UNIVERSITY OF OKLAHOMA

GRADUATE COLLEGE

SITE-DIRECTED MUTAGENESIS AS A PROBE OF NAD^+-BINDING SITE IN MALIC ENZYME

A DISSERTATION

SUBMITTED TO THE GRADUATE FACULTY

in partial fulfillment of the requirements of the

Degree of

DOCTOR OF PHILOSOPHY

By

DENIZ FULYA AKTAS
Norman, Oklahoma
2008

SITE-DIRECTED MUTAGENESIS AS A PROBE OF
NAD^+-BINDING SITE IN MALIC ENZYME

A DISSERTATION APPROVED FOR THE
DEPARTMENT OF CHEMISTRY AND BIOCHEMISTRY

BY

Dr. Paul F. Cook, Chair

Dr. Ann H. West

Dr. Phillip E. Klebba

Dr. Kenneth M. Nicholas

Dr. Roger G. Harrison

ACKNOWLEDGEMENT

I would like to express my deepest gratitude for my academic advisor Dr. Paul F. Cook. I want to thank him for encouraging and challenging me throughout my graduate studies. He has been more than an advisor to me. Besides being a great mentor, he has an amazing personality, and he is always nice, kind and humorous. I will always miss the days I have spent in his lab.

I also would like to thank my advisory committee, Dr. Ann H. West, Dr. Philip E. Klebba, Dr. Kenneth M. Nicholas and Dr. Roger G. Harrison who have generously given their time and expertise to better my work. Their comments and suggestions which positively guided this work were invaluable.

There are many who have contributed to this work in various ways. Among those, I want to express my deepest appreciation to Dr. William Karsten. He was always helpful whenever I needed his expertise from the very beginning. He not only taught me almost all the techniques I needed, but also helped me to interpret my data. I also want to acknowledge all my lab mates who supported and helped me throughout my Ph.D, especially Dr. Babak Andi, Dr. Lei Li, Dr. Ying Lin, Dr. Hengyu 'Carina' Xu and Dr. Lillian Chooback. I want to thank my lab mate and very good friend Devi Kosala Ekanayake whose friendship and hospitality have supported and entertained me over the many years of our friendship. I want to thank as well Jean Keil, Arlene Crawford and Carol Jones for helping me with all the paperwork.

This dissertation could not have been written without the support and love of my parents, Tulay and Kenan Bolukbasi, my grandparents Serife and Ramazan Acarturk and my sister Begum Bolukbasi. They always have been an inspiration and support to me. I

also want to thank my parents-in-law, Vefa and Gultekin Aktas, my brother-in-law Mert Can Aktas, my uncle-in-law Reha Aktas and his family for loving and supporting me all those years.

And finally, I want to thank and dedicate this dissertation to my husband Levent Aktas, who has always been there for me, who gave me strength to go on, who always made me feel that I could achieve anything I wanted! Thanks for loving and trusting me.

TABLE OF CONTENTS

LIST OF TABLES

LIST OF FIGURES

ABSTRACT

The mitochondrial NAD-malic enzyme catalyzes the oxidative decarboxylation of malate to pyruvate and CO_2. The role of the dinucleotide substrate in oxidative decarboxylation is probed in this study using site-directed mutagenesis to change key residues that line the dinucleotide binding site. Mutant enzymes were characterized using initial rate kinetics, and isotope effects were used to obtain information on the contribution of these residues to binding energy and catalysis.

The first part of the project was to investigate the contribution of binding energy and catalysis of the groups that interact with the nicotinamide and ribose rings of NAD. Results obtained for the N479 mutant enzymes, indicate that the hydrogen bond donated by N479 to the carboxamide side chain of the nicotinamide ring is important for proper orientation of the cofactor in the hydride transfer step. The stepwise oxidative decarboxylation mechanism observed for the wt enzyme changed to a concerted one, which is totally rate limiting, for the N479Q mutant enzyme. In this case, it is likely that the longer glutamine side chain causes reorientation of malate such that it binds in a conformation that is optimal for concerted oxidative decarboxylation. Converting N479 to the shorter serine side chain gives very similar values of K_{NAD}, K_{malate} and isotope effects relative to wt, but $V/\mathbf{E_t}$ is decreased 2,000-fold. Data suggest an increased freedom of rotation, resulting in nonproductively bound cofactor, perhaps with the nicotinamide ring occupying the site that favors the reduced ring. Changes were also made to two residues, S433 and N434, which interact with the nicotinamide ribose of NAD. In addition, N434 donates a hydrogen bond to the β-carboxylate of malate. The K_{NAD} for the S433A mutant enzyme increased by 80-fold, indicating that this residue

provides significant binding affinity for the dinucleotide. With N434A, the interaction of the residue with malate is lost, causing the malate to reorient itself, leading to a slower decarboxylation step. The longer glutamine and methionine side chains stick into the active site and cause a change in the position of malate and/or NAD, and results in more than a 10^4-fold decrease in $V/\mathbf{E_t}$ for these mutant enzymes. Overall, data indicate that subtle changes in the orientation of the cofactor and substrate dramatically influence the reaction rate.

The second part of this project focused on the residues that form the adenosine binding site of NAD. Site-directed mutagenesis was performed to determine the role of these residues in binding of the cofactor and/or catalysis. D361, which is completely conserved among species, is located in the dinucleotide-binding Rossmann fold and makes a salt bridge with R370, which is also highly conserved. D361 was mutated to E, A and N. R370 was mutated to K and A. D361E and A mutant enzymes were inactive, likely a result of the increase in the volume, in the case of the D361E mutant enzyme that caused clashes with the surrounding residues, and loss of the ionic interaction between D361 and R370, for D361A. Although the K_m for the substrates and isotope effect values did not show significant changes for the D361N mutant enzyme, $V/\mathbf{E_t}$ decreased by 1400-fold. Data suggested the nonproductive binding of the cofactor, giving a low fraction of active enzyme. The R370K mutant enzyme did not show any significant changes in the kinetic parameters, while the R370A mutant enzyme gave a slight change in $V/\mathbf{E_t}$, contrary to expectations. Overall, results suggest that the salt bridge between D361 and R370 is important for maintaining the productive conformation of the NAD binding site. Mutation of residues involved leads to nonproductive binding of NAD. The interaction

stabilizes one of the Rossmann fold loops that NAD binds. Mutation of H377 to lysine, which is conserved in NADP-specific malic enzymes and proposed to be a cofactor specificity determinant, did not cause a shift in cofactor specificity of the *Ascaris* malic enzyme from NAD to NADP. However, it is confirmed that this residue is an important second layer residue that affects the packing of the first layer residues that directly interact with the cofactor.

The last part of this dissertation consists of a review on the acid-base chemical mechanism of the enzyme class, metal ion-dependent pyridine nucleotide-linked β-hydroxyacid oxidative decarboxylases. This family includes malic enzyme (ME), isocitrate dehydrogenase (IcDH), and isopropylmalate dehydrogenase (IPMDH), which require a divalent metal ion, and homoisocitrate dehydrogenase (HIcDH), and tartrate dehydrogenase (TDH), which require a monovalent and divalent metal ion for activity. Overall structure gives two distinct classes, with the MEs as the only member of one of the two classes, ME subfamily, while all of the others exhibit the same fold, the IcDH subfamily. The active sites of all of the enzymes have a similar overall geometry and most of the active site residues are conserved throughout the family; they are completely conserved within the IcDH subfamily. Data available for all of the enzymes in the family have been considered and a general mechanism is proposed for the family that makes use of a lysine (general base), tyrosine (general acid) pair. Differences exist in the mechanism of generating the neutral form of lysine so that it can act as a base.

CHAPTER 1:

INTRODUCTION

1.1. Pyridine-nucleotide dependent oxidative decarboxylases

The malic enzyme is in a class of enzymes called pyridine-nucleotide dependent decarboxylases that includes isocitrate dehydrogenase (ICDH), 6-phosphogluconate dehydrogenase (6PGDH), tartrate dehydrogenase (TDH), isopropylmalate dehydrogenase (IPMDH), cholestenoate dehydrogenase (CDH) and malic enzyme (ME). Those enzymes catalyze the oxidative decarboxylation of β-hydroxyacids with the use of NAD(P) as the oxidant Figure 1.1 [1]. This class can be divided into three based upon the metal ion requirement features. 6PGDH does not need the metal ion for activity because the electron-withdrawing hydroxyl groups vicinal to the β-hydroxyl group can act like the metal ion in activating the substrate for decarboxylation [2]. Malic enzyme needs a divalent cation, like Mg^{+2} or Mn^{+2}, and the rest of the enzymes fall into the third class requiring both a monovalent and a divalent metal ion.

The enzymes of this class are either homodimeric or homotetrameric. TDH, IPMDH and ICDH show amino acid sequence homology whereas ME and 6PGDH do not. 6PGDH has a rapid equilibrium random kinetic mechanism whereas the others have a steady-state random kinetic mechanism [1].

Pyridine-nucleotide dependent oxidative decarboxylases have the same general acid-base mechanism. In the first step, a general base assists in the oxidation of β-hydroxyacid to β-ketoacid. Then the same residue acts as a general acid and aids in the decarboxylation of the β-ketoacid to the enol, with the divalent ion acting as a Lewis acid

Figure 1.1 General reaction of Pyridine-nucleotide dependent oxidative decarboxylases. R_1=H, OH, $CH_2CO_2^-$, $CH(CH_3)_2$. R_2= CO_2^-, $CH(OH)CH(OH)CH_2OPO_3^{2-}$ M^{2+} is the metal ion [3].

(exception of 6PGDH). In the last step, the enol is tautomerized to a ketone, with the aid of a second general acid [1]. This class is an excellent example of multistep catalysis.

1.2. Background and significance

In the early 1940's, an enzyme catalyzing the oxidative decarboxylation of malate was reported independently by a number of scientists [4-6]. The enzyme, named as 'malic enzyme' by Ochoa [7], was first found in pigeon liver and has since been isolated from many living organisms from bacteria to humans.

Malic enzyme is an oxidative decarboxylase which catalyzes the divalent metal ion (Mg^{+2} or Mn^{+2}) dependent conversion of L-malate to pyruvate and CO_2, with concomitant reduction of $NAD(P)^+$ to NAD(P)H. Three different isoforms of malic enzyme have been found in mammals: cytosolic $NADP^+$-dependent malic enzyme (c-NADP-ME), mitochondrial $NADP^+$-dependent malic enzyme (m-NADP-ME) and mitochondrial $NAD(P)^+$-dependent malic enzyme (m-NAD-ME). m-NAD-ME can use both NAD^+ and $NADP^+$, but under physiological conditions it prefers NAD^+.

Malic enzyme is involved in many important biological pathways. With its products pyruvate, NAD(P)H and CO_2, malic enzyme plays a significant role in metabolic processes such as photosynthesis and energy production. Photosynthetic NADP-MEs have been found in both C4 and CAM (Crassulacean Acid Metabolism) plants. The isoform in C4 plants is the best studied plant enzyme and it plays a very important role in providing CO_2, via malate decarboxylation, to be used in carbon fixation by ribulose-1,5-bisphosphate carboxylase/oxygenase. The malic enzyme is specifically localized in bundle sheath chloroplasts [8] and its expression is regulated by light [9]. Another isoform has been found in CAM plants, having a similar function to the

C4 isoform. NADP-ME is also present in C3 plants where it has a non-photosynthetic role. It is induced by UV-B radiation exposure [10] and plays a role in the plant defense system by providing NADPH for deposition of lignin and for biosythesis of flavonoids [11]. This function of the enzyme has also been documented for C4 and CAM non-photosynthetic isoforms.

NADP-ME is also suggested to be involved in lipid biosythesis in mammals. It participates in the transfer of a hydride from NADH to NADPH [12] and is one of the major sources of NADPH required in fatty acid biosynthesis in adipose tissue [13]. It has also been reported that when cells are passing from growing state to resting state, the increase in triacylglycerol synthesis is due to the increased activity of triacylglycerol synthesizing enzymes, one of which is malic enzyme [14]. In another study by Ayala *et al*, it has been reported that the activation of NADPH-consuming pathways, such as detoxification processes, increases the ME amount; suggesting that NADPH requirement can be a factor for ME induction [15].

Several studies suggest that there is a significant increase in expression of malic enzyme in rapidly proliferating tissues [16-18]. In normal tissues, malic enzyme provides NADPH for fatty acid biosythesis. However, in tumor cells, rather than contributing to the NADPH pool, malic enzyme is thought to participate in energy production. Glutamate, rather than glucose, has been reported to be the preferred energy fuel in tumor cells [18,19]. Malic enzyme participates in a pathway called glutaminolysis in which glutamine is converted to lactate. This pathway provides energy and intermediates for synthetic purposes in the tumor cells [18]. In addition, malic enzyme converts excess malate to pyruvate which in turn is converted to lactate to be secreted from the cell [20].

1.3. Reactions of malic enzymes

Malic enzymes catalyze the metal-dependent oxidative decarboxylation of L-malate (Figure 1.2A) with concomitant reduction of NAD(P) to NAD(P)H. In addition to oxidative decarboxylation, malic enzymes can catalyze the decarboxylation of oxaloacetate (Figure 1.2B) and the reduction of α-ketoacids (Figure 1.2C).

According to their dinucleotide specificity and oxalaoacetate decarboxylase activity, malic enzymes are divided into three different classes [21]. The first class is **EC 1.1.1.40**, that is L-malate:NADP oxidoreductase (oxaloacetate-decarboxylating), which includes malic enzymes from the livers of pigeon and chicken. The second class is **EC 1.1.1.39**, that is L-malate:NAD oxidoreductase (decarboxylating) which includes group D streptococcus, cauliflower and potato tuber malic enzymes. The third class is **EC 1.1.1.38**, that is the L-malate:NAD oxidoreductase (oxaloacetate-decarboxylating), which includes the malic enzyme from *Lactobacillus arabinosus*, the dung beetle *Catharsius* and *Ascaris suum*.

1.4. Malic enzyme from *Ascaris suum*

Ascaris suum, which is a parasitic nematode, has been a major source for malic enzyme studies, especially before recombinant techniques, since it could be easily obtained in large quantities (the female parasite can lay an estimated 2 million eggs daily). *Ascaris suum* infects intestines of pigs, while *Ascaris lumbriocides* infects humans. In the latter case, with the ingestion of *Ascaris* eggs, growing larvae travel to lung tissue via circulatory system, causing ascariasis.

A.

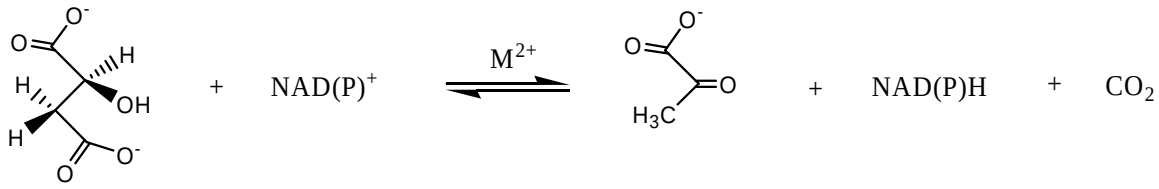

L-Malate Pyruvate

B.

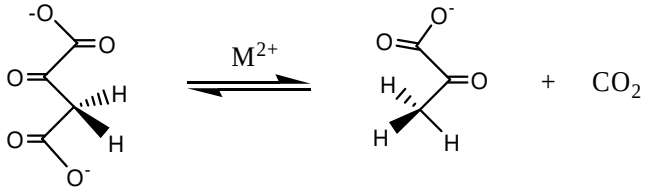

Oxaloacetate Pyruvate

C.

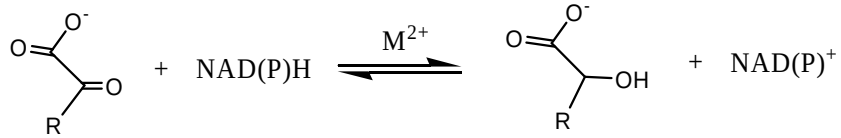

alpha-ketocid alpha-hydroxyacid

Figure 1.2 Reactions catalyzed by Malic Enzymes. R stands for CO_2^-, $CH_2CO_2^-$ or CH_3. M^{2+} stands for the divalent metal ion [3].

Ascaris suum malic enzyme is one of the best-studied malic enzymes and it is also the subject of this study. NAD-ME was isolated from *A. suum* in 1956 by Saz and Hubbard [21]. Malic enzyme plays an important role in carbohydrate metabolism in this organism, Figure 1.3. *Ascaris suum* has an anaerobic energy metabolism where the Kreb cycle is not functional [22]. The organism stores its energy in terms of glycogen at high concentration, which can be converted to glucose in the cytosol. The glucose is then converted to phosphoenolpyruvate via the glycolytic pathway. PEP is converted to oxaloacetate which in turn is converted to malate by malate dehydrogenase. Malate enters the mitochondria and malic enzyme catalyzes the oxidative decarboxylation of malate to pyruvate, CO_2 and NADH. These reactions are responsible for transfer of reducing equivalents from cytosol to mitochondrion.

Fumarase also acts on malate, converting it to fumarate, maintaining the two at equilibrium. Fumarate is converted to succinate by fumarate reductase which uses the NADH produced by the malic enzyme reaction and fumarate reduction is coupled to electron transport-associated ADP phosphorylation. Mitochondrial NAD-ME is the key enzyme in the only mitochondrial ATP producing pathway of the organism. The succinate produced can be used to synthesize branched-chain fatty acids and other endo products of metabolism.

1.5. Purification, cloning and expression of *Ascaris suum* ME

In 1957, Saz and Hubbard [21] partially purified *A. suum* ME and in 1981, Allen and Harris [23] purified it to homogeneity. DEAE-cellulose and cellulose phosphate chromatographies and ammonium sulfate fractionation were used in these studies. In 1957, Saz and Hubbard [21] partially purified *A. suum* ME and in 1981, Allen and Harris

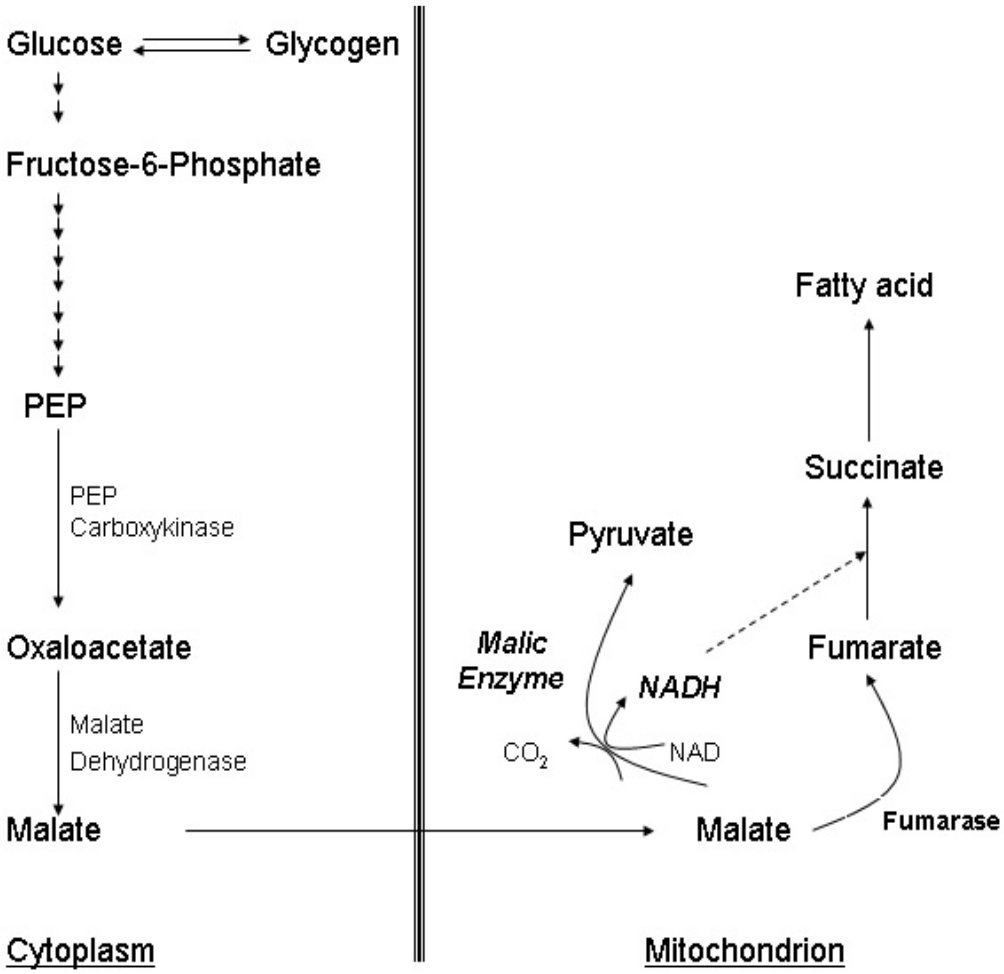

Figure 1.3 Abbreviated Carbohydrate and Energy Metabolism in *Ascaris suum* [24].

[23] purified it to homogeneity. DEAE-cellulose and cellulose phosphate chromatographies and ammonium sulfate fractionation were used in these studies. In 1994, Karsten and Cook [25] developed a procedure, which was modified from the method of Allen and Harris, that utilized tandem column affinity chromatography with Blue-B and Orange-A agarose resins.

In 1992, Kulkarni *et al*. obtained the nucleotide sequence of *A. suum* ME cDNA [26]. It consisted of 2269 bases, with a 5'-leader sequence, single open reading frame of 1851 bases and a 3'-noncoding region of 340 bases. The first 12 amino acid residue sequence is a mitochondrial translocation signal sequence. The mature protein consists of 605 amino acids, 73 are acidic and 84 are basic. There are 3 tryptophan, 13 histidine and 9 cysteine residues. The molecular weight of the monomer is 68,478 Da.

The *A. suum* NAD-ME was first subcloned into expression vector pKK223-3 [27]. In 1999, Karsten *et al*. [28] subcloned it into the pQE.30 expression vector which adds a six histidine tag to the C-terminus. The pQE.30 vector gives good expression and the his-tag makes it very easy to purify the recombinant protein by using nickel-NTA column chromatography.

1.6. The structure of the malic enzyme

Crystals of malic enzyme were obtained from rat liver in 1987 [29], *A. suum* in 1991 [30] and pigeon liver in 1999 [31]. However, the first structure of an NAD(P)-ME from human mitochondria was solved in 1999 at 2.5 Å resolution and refined to 2.1 Å resolution [32]. In that study it was found that human mitochondrial NAD(P)-ME is a homotetramer, which is comprised of a dimer of dimers. The monomer structure consists of four domains, A, B, C and D. Domain A is mostly helical while domain B consists of

a parallel five-stranded β-sheet surrounded by helices on both sides, which represented a new backbone fold. Domain C has a Rossmann fold indicating a dinucleotide-binding motif, while domain D contains one helix and a long extended structure. A second NAD-binding site was found and is ~35 Å away from the active site, which is a deep cleft at the interface between three of the domains. The second NAD-binding site is thought to be an inhibitory site for ATP.

In 2002, the crystal structure of the ME from *A. suum* was solved to 2.3 Å resolution [33]. The 3D structures of *A. suum* ME and human ME are very similar as expected since there is 82% sequence homology between them. *A. suum* ME is also a homotetramer and a dimer of dimers, Figure 1.4. The tetramer exhibits 222 symmetry. For the formation of the tetramer 4900 $Å^2$ per monomer is buried. The monomer consists of four domains that correspond to those assigned by Xu *et al*. [32], Domain A and B participate in the dimer and tetramer interfaces and are considered to be the core of the molecule. Domain C contains the Rossmann fold to which NAD binds, while domain D contains the amino- and carboxy-termini, which has unique features in the *A. suum* ME.

Some of the carboxy-terminal residues are not present in human ME and they form a short four-residue helix and a coil. In addition, the amino-terminus contains 30 additional residues that enable a more extensive tetramer interface interaction. The other domains are very similar to human ME domains, with the exception of the position of their C domains relative to A/B domain core. When the tetramer organizations of *A. suum* and human MEs are compared, it can be seen that *A. suum* enzyme is more flat than the human ME.

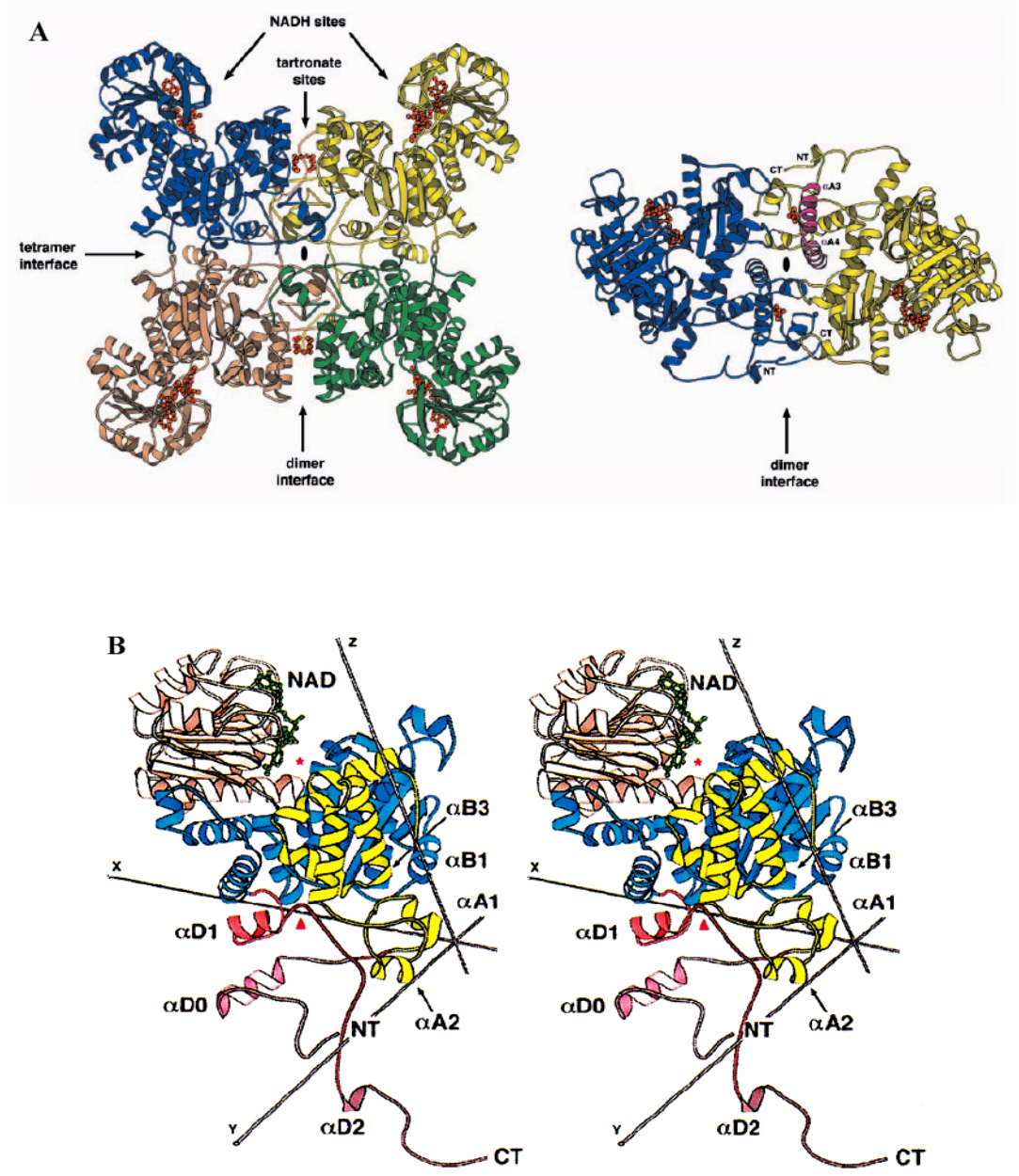

Figure 1.4 Ribbon diagrams of the structure of *Ascaris* mitochondrial ME. A) in complex with NADH, Mg, and tartronate. The tetramer viewed down one 2-fold axis (indicated by the *black oval*) with the tetramer and dimer interfaces indicated by the *arrows*. The four subunits are *colored blue*, *yellow*, *green*, and *tan*. The four NADH and four tartronate ligands are shown as *red ball-and-stick models*, and their binding sites are indicated for one dimer. Right: the *Ascaris* ME dimer viewed down the 2-fold axis corresponding to the dimer interface showing the locations of the two tartronate binding sites more clearly [34] B) in binary complex with NAD. The NAD ligand and the amino and carboxyl termini are indicated, and the four domains are colored as follows: yellow, A domain; blue, B domain; tan, C domain; red and purple, D domain [33].

The human ME active site has been crystallized in several different conformations [35]. The enzyme in complex with NAD is in an open form, the active site is fully exposed to solvent and the residues are not positioned to carry out catalysis. However, upon binding of the metal ion and the substrate the enzyme undergoes a conformational change via rigid body movements of domain C with respect to domain B and the active site is closed to carry out catalysis. It has been suggested that the open form is required for substrate binding and product release whereas the closed form is required for catalysis.

In the *A. suum* NAD-ME, the active site in the binary complex is similar to the open form of the human ME binary complex, but more open, providing a more intensive interaction between NAD and domain C [33]. Domains B and C provide almost all of the active site residues, whereas residue Y126 is contributed from domain A, Figure 1.5. The suggested residues contributing to substrate binding and catalysis are R181, K199, D295, N434 and N479. As in the human ME, the conformational change in the active site from the open to closed state is by the rigid body movements of domain C and the closed form of the active site of *A. suum* ME is similar to that of human ME.

One of the most notable differences between *A. suum* and human ME is that human ME has an exo-site, at the tetramer interface, which is suggested to be an ATP-inhibitory binding site. However, in *A. suum* ME this exo site is not present and the enzyme is not inhibited by physiological concentrations of ATP [34].

1.6.1. Metal-ion binding site

The *A. suum* NAD-ME needs a divalent metal ion to carry out its reaction and can use either Mg^{2+} or Mn^{2+}. Hung *et al* [36], showed that with other divalent cations (Zn^{2+},

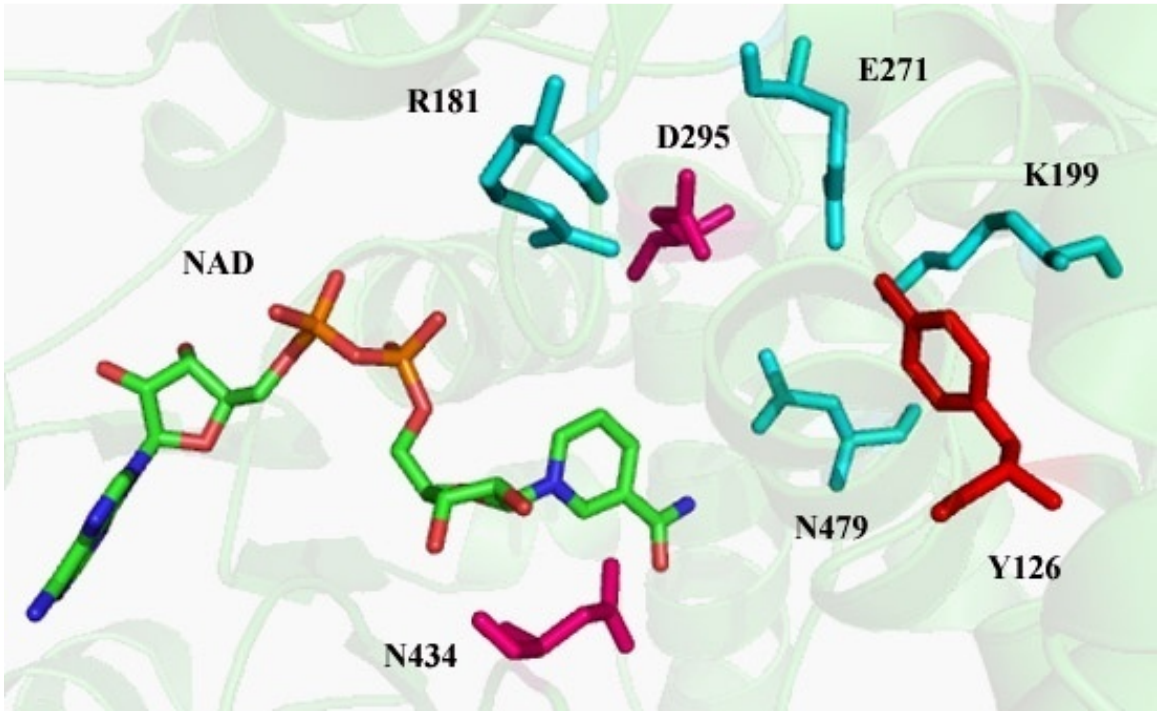

Figure 1.5 Active site residues in *Ascaris* malic enzyme (PDB code: 1LLQ). The residues shown in cyan and magenta are contributed by domain B and C, respectively. Y126, shown in red, is from domain A. NAD is shown in spectrum. The figures are generated by PyMOL molecular visualization program (website: http://pymol.sourceforge.net/).

Cu^{2+} and Fe^{2+}) the conformational change was slowed down and active site geometry was altered. In addition, the resulting conformation was unfavorable for catalysis. Evidence has suggested that the nature of the metal ion and its coordination in the active site are crucial for the catalysis. In all malic enzymes studied thus far, it has been found that the sequence around the metal ion binding site is highly conserved. In the *A. suum* NAD-ME, the metal ion binding site is made up of E271, D272 and D295, which correspond to E255, D256 and D279 in human NAD-ME [35].

1.6.2. Tartronate binding site

The *A. suum* NAD-ME was known to be activated by fumarate and an activation constant of 40 µM was reported [37]. Recently, Rao *et al*. [34] obtained the crystal structure of the *A. suum* mitochondrial NAD-ME in a quaternary complex with NADH, tartronate and magnesium, at 2.0 Å resolution. In this study tartronate (2-hydroxymalonic acid), a dicarboxylic analogue of malate and fumarate, was tightly bound to a positively charged pocket at the dimer interface (Figure 1.4A). The residues providing hydrogen bondings to tartronate are reported as R105, R81 and Q78, Figure 1.6.

These residues are homologous to those interacting with the activator fumarate in the human ME [38]. Therefore, it has been suggested that the tartronate binding site in *A. suum* NAD-ME is an allosteric site for the activator fumarate. However, there is approximately 30 Å distance between the active site and the allosteric site, suggesting that there must be structural interactions between the sites to transmit the allosteric signal [34].

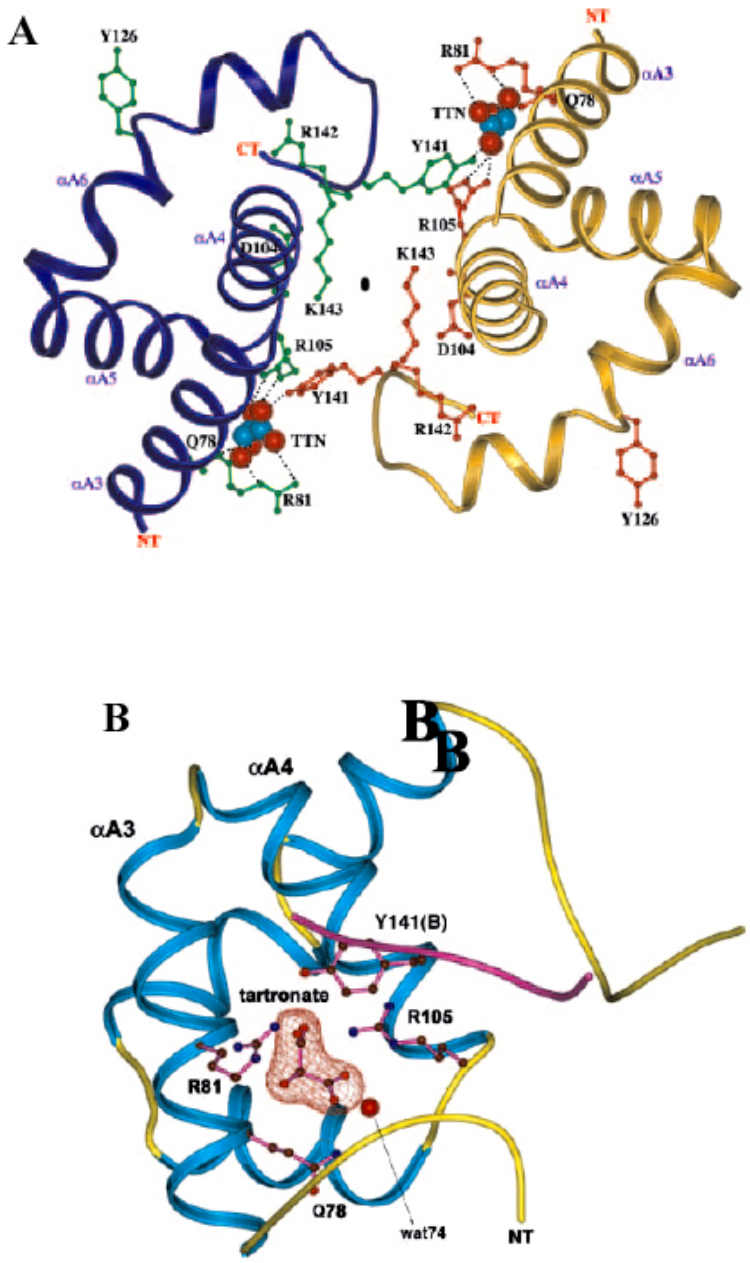

Figure 1.6 Binding of tartronate to *Ascaris suum* malic enzyme**.** A) Tartronate (TTN), 2-hydorxymalonic acid, in *Ascaris* ME is shown as red and cyan CPK models. Key residues involved in binding ligands are shown as ball-and-stick models. B) Ribbon diagram of the tartronate-binding site within the dimer interface of *Ascaris* ME with tartronate and key residues indicated as ball-and-stick models and a water molecule bound to tartronate shown as a sphere [34].

1.6.3. NAD binding site

The NAD cofactor is bound by three loops (361-362, 326-329, 405-408). It binds to the C domain with the nicotinamide ring in anti-conformation *re*-face exposed to solvent [33]. However, in the structure obtained with NADH bound there is a dramatic difference in the conformation and interactions of the nicotinamide ring (Figure 1.7) [34]. In the ME-NADH complex there is +198º rotation about the N-glycosidic bond relative to the ME-NAD complex. As a consequence of this rotation, the interactions between NAD and G477, N479 are broken; new interactions between NADH and D295, R181 are formed.

Recently, Karsten and Cook [39] mutated R181 to lysine and glutamine. In the crystal structures of *A. suum* malic enzyme R181 is within hydrogen bonding distance with malate and nicotinamide ring of NADH, but not with NAD. The significant increase in K_{malate} and $K_{ioxalate}$ for both mutants suggested that R181 plays an important role in binding the substrate. The mutant enzymes showed a >10-fold increase in K_{iNADH} without affecting K_{NAD}. This supported the rotation of the nicotinamide ring upon reduction of the cofactor. This rotation is important in catalysis for proper positioning of the oxaloacetate intermediate prior to decarboxylation. This ring flip was also observed in 6-phosphogluconate dehydrogenase [40,41].

1.7. Kinetic mechanism of the *Ascaris suum* malic enzyme

Ochoa *et al.* [6] found out that the malic enzyme in pigeon liver extracts catalyzed the conversion of malate to pyruvate, with the concomitant reduction of NAD, in the presence of a divalent metal ion. In 1957, Saz and Hubbard [21] showed that the malic enzyme from *Ascaris lumbriocides* muscle could use both NAD and NADP as the

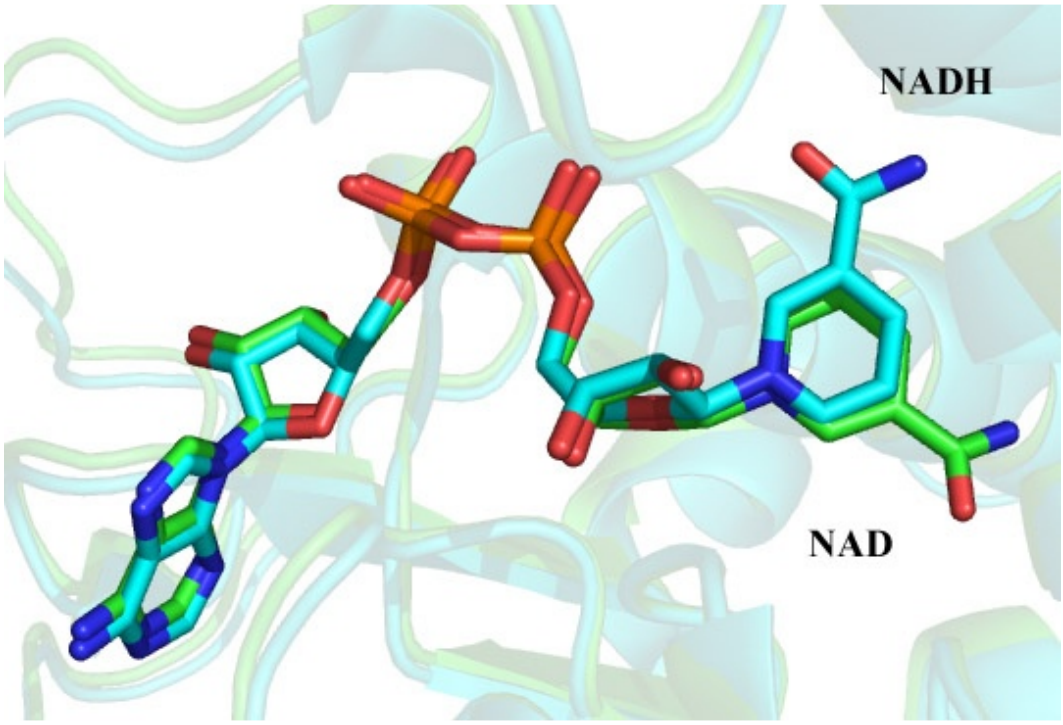

Figure 1.7 Overlay of NAD and NADH bound to the active site of *Ascaris suum* malic enzyme. NAD is shown in green and NADH is shown in cyan. The PDB codes for NAD and NADH are 1LLQ and 1O0S, respectively.

cofactor. It was also suggested that the enzyme did not have the oxaloacetate decarboxylation activity. However, Hsu and Lardy [42] proposed that the oxaloacetate was an intermediate in the enzyme reaction. Therefore, the enzyme must have the oxaloacetate decarboxylation ability. This was confirmed by Park *et al*. [43] that the malic enzyme from *Ascaris suum* could decarboxylate oxaloacetate with no requirement of NAD although the presence of the dineucleotide increased the affinity of the enzyme for the oxaloacetate. Therefore, the classification of *Ascaris suum* malic enzyme changed to E.C.1.1.1.38.

Landsperger *et al.* [44]carried out the first initial velocity studies on malic enzyme in both forward and reverse directions. Data suggested a sequential kinetic mechanism. However, the chelate complexes formed between the metal ion and the substrates were not considered. Therefore, extensive initial velocity studies were carried out by Part *et al*. [45] in the absence and presence of products and dead-end inhibitors. Data showed that the *A. suum* ME has a steady-state random kinetic mechanism in the direction of oxidative decarboxylation, in which either malate or NAD can add to the enzyme-metal ion complex (Figure 1.8). However, when low concentrations of Mg^{+2} were used the mechanism became ordered with the sequential addition of NAD, Mg and malate; the enzyme-NAD-malate was unproductive. It was suggested that the ordered mechanism was optimal *in vivo*. In the same study, it was shown that NAD and malate form chelate complexes with the metal ion and that the final concentrations of the substrates must be adjusted for this complex. These results were confirmed by finite and equal values of V, V/K_{malate} and V/K_{NAD} at pH 7.0 [46] and by isotope partitioning experiments [47].

The kinetic mechanism in the reductive carboxylation direction was also suggested to be steady-state random [48]. No binding site for CO_2 was observed, so the reaction should happen when enolpyruvate collides with CO_2. The data suggested the requirement of metal ion binding prior to pyruvate for a productive complex formation [45].

Cook and Cleland [49] reported that if the substrates bind to only the correctly protonated enzyme form, the *V* profile will be pH-independent. However, for the *A. suum* malic enzyme, the maximum rate shows a pH dependence and decreases below a pK of 4.8 [46]. On the basis of this, it is suggested that when a group with an apparent pK of 4.8 becomes protonated some step after catalysis, which is pH-dependent, becomes rate-determining. This slow step could be 1) pH-dependent release of a product after the first product. Since CO_2 is the most likely product to be released first, then the slow step involves release of pyruvate or NAD(P)H. For some of the NAD(P) MEs release of NAD(P)H is indeed proven to be totally rate limiting, where the deuterium isotope effect on V is unity. However, for the *A. suum* NAD-ME this can not be the case since ^{D}V is finite with a value of 1.45 [46]; 2) pH-dependent isomerization of free enzyme or enzyme-substrate complex. In 1993, Rajapaksa *et al*. [50] carried out pre-steady state kinetic studies in which a lag period was observed prior to steady state attainment. This study showed that there is slow isomerization of enzyme-NAD complex.

1.8. Chemical mechanism of *Ascaris suum* malic enzyme

1.8.1. Stepwise chemical mechanism of NAD-malic enzyme

Hermes *et al* [51] determined deuterium isotope effects and ^{13}C isotope effects

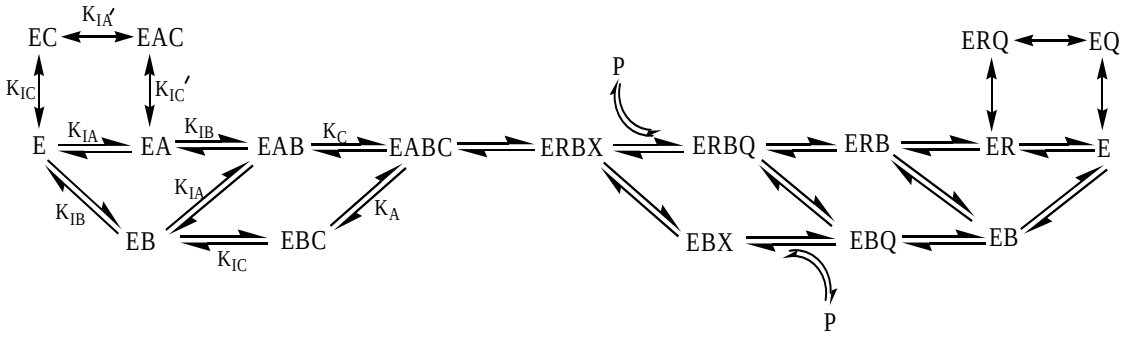

Figure 1.8 Random kinetic mechanism of *A. suum* NAD-ME. A, B and C represent NAD^+, Mg^{+2} and L-malate, respectively. X, P, Q and R represent oxaloacetate, CO_2, pyruvate and NADH, respectively [3]. K_i represents the dissociation constant for the binary enzyme-reactant complexes, whereas K_I represents the dissociation of the ternary EAB complex. $K_{I'}$ represents the dead-end complexes. Known dissociation constants are listed in Table 1.1.

Table 1.1 Known Dissociation Constants in *Ascaris suum* ME Reaction [3]

Dissociation Constants (mM)	**Mg^{2+} as metal ion**
K_A	0.005 ± 0.001
K_{iA}	0.080 ± 0.001
K_{IA}	0.078 ± 0.004
K_{IA}'	0.14 ± 0.03
K_{iB}	14.0 ± 1.0
K_{IB}	29.3 ± 1.3
K_C	1.2 ± 0.1
K_{iC}	20.0 ± 2.0
K_{IC}	1.6 ± 0.3
K_{IC}'	35.0 ± 0.8

The definition of the parameters are given in the legend of Figure 1.8.

with both deuterated and protoated malate. Results showed that the malic enzyme from chicken liver had a stepwise mechanism with hydride transfer preceding decarboxylation. It was also determined that the reverse hydride transfer was 6-12 times faster than decarboxylation. Grissom and Cleland confirmed the stepwise nature of the NADP-malic enzyme [52]. The mechanism of NAD-malic enzyme from *Ascaris suum* was also considered to be stepwise, hydride transfer preceding decarboxylation and this was proved by Weiss *et al* [53] using multiple isotope effects on different dineucleotides. ^{13}C isotope effect values were smaller with the deuterated malate than the ones with the unlabeled malate for the nicotinamide-containing dinucleotides. This suggested a stepwise mechanism with hydride transfer followed by decarboxylation. However, with the modified nicotinamide-containing dinucleotides the mechanism either changed from stepwise to concerted or was still stepwise with a β-secondary C isotope effect associated with the hydride transfer. In 1994, Karsten *et al*. [25] carried out deuterium and tritium isotope effect studies and oxaloacetate-partioning experiments and confirmed the stepwise nature of the NAD-malic enzyme from *A. suum*. They reported ^{D}V=2.02 ± 0.07, $^{D}(V/K_{NAD})$=1.57 ± 0.07, $^{13}(V/K)_{H}$= 1.0342 ± 0.0002 and $^{13}(V/K)_{D}$= 1.0252 ± 0.0001, when Mg^{2+} was used as the metal ion. They also showed that the mechanism changed to a concerted one with alternative dinucleotides, like PAAD and 3-APAD, most likely because of the different configuration of bound malate. This was also confirmed by the ^{13}C isotope effect studies carried out for all four carbons of L-malate [54].

1.8.2. General acid/general base mechanism of A. suum ME

The pH dependence of the kinetic parameters and the primary deuterium isotope effects showed that the two enzyme groups were necessary for binding and catalysis and

substrates bind only to correctly protonated form of *Ascaris suum* NAD-malic enzyme [46]. A group with a pK of 4.9 must be unprotonated and a group with a pK of 8.9 must be protonated for optimum binding and activity. This was consistent with the results obtained for pH dependence of dissociation constants using the competitive inhibitors against malate. Based on those, a general acid/general base mechanism was proposed for *A. suum* NAD-malic enzyme [43,46]. The proposed mechanism can be summarized as: the general base with a pK of 4.9 accepts a proton from the 2-hydroxyl group of L-malate simultaneously with the hydride transfer to NAD. The proton is shuttled back and forth between the general base and the C2 oxygen. The general acid with a pK of 8.9 plays a role in the tautomerization step.

Liu *et al*. [55] suggested that K199 was the general acid and D295 was the general base in *A. suum* NAD-ME reaction. However, with the availability of the structure of *A. suum* malic enzyme, Karsten *et al*. [56] proposed that a catalytic triad was responsible for the acid-base chemistry. In that study it was reported that the enzyme was in an open conformation before the binding of malate (Figure 1.9, I). Upon binding of malate the active site of the enzyme is closed and a hydrogen bond is formed between K199 and Y126. A proton is transferred to D294 as it comes closer to E271, and this enables K199 to act as a general base. First, malate is oxidized to oxaloacetate with K199 acting as a general base. In this hydride transfer step (Figure 1.9, II), K199 accepts a proton from the 2-hydroxyl group of malate converting it to oxaloacetate intermediate which is subsequently decarboxylated (Figure 1.9, III) with the aid of metal ion, acting as a Lewis acid. A proton is shuttled from K199 to the carbonyl oxygen of oxaloacetate, forming an enolpyruvate. Tautomerization step (Figure 1.9, IV) involves general base-general acid

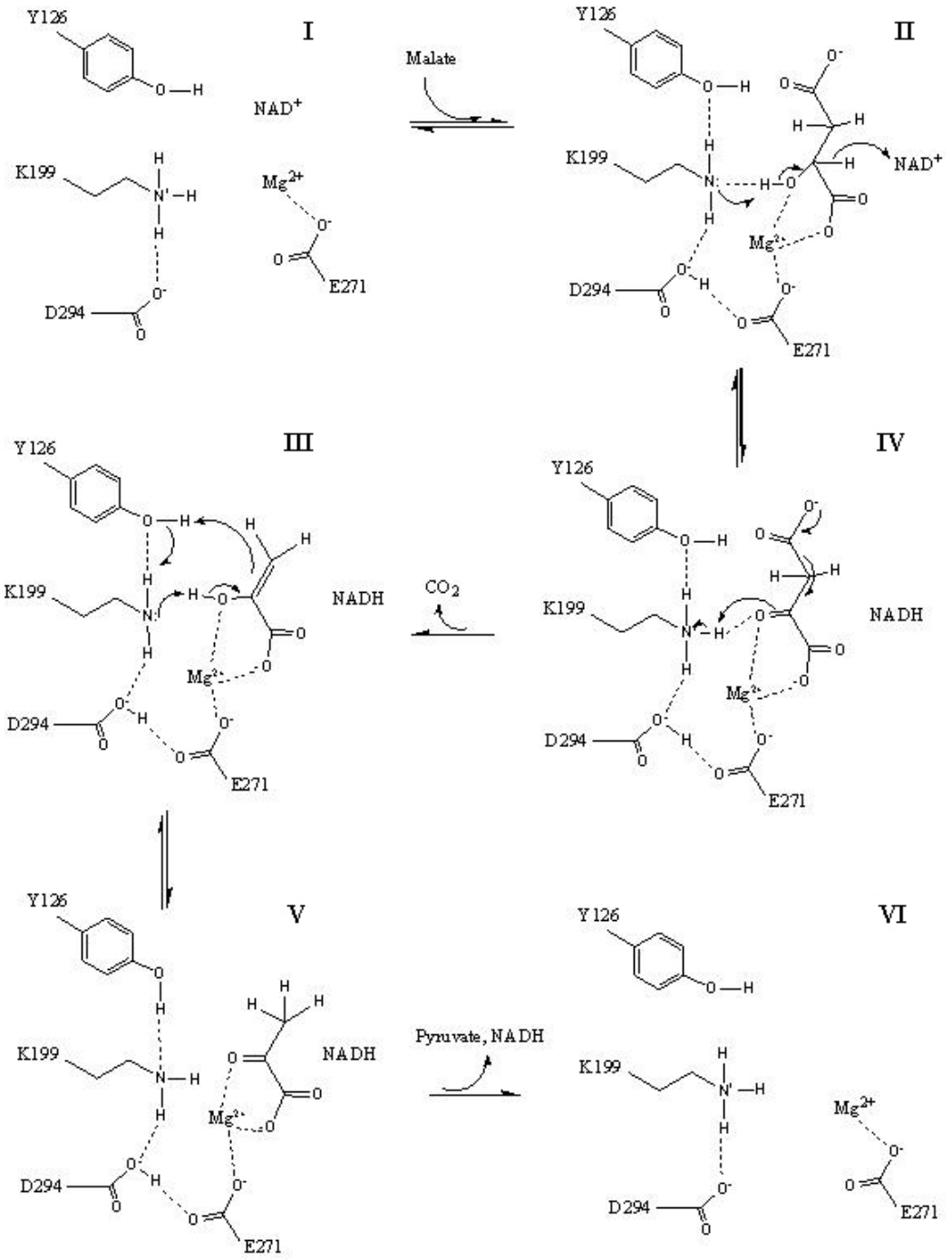

Figure 1.9 Proposed General Acid/Base Chemical Mechanism for Malic Enzyme [56]

catalysis, K199 accepting a proton from the enol hydroxyl and Y126 donating a proton to pyruvate. Then the pyruvate is released from the enzyme (Figure 1.9, V), regenerating the enzyme in the correct protonation state (Figure 1.9, VI). The hydride transfer and decarboxylation steps are partially rate-limiting whereas tautomerization step is fast and not rate-limiting.

1.9. Regulation of malic enzyme

As stated previously, when malate enters the mitochondrion of *Ascaris suum* it reacts with malic enzyme generating NADH as reducing power. The malate also reacts with fumarase, producing fumarate, which is reduced to succinate utilizing the NADH formed by the malic enzyme. ATP is generated through this reduction. Therefore, there is a competition between fumarase and malic enzyme for malate. A regulation should exist to balance the production of NADH by malic enzyme and consumption of it by fumarase.

Landsperger and Harris [37] reported that the malate saturation curve exhibits sigmoidicity which increases with increasing pH. They also reported that the fumarate is an activator of the malic enzyme, whereas the end product branched chain fatty acids, tiglate, 2-methylbutanoate and 2-methylpentanoate are inhibitors. These end products act by depleting Mg^{2+} required for the activity of the enzyme. Oxalate was reported to be the most potent inhibitor of the NAD-ME (K_{is}=0.16 mM) [46]. It is a structural analogue of the enolpyruvate. There is a competitive inhibition above pH 7 and noncompetitive inhibition below pH 7.

It was suggested that when fumarate production is increased, the fumarate activated the enzyme by increasing the affinity of the enzyme for malate. Low

concentration of fumarate was enough to stimulate the malic enzyme (K_{act}= 0.5 mM). Both fumarate activation and end product inhibition were competitive with malate. ATP and several other nucleotides did not inhibit *Ascaris suum* malic enzyme. Lai *et al*. [24] confirmed that the activation of malic enzyme by fumarate operates by reducing the K_m for malate resulting from a decrease in the off-rate for malate from E:Mg:malate and E:NAD:Mg:malate complexes. It was also reported that besides being a positive heterotropic effector at low concentrations, fumarate is also an inhibitor against malate at higher concentrations (K_i around 25 mM). They also suggested that there are two sites for fumarate to bind to exert its activation and inhibition effects. Mallick *et al*. [48] showed that L-malate is also an activator of the enzyme in reductive carboxylation direction (K_{act}=50 µM). Following that study, with the help of the crystal structure, fluorescence and kinetic studies, it was shown that the malate and fumarate bind to different activator binding sites. However, they also observed a synergistic binding of fumarate and malate, indicating the two binding sites must be interacting [57].

The human ME is inhibited by ATP [58]. There are two NAD-binding sites, one at the active site and one (exo site) at the tetramer interface. Inhibition of the enzyme with ATP is the result of competition between NAD and ATP for the active site. The inhibition constant is reported to be 81 µM. *A. suum* is not inhibited by the physiological concentrations of ATP and several other nucleotides.

The level of expression of malic enzyme in rat liver is regulated by thyroid hormone in a tissue specific manner [58,59]. Hormonal stimulation affects the synthesis rate of ME mRNA. In responsive tissues, like heart, kidney and liver, ME activity was modulated by thyroid hormone at pretranslational level [60]. In a study by Goldman *et al*.

[61], when the starved ducks were fed with a carbohydrate rich diet, there was a 20-fold increase in NADP-ME mRNA resulted both by increased transcription and decreased degradation.

1.10. Scope of this study

The kinetic and chemical mechanism of *Ascaris suum* NAD-malic enzyme have been proposed by our group. However, the functional roles of key residues lining the dinucleotide binding site were still unclear. The purpose of this study is to investigate the functions of these residues and have a better understanding of the role of the dinucleotide substrate in oxidative decarboxylation. For this purpose, site directed mutagenesis, initial velocity and isotope effect studies have been carried out.

The content of this research can be divided mainly into three:

1) Roles of residues interacting with the nicotinamide ring (N479) and nicotinamide ribose (S433 and N434):
   a) Hydrogen bond donated by N479 to the carboxamide side chain of the nicotinamide ring is crucial for proper orientation in the hydride transfer step.
   b) S433 provides significant binding affinity for NAD.
   c) The effect of N434 is more pronounced in both positioning of malate and NAD.
2) Role of residues lining the adenosine binding site of NAD (D361 and R370), and potential cofactor specificity determinant (H377):
   a) The ionic interaction between D361 and R370 is very important for the binding of the adenosine portion of the cofactor. Mutations to these residues can lead to nonproductive binding of the dinucleotide.

b) H377 is not a cofactor specificity determining residue in *Ascaris suum* malic enzyme.

3) Review on general acid/base mechanism of metal ion dependent pyridine nucleotide linked β-hydroxyacid decarboxylases.

Overall, data suggested that the binding and orientation of the cofactor is strictly controlled by the residues lining the dinucleotide binding site. Correct positioning of the cofactor is a key to the efficient catalysis of the *Ascaris suum* malic enzyme.

-Chapter 2 and Chapter 3 in this dissertation have been published in *Biochemistry, 47* (8), 2539-2546, 2008 and *Biochimica et Biophysica Acta, 1784*, 2059-2064, 2008, respectively.

CHAPTER 2:

2.1. Introduction

Malic enzyme is a pyridine nucleotide-linked β-hydroxyacid oxidative decarboxylase, which catalyzes the divalent metal ion (Mg^{2+} or Mn^{2+}) dependent conversion of L-malate to pyruvate and CO_2 , with concomitant reduction of $NAD(P)^+$ to NAD(P)H [1,6,42].

The malic enzyme was first found in pigeon liver and was a cytosolic enzyme that required NADP as an oxidant [6]. The *Ascaris suum* mitochondrial NAD-malic enzyme (E.C. 1.1.1.38) was isolated from the anaerobic parasitic nematode in 1956 [21]. Malic enzyme plays an important role in the energy metabolism of the nematode. L-Malate is the product of anaerobic glycolysis and malic enzyme, in the mitochondrion, is responsible for producing NADH, which is the main source of ATP synthesis via site I oxidative phosphorylation [22,62,63].

On the basis of initial velocity, product inhibition, isotope partitioning and deuterium isotope effect studies [45,46,64], a steady-state random kinetic mechanism was proposed for the *A. suum* malic enzyme, with the requirement that Mg^{+2} adds prior to malate. A general acid/base mechanism was proposed on the basis of the pH dependence of kinetic parameters and isotope effects [43,46]. Recently, according to Karsten *et al*. [56], a catalytic triad, involving residues K199, Y126 and D294, was shown to be responsible for the acid-base chemistry in the *Ascaris* enzyme, Figure 2.1.

The catalytic pathway, comprising a conformational change, followed by hyride transfer and decarboxylation, contributes to rate limitation of the overall reaction. In

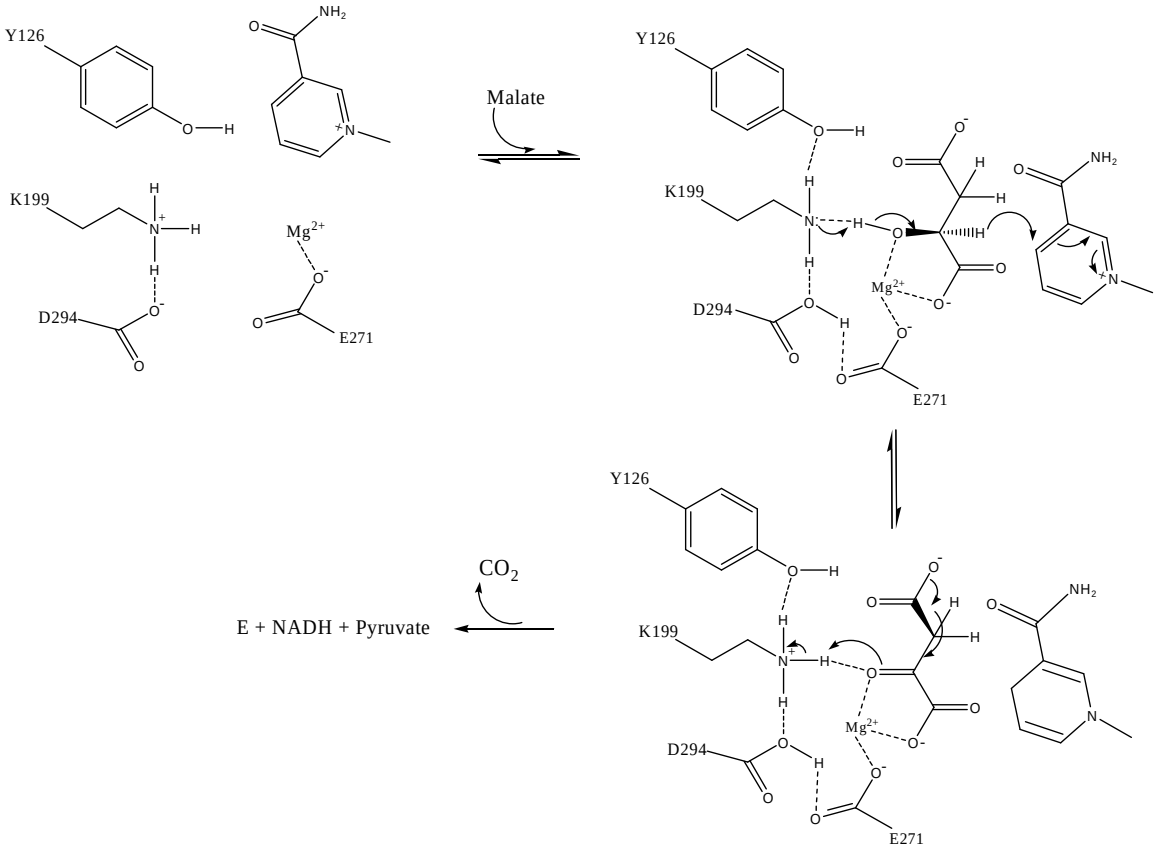

Figure 2.1 Proposed General Acid/Base Chemical Mechanism for *Ascaris suum* Malic Enzyme.

addition, malate is sticky and has an off-rate constant from the central E-NAD-Mg-malate complex equal to the net rate constant for catalysis [46,64], while at saturating concentrations of reactants an isomerization of E-NAD also contributes to rate limitation [50].

The aim of this study was to determine the possible functional roles of several residues in the dinucleotide binding site. Site-directed mutagenesis has been used as a probe of the NAD and NADH binding sites. Residues N479, S433 and N434 were mutated to a number of different amino acids to alter the side chain functionality. The mutant enzymes were characterized by initial rate, inhibition and isotope effect studies. The contribution to binding energy and catalysis of the groups that interact with NAD and NADH have been investigated and the implications to the catalytic mechanism are discussed.

2.2. Materials and Methods

2.2.1. Chemicals and Enzymes.

Malate, NAD and NADH were obtained from USB. Hepes and Ches buffers were from Research Organics, while Pipes buffer and fumarate were purchased from Sigma. Magnesium sulfate and manganese sulfate were obtained from Fisher Scientific. Sodium borodeuteride (98 atom %) was from Aldrich and IPTG was from GoldBio Tech. The QuikChange site-directed mutagenesis kit was from Stratagene. The recombinant *A. suum* malic enzyme used in these studies has a 6-histidine N-terminal tag, and both the wild type and mutant enzymes were prepared and purified as described previously [28]. Protein concentrations were obtained using the method of Bradford [65]. All other

chemicals and reagents used were obtained commercially and were of the highest purity available.

2.2.2. Malate-2-d.

Malate-2-d was synthesized by the reduction of oxaloacetate with sodium borodeuteride [39]. A solution of 40 mM oxaloacetate was prepared and its pH was adjusted to 7 with KOH. 40 mM sodium borodeuteride was added to this solution and allowed to incubate at room temperature for 1 hour and the pH was then adjusted to 5 with acetic acid. Pipes buffer and NAD were added to final concentrations of 25 mM and 0.2 mM, respectively, and the pH was adjusted to 7 with KOH. KCl (30 mM), $MnSO_4$ (1 mM), TDH (170 units) and LDH (50 units) were added and the solution was allowed to incubate at room temperature for 48 hours to remove D-malate-2-d. The amount of the remaining D-malate-2-d in the solution was determined by end-point assay using tartrate dehydrogenase. The end-point assay contained 100 mM Ches, pH 8.5, 1 mM $MnSO_4$, 1 mM NAD, 30 mM KCl, ~1 unit TDH and 5 µL of the synthesis solution. More than 95% of the D-malate-2-d was removed. The pH of the resulting solution was adjusted to 5 with perchloric acid and activated charcoal was added to remove the dinucleotides. After filtration and concentration via rotary evaporation, L-malate-2-d was purified by Dowex AG-1-X8 column chromatography. The L-malate-2-d concentration was determined by end-point assay containing 1.5 units of wild type *A. suum* malic enzyme, 100 mM Ches, pH 8.5, 1 mM $MnSO_4$, 1 mM NAD, 2 mM fumarate and ~0.1 mM L-malate-2-d.

2.2.3. Enzyme assays.

Enzyme assays were carried out at 25°C in 1 cm cuvettes using a Beckman DU640 UV-visible spectrophotometer. In the direction of oxidative decarboxylation of malate, malic enzyme activity was measured at varying concentrations of L-malate, divalent metal ion, and NAD as indicated in the text. The non-varied substrate was maintained at a concentration at least 10 times its K_m value, and reaction mixtures were maintained at pH 7 with 100 mM Hepes buffer. The reaction was followed at 340 nm to monitor the production of NADH (ε_{340}, 6220 $M^{-1}cm^{-1}$). Malic enzyme uses the uncomplexed form of the divalent metal ion and substrates, and corrections for chelate complexes were made using the following dissociation constants: Mg-malate, 25.1 mM; Mn-malate 5.4 mM; Mg-NAD 19.6 mM; Mn-NAD and Mn-NADH 12.6 mM [45]. All substrate concentrations reported in the text refer to the uncomplexed concentrations of substrates, and divalent metal ion.

The primary kinetic deuterium isotope effects were determined by direct comparison of initial velocities using 100 mM Hepes, pH 7, saturating concentrations of NAD and metal ion, and varied concentrations of L-malate-2-h(d). The inhibition constant for NADH was obtained by measuring the initial rate as a function of NAD with metal ion and malate fixed at their respective K_m values and at different concentrations of NADH, including zero.

2.2.4. ^{13}C kinetic isotope effects.

The ^{13}C isotope effects on the malic enzyme reaction were determined using the natural abundance of ^{13}C in the substrate as the label [66]. Both high-conversion (100%) and low-conversion (15%) samples were measured. The low conversion reactions

contained 25 mM Hepes, pH 7, 12 mM L-malate-2-h(d), 30 mM $MgSO_4$, and 10 mM NAD, in a total volume of 33 mL. The high-conversion sample contained the same components, with the exception that the concentration of L-malate-2-h(d) was 2 mM. The reaction mixtures were adjusted to pH ~6 and sparged with CO_2 free nitrogen for at least 3 hours. The pH was then adjusted to 8.2 with KOH and the mixture was sparged for an additional 2 hours. The high-conversion reaction was initiated by the addition of 0.6 mg of wild type malic enzyme and the reaction was allowed to incubate overnight. The completeness of the reaction was determined by taking an aliquot of the sample mixture and determining the absorbance at 340 nm. The low-conversion reaction was initiated by the addition of one of the mutant enzymes. The progress of the reaction was checked by measuring the absorbance of the aliquots at 340 nm. All the reactions were quenched by the addition of 100 µL of concentrated sulfuric acid prior to CO_2 isolation. The $^{12}C/^{13}C$ ratio of the isolated CO_2 was determined using an isotope ratio mass spectrometer (Finnigan Delta E). All ratios were corrected for ^{17}O according to Craig [67].

2.2.5. Data analysis.

Initial velocity data were fitted with BASIC versions of the FORTRAN programs developed by Cleland [68]**.** Saturation curves for malate, NAD and the metal ion were fitted using equation 1. Data conforming to an equilibrium ordered or sequential kinetic mechanism were fitted using equations 2 and 3, while data for competitive inhibition were fitted to equation 4.

$$v = \frac{V\mathbf{A}}{K_a + \mathbf{A}} \tag{1}$$

$$v = \frac{V\mathbf{AB}}{K_{ia}K_b + K_b\mathbf{A} + \mathbf{AB}} \tag{2}$$

$$v = \frac{V\mathbf{AB}}{K_{ia}K_b + K_a\mathbf{B} + K_b\mathbf{A} + \mathbf{AB}} \tag{3}$$

$$v = \frac{V\mathbf{A}}{K_a\left(1 + \frac{I}{K_{is}}\right) + \mathbf{A}} \tag{4}$$

In equations 1-4, v represents the initial velocity, V is the maximum velocity, **A** and **B** are reactant concentrations, K_a and K_b are the Michaelis constants for **A** and **B**, I is the inhibitor concentration, K_{ia} is the inhibition constant for **A**, K_{is} is the slope inhibition constant.

Data for primary kinetic deuterium isotope effects were fitted using equation 5, where F_i is the fraction of deuterium in the labeled compound, and $E_{V/K}$ and E_V are the isotope effects minus 1 on V/K and V, respectively.

$$v = \frac{V\mathbf{A}}{K_a(1 + F_i E_{V/K}) + \mathbf{A}(1 + F_i E_V)} \tag{5}$$

^{13}C isotope effects were calculated using equation 6, where f is the fraction of completion of reaction, and R_f and R_o are the $^{12}C/^{13}C$ isotopic ratios of CO_2 at low and high conversion representing the ratio in the substrate, respectively. Isotope ratios are measured as $\delta^{13}C$, equation 7, where R_{smp} and R_{std} are $^{12}C/^{13}C$ isotopic ratios for sample and standard, respectively. The standard for CO_2 was Pee Dee Belemnite [67] with $^{12}C/^{13}C$ of 0.0112372.

$$^{13}\left(\frac{V}{K}\right) = \frac{\log(1-f)}{\log\left(1-f\left[\frac{R_f}{R_0}\right]\right)} \qquad (6)$$

$$\delta^{13}C = (R_{smp} / R_{std} - 1) \times 1000 \qquad (7)$$

2.2.6. Calculation of intrinsic isotope effects and commitment factors.

Estimates of intrinsic isotope effects and commitment factors were obtained according to Karsten and Cook [25,39] using an iterative method to search for the best fit. Wild type *A. suum* malic enzyme has a stepwise mechanism [25,53] with the requirement that the metal ion must bind to the enzyme prior to malate [45,48,64]. The kinetic mechanism may be described as below, where M is Mg^{2+}, A is oxidized dinucleotide, B is L-malate, X is enzyme-bound oxaloacetate intermediate and R is reduced dinucleotide.

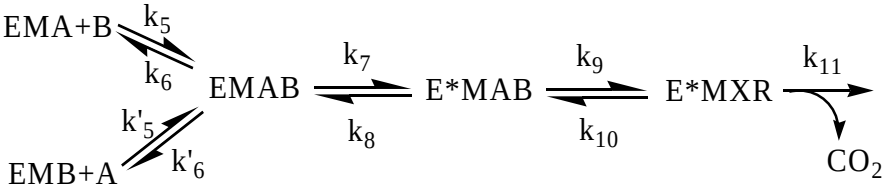

(8)

Since this is a random kinetic mechanism, the rate constants k_5 and k_6 are for the malate-binding and release at saturating concentrations ($10K_m$) of NAD and Mg^{2+}, and the rate constants k'_5 and k'_6 are for the dinucleotide-binding and release at saturating malate and Mg^{2+}. The rate constants k_7 and k_8 represent any precatalytic conformational change leading to a Michaelis complex while k_9 and k_{10} are for hydride transfer and k_{11} represents decarboxylation. There is likely no binding site for CO_2, and thus the release of CO_2 is likely very fast [48,64] and the decarboxylation step is practically irreversible. On the basis of this mechanism, the equations for the isotope effects are as follows:

$$^{D}\left(\frac{V}{K_{malate}}\right)=\frac{^{D}k_9+c_f+^{D}K_{eq}(c_r)}{1+c_f+c_r} \tag{9}$$

$$^{13}\left(\frac{V}{K_{malate}}\right)_{H}=\frac{^{13}k_{11}+\left(\frac{1+c_f}{c_r}\right)}{1+\left(\frac{1+c_f}{c_r}\right)} \tag{10}$$

$$^{13}\left(\frac{V}{K_{malate}}\right)_{D}=\frac{^{13}k_{11}+\left(\frac{1+c_f/^{D}k_9}{^{D}K_{eq}(c_r)/^{D}k_9}\right)}{1+\left(\frac{1+c_f/^{D}k_9}{^{D}K_{eq}(c_r)/^{D}k_9}\right)}=\frac{^{13}k_{11}+\left(\frac{^{D}k_9+c_f}{^{D}K_{eq}(c_r)}\right)}{1+\left(\frac{^{D}k_9+c_f}{^{D}K_{eq}(c_r)}\right)} \tag{11}$$

The commitment factors are relative to the hydride transfer step, where c_f is the forward commitment to catalysis, $(k_9/k_8)(1 + k_7/k_6)$, and c_r is the reverse commitment to catalysis (k_{10}/k_{11}). The intrinsic primary kinetic deuterium isotope effect is $^{D}k_9$, while

$^{l3}k_{11}$ is the intrinsic primary kinetic ^{13}C isotope effect. $^{D}K_{eq}$,$^{D}k_9/^{D}k_{10}$, is the deuterium isotope effect on the equilibrium constant which was determined by Cook *et al*. as 1.18 [69].

Assuming a concerted mechanism, the intrinsic isotope effects and forward commitment factor were calculated according to Weiss *et al*. [53]. The kinetic mechanism is illustrated in equation 12 where M, A and B are as defined in equation 8.

$$\mathrm{EMA} + \mathrm{B} \underset{k_6}{\overset{k_5}{\rightleftharpoons}} \mathrm{EMAB} \underset{k_8}{\overset{k_7}{\rightleftharpoons}} \mathrm{E^*MAB} \xrightarrow{k_9} \mathrm{CO_2} \tag{12}$$

The rate constants k_5, k_6, k_7 and k_8 are as defined for equation 8. The rate constant k_9 is for the concerted oxidative decarboxylation step. For this mechanism, the equations for the isotope effects are as follows:

$$^{D}\left(\frac{V}{K_{malate}}\right) = \frac{^{D}k_9 + c_f}{1 + c_f} \tag{13}$$

$$^{13}\left(\frac{V}{K_{malate}}\right)_{H} = \frac{^{13}k_9 + c_f}{1 + c_f} \tag{14}$$

$$^{13}\left(\frac{V}{K_{malate}}\right)_{D} = \frac{^{13}k_9 + \frac{c_f}{^{D}k_9}}{1 + \frac{c_f}{^{D}k_9}} \tag{15}$$

The c_f term is as for equation 8, while c_r is zero for this mechanism and does not appear in the equations. All other terms are as defined for equation 8.

2.3. Results.

2.3.1. Initial velocity studies.

In order to characterize the mutant enzymes, initial rate studies were carried out. Initial velocity patterns were obtained by measuring the initial rate as a function of NAD at different concentrations of malate, and with metal ion maintained at saturation ($10K_m$). Kinetic parameters are summarized in Table 2.1 and Table 2.2.

Asparagine-479, which interacts with the carboxamide side chain of NAD, Figure 2.2, was mutated to glutamine, serine and methionine (the kinetic parameters for the N479M mutant enzyme could not be determined because of its estimated 10^5-fold decreased activity). A 2-fold increase in K_{malate} was observed for the Q and S mutant enzymes, Table 2.1. The N479Q mutant enzyme exhibited no significant change in K_{NAD}, while the N479S mutant gave only a 2-fold increase. However, both mutant enzymes had significantly reduced values of $V/\mathbf{E_t}$ ($>10^3$-fold). Inhibition constants for NADH, as a competitive inhibitor vs NAD, were 15 μM and 17 μM, respectively, for the N479Q and N479S mutant enzymes compared to a value of 19 μM for the wild type enzyme. Mutations of N479 thus affect the catalytic pathway, which includes the conformational change to close the site in preparation for catalysis, hydride transfer and decarboxylation.

Serine-433 and asparagine-434 interact with the nicotinamide ribose of NAD, Figure 2.2. In addition, N434 interacts with β-carboxylate of malate. Table 2.2 lists the kinetic parameters for the S433 and N434 mutant enzymes.

Table 2.1 Kinetic parameters for the N479 mutant enzymes

Parameter	Wild Type	N479Q	N479S
K_{malate} (mM)	0.8 ± 0.1	1.8 ± 0.2	1.7 ± 0.3
Fold increase		2.2 ± 0.4	2.1 ± 0.5
K_{NAD} (mM)	0.032 ± 0.004	0.034 ± 0.005	0.057 ± 0.009
Fold increase		1.1 ± 0.2	1.8 ± 0.3
$V/\mathbf{E_t}$ (s^{-1})	31 ± 1	(20 ± 1) x 10^{-3}	(15 ± 1) x 10^{-3}
Fold decrease		1,500 ± 100	2,000 ± 150
$V/(K_{malate}.\mathbf{E_t})$ ($M^{-1}s^{-1}$)	(3.8 ± 0.5) x10^4	11 ± 1	8.8 ± 0.2
Fold decrease		3,500 ± 500	4,300 ± 500
$V/(K_{NAD}.\mathbf{E_t})$ ($M^{-1}s^{-1}$)	(1.0 ± 0.2) x 10^6	600 ± 80	260 ± 60
Fold decrease		1,700 ± 400	3,800 ± 1,000

Table 2.2 Kinetic parameters for S433 and N434 mutant enzymes

Parameter	Wild Type	S433A	N434Q	N434M	N434A
K_{malate} (mM)	0.8 ± 0.1 [0.24 ± 0.08][a]	1.3 ± 0.3	4.3 ± 0.5	2.2 ± 0.7	[0.50 ±0.03]
Fold increase		1.6 ± 0.5	5 ± 1	3 ± 1	2 ± 0.7
K_{NAD} (mM)	0.032 ± 0.004 [0.07 ± 0.01]	2.6 ± 0.3	0.08 ± 0.02	0.23 ± 0.06	[0.050 ± 0.008]
Fold increase		80 ± 15	2.5 ± 0.7	7 ± 2	1.4 ± 0.3[b]
$V/\mathbf{E_t}$ (s^{-1})	31 ± 1 [45 ± 4]	5.3 ± 0.2	(2.2 ± 0.2) x10^{-3}	(2.8 ± 0.2) x10^{-3}	[(1.30 ± 0.05) x10^{-2}]
Fold decrease		6 ± 0.3	14,000 ± 1,500	10,000 ± 1,000	3,500 ± 350
$V/(K_{malate}.\mathbf{E_t})$ ($M^{-1}s^{-1}$)	(3.8 ± 0.5) x10^4 [(1.9 ± 0.6) x10^5]	(4.0 ± 0.3) x10^3	0.51 ± 0.04	0.64 ± 0.04	[3.0 ± 0.1]
Fold decrease		10 ± 1	75,000 ± 11,000	30,000 ± 9,000	63,000 ± 20,000
$V/(K_{NAD}.\mathbf{E_t})$ ($M^{-1}s^{-1}$)	(1.0 ± 0.2) x10^6 [(6.5 ± 1.0) x10^5]	(2.0 ± 0.2) x10^3	28.0 ± 0.3	6.1 ± 0.3	[260 ± 60]
Fold decrease		500 ± 100	35,000 ± 7,000	75,000 ± 30,000	2500 ± 700

[a]Values in brackets are kinetic parameters with Mn^{2+}.
[b]Fold decrease.

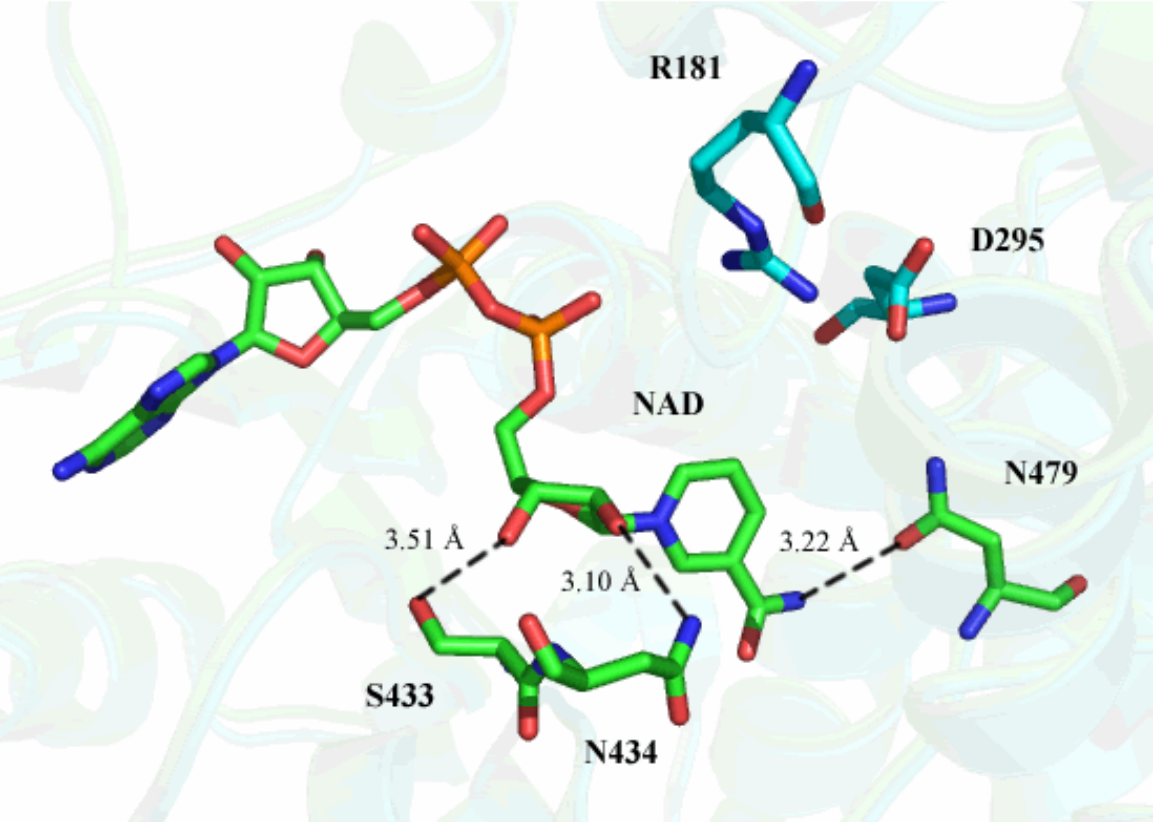

Figure 2.2 Close-up of the binding site for NAD (PDB code 1llq) in the *Ascaris* malic enzyme and the residues with the hydrogen bonding distances. This figure was generated using the PyMOL molecular visualization program (website: http://pymol.sourceforge.net/).

All of the mutant enzymes, with the exception of S433C, exhibited modest changes in K_{malate}. The S433C mutant enzyme exhibited apparent 9- and 500-fold increases in K_{malate} and K_{NAD}, respectively. (Since the enzyme could not be saturated with NAD, kinetic parameters were not determined). The S433A mutant enzyme showed an 80-fold increase in K_{NAD}. The N434Q and M mutant enzymes exhibited modest changes in K_{NAD}, while the N434A mutant enzyme showed a slight decrease in K_{NAD}. Replacing the β-hydroxyl of serine with a β-thiol as in cysteine, gave an enzyme with a very high apparent K_{NAD} (16 mM), which made it impossible to determine $V/\mathbf{E_t}$ and $V/K_{malate}\mathbf{E_t}$, but $V/K_{NAD}\mathbf{E_t}$ decreased significantly ($3x10^5$-fold), likely as a result of the bulky sulfur causing crowding. In agreement, $V/\mathbf{E_t}$ and $V/K_{malate}\mathbf{E_t}$ decreased only 6-fold and 10-fold, respectively, for the S433A mutant enzyme when the β-hydroxyl group was replaced by a hydrogen compared to wild type enzyme. More pronounced effects were observed for the N434 mutant enzymes which gave more than a 10^3-fold decrease in $V/\mathbf{E_t}$, $V/K_{malate}\mathbf{E_t}$ and $V/K_{NAD}\mathbf{E_t}$. The inhibition constant for NADH for the S433 and N434 mutant enzymes could not be accurately determined, but was greater than 0.3 mM in all cases.

2.3.2. Isotope effect studies.

Kinetic deuterium isotope effects, ${}^{D}V$ and ${}^{D}(V/K_{malate})$, were determined by direct comparison of initial velocities for the wild type and mutant malic enzymes at saturating concentrations ($10K_m$) of metal ion and NAD, varying L-malate-2-(h,d). ${}^{13}(V/K)_H$ and ${}^{13}(V/K)_D$ were also determined as described in the Material and Methods section. The values of ${}^{D}V$ and ${}^{D}(V/K_{malate})$ are the mean averages of at least six separate determinations and the effects are equal to one another for all mutant enzymes (with the possible exception of S433A) within error. All results are listed in Table 2.3.

Table 2.3 Primary Deuterium and ^{13}C Kinetic Isotope Effects for The Wild Type and Mutant Malic Enzymes

	^{D}V	$^{D}(V/K_{malate})$	$^{13}(V/K)_{H}$	$^{13}(V/K)_{D}$
Wild Type	2.0 ± 0.2 (2.1 ± 0.2)[c]	1.6 ± 0.3 (1.8 ± 0.1)	1.0342 ± 0.0002[a] (1.0353 ± 0.0005)	1.0252 ± 0.0001[ab] (1.02348 ± 0.00008)
N479Q	1.8 ± 0.1	2.1 ± 0.2	1.0235 ± 0.0015	1.0250 ± 0.0007[d]
N479S	1.8 ± 0.1	1.5 ± 0.3	1.0313 ± 0.0032	1.0242 ± 0.0003[b]
S433A	2.8 ± 0.8	2.1 ± 0.2	1.0300 ± 0.0032	1.0166 ± 0.0001[b]
S433C	ND[e]	1.8 ± 0.1	1.0200 ± 0.0001	1.0129 ± 0.0015[b]
N434A	(1.9 ± 0.1)	(1.77 ± 0.15)[f]	(1.0447 ± 0.0006)	(1.030 ± 0.001)
N434M	1.03 ± 0.16	1.08 ± 0.74	ND	ND

[a]Values from Weiss *et al.* [53].

[b]Stepwise mechanism applying $\frac{^{13}(V/K)-1}{^{13}(V/K)-1} = \frac{^{D}(V/K)}{^{D}K_{eq}}$

[c]Values in paranthesis are isotope effects with Mn^{2+}.

[d]Concerted mechanism

[e]ND is for Not Determined (K_{NAD}= 16 mM).

[f]Calculated value using the equation in footnote b.

No significant change in ^{D}V or $^{D}(V/K_{malate})$ compared to wt was observed for the N479Q and S and the N434A mutant enzymes. ^{D}V and $^{D}(V/K)$ may have increased slightly for S433A, while both values were unity, within error, for N434M.

Primary ^{13}C kinetic isotope effects decreased for all mutant enzymes compared to the wild type enzyme, with the exception of N434A. $^{13}(V/K)_{D}$ values were smaller than the $^{13}(V/K)_{H}$ values, indicating that the mechanism is stepwise for all mutant enzymes, with the exception of N479Q mutant enzyme (see footnote d in Table 2.3). In the case of N479Q, $^{13}(V/K)_{H} = {}^{13}(V/K)_{D}$ indicates a concerted mechanism.

2.4. Discussion.

The purpose of this study was to investigate the function of the residues that interact with the nicotinamide and ribose rings of the dinucleotide substrate. Site-directed mutagenesis, initial rate kinetics and isotope effects were used to probe the contribution of these groups to binding energy and catalysis.

2.4.1. Kinetic parameters of N479Q, S mutant enzymes.

The mutant enzymes show a 2-fold increase in K_{malate}, which is indicative of a decrease in affinity. The K_m is equal to K_d for the malic enzyme, given the equality of ^{D}V and $^{D}(V/K_{malate})$ [70]. A maximum 2-fold change in K_{NAD} is observed, even though N479 interacts with NAD, suggesting it provides only modest affinity for the cofactor, while K_{iNADH} does not change. Conformational changes are induced upon binding of NAD and malate [50], so it is not surprising that the affinity for both NAD and malate are affected, although only slightly. The main effect of the mutation, however, is a $>10^3$-fold decrease in $V/\mathbf{E_t}$ and $V/K\mathbf{E_t}$ for both substrates. The likely reason for this is a change in the

orientation of the nicotinamide ring relative to C2 of malate as a result of hydrogen-bonding to the longer side chain of Q compared to N in the case of N479Q and the lack of the hydrogen bond for N479S. This will be discussed further below.

2.4.2. Isotope effects.

Data for the wild type malic enzyme indicate a stepwise mechanism with hydride transfer preceding decarboxylation [50]. ^{D}V and $^{D}(V/K_{malate})$ values measured for the N479 mutant enzymes are similar to those of the wild type enzyme, Table 2.3. Although $V/\mathbf{E_t}$ has decreased by $>10^3$-fold it appears at face value that the contribution of the hydride transfer to rate limitation is similar to the wild type enzyme. In the case of a stepwise mechanism, the ^{13}C isotope effect measured with L-malate-*2-d* will be lower than that observed with L-malate, as found for the wild type enzyme [51]. For the N479Q mutant enzyme, $^{13}(V/K)_H$ and $^{13}(V/K)_D$ are equal within error, which indicates the mechanism has become concerted, with hydride transfer and decarboxylation taking place in the same step, and that the step is completely rate-limiting for the reaction. Converting asparagine to glutamine conserves the functional group but the glutamine side chain is a methylene longer than that of asparagine. When the asparagine to glutamine mutation is modeled using PyMOL molecular visualization software, it is observed that the glutamine side chain clashes with both NAD and malate. In order to accommodate the longer side chain of glutamine, which comes into close proximity of the nicotinamide ring and malate, the position of malate and/or the nicotinamide ring relative to one another would be expected to change. In this case, malate may already be in the proper conformation for decarboxylation to occur as it is oxidized to oxaloacetate, generating

more favorable molecular orbital overlap as the π bond is formed at C2-C3. That is, the oxaloacetate intermediate may either not exist or have a very short life time.

The change from stepwise to concerted oxidative decarboxylation is not unprecedented for the NAD-malic enzyme reaction. Multiple isotope effect studies with a variety of alternative dinucleotide substrates were measured for the malic enzyme [25,53]. When NAD and NADP were used as substrates the mechanism was stepwise, with oxidation preceding decarboxylation. The mechanism changed to concerted with the more oxidizing 3-APAD(P), 3-PAAD and thio-NAD(P). For the stepwise mechanism, malate binds such that its C4 carboxylate is in the C2-C3 plane, which does not favor decarboxylation, and it is slow as suggested by the ^{13}C isotope effect of 1.034 measured for the wt enzyme [53]. With the alternative, more oxidizing dinucleotide substrates, the hydride transfer step contributes more to rate limitation, resulting in a very short life-time (no potential energy well) for the oxaloacetate intermediate. The result is an asynchronous concerted reaction with cleavage of the C3-C4 bond lagging behind C-H bond cleavage [54]. In the case of the N479Q mutant enzyme, either an asynchronous oxidative decarboxylation takes place as observed for the wt enzyme with more oxidizing dinucleotide substrates or malate is bound with its β-carboxyl group already out of the C1-C2-C3 plane and trans to the hydride to be transferred to C4 of the nicotinamide ring of the dinucleotide, i.e., a true concerted reaction. Given the intrusion of the glutamine side chain into the malate and NAD sites, it is likely that a change in conformation of the bound malate has occurred for the N479Q mutant enzyme, placing the β-carboxyl in a better position for decarboxylation as C2 is oxidized.

A quantitative analysis, on the basis of theory presented in the Materials and Methods section, was used to generate estimates of forward and reverse commitment factors, intrinsic deuterium and ^{13}C isotope effects, Table 2.4. For the wild type malic enzyme, the forward and reverse commitment factors are high, suggesting a significant contribution of the precatalytic conformational change to rate limitation and a partitioning of the oxaloacetate intermediate in favor of malate. For the N479Q mutant enzyme, the mechanism is concerted, and the equality of $^{13}(V/K)_H$ and $^{13}(V/K)_D$ indicates oxidative decarboxylation is completely rate limiting. The estimated intrinsic deuterium isotope effect is smaller than that observed for the wild type enzyme, as is the intrinsic ^{13}C isotope effect. The ^{13}C kinetic isotope effect of 1.025 compared to the value of 1.05 for the intrinsic ^{13}C isotope effect for decarboxylation of the oxaloacetate intermediate suggests a transition state with about 50% C2-H and C3-C4 bond cleavage if the mechanism is truly concerted.

If the above interpretation concerning the N479Q mutant enzyme is correct, the smaller serine side chain would be expected to behave differently. For the N479S mutant enzyme, the primary deuterium and ^{13}C isotope effects are very similar to those of the wt enzyme. Deuteration of malate causes the ^{13}C isotope effect to decrease, indicating a stepwise mechanism for the N479S mutant enzyme and the data adhere to the equality for a stepwise mechanism, with oxidation preceding decarboxylation. However, there is still a $>10^3$-fold decrease in $V/\mathbf{E_t}$, suggesting the nicotinamide ring must be bound differently.

When the asparagine to serine mutation is modeled using PyMOL molecular visualization software, it is observed that the hydrogen-bonding interaction between this residue and the nicotinamide ring of NAD is lost, since the serine functional group is

Table 2.4 Commitment factors and intrinsic isotope effects.

	c_f	c_r	${}^{D}k_9$	${}^{13}k$
Wild type	7[a] (1)[bc]	14[a] (2.2)[bc]	11[a] (4)[bc]	1.052[a] (1.069)[bc]
N479Q	NA[d]	NA[d]	2.2	1.026
N479S	8.2	15	11	1.050
S433A	3	5	10	1.050
S433C	8	6	11	1.050
N434A	(1)[c]	(3)[c]	(4)[c]	(1.07)[c]

[ab] Values from Karsten *et al.* [25].
[c] Values in parentheses are with Mn^{2+}.
[d] NA is not applicable

shorter than that of asparagine. None of the possible orientations of NAD or serine residue could generate a reasonable hydrogen-bonding distance. This situation likely results in an increased freedom of rotation of the nicotinamide ring, giving nonproductively bound cofactor, with a small fraction (~0.05% on the basis of $V/\mathbf{E_t}$) of the dinucleotide productively bound. In agreement with this suggestion, the relative rates of steps within the catalytic pathway (precatalytic conformational change, hydride transfer and decarboxylation), relative to one another, are similar to the wild type enzyme. (This is also supported by the estimates of the commitment factors and intrinsic isotope effects, which are very similar to those of wild type).

2.4.3. Kinetic parameters for S433 and N434 mutant enzymes.

In order to obtain information on the interactions with the nicotinamide ribose, S433 was mutated to A and C, while N434 was mutated to Q, A and M. Both residues hydrogen bond to the nicotinamide ribose, Figure 2.2. N434 also interacts with β-carboxylate of malate.

All of the mutant enzymes exhibit a slight increase in K_{malate}, which indicates a decrease in affinity, considering the very similar values of ${}^{D}V$ and ${}^{D}(V/K_{malate})$ [70]. (${}^{D}V$ could not be determined for the S433C mutant enzyme, but it likely behaves as the others). The S433A mutant enzyme exhibits an 80-fold increase in K_{NAD}. Since the only difference between S and A is the loss of the hydrogen bond donor, data suggest S433 provides significant binding affinity for NAD. Using a value of 80 for the fold change, $\Delta\Delta G^{\circ\prime}$ is 2.6 kcal/mol ($\Delta\Delta G^{\circ\prime} = RT \ln((K_{NAD})_{S433A}/(K_{NAD})_{wt})$). For the S433C mutant enzyme, replacement of the β-hydroxyl of S433 with the larger thiol gives a 500-fold increase in the apparent K_{NAD}, about 6-fold higher than that observed with the S to A

mutation. The large increase in K_{NAD} likely results from crowding by the larger thiol, which changes the position of the bound NAD ribose, translating into a change in position of the nicotinamide ring. The inhibition constant for NADH for the S433 and N434 mutant enzymes could not be accurately determined, but was greater than 0.3 mM in all cases. $V/\mathbf{E_t}$ and $V/K\mathbf{E_t}$ could not be determined for the S433C mutant enzyme because of the high value of K_{NAD}. However, the apparent $V/K_{NAD}\mathbf{E_t}$ decreased 300,000-fold compared to wild type and this likely includes a decrease in $V/\mathbf{E_t}$ and an increase in K_{NAD}.

When mutations at N434 are modeled using PyMOL software, the longer glutamine and methionine side chains stick into the active site, in close proximity to the bound malate, which likely results in reorientation of NAD and malate. However, changes in the K_m for malate and NAD were moderate for the N434 mutant enzymes, suggesting that the affinity for reactants was not altered. Nonetheless, $V/\mathbf{E_t}$ decreased on the order of 10^3-10^4 with the smallest change observed for N434A.

2.4.4. Isotope effects.

In the case of the S433A mutant enzyme, the loss of a hydrogen-bonding interaction results in a large decrease in $V/\mathbf{E_t}$, suggesting a change in the orientation of the nicotinamide ring relative to C2 of malate. A slight increase in ^{D}V and $^{D}(V/K)$, coupled to a slight decrease in the ^{13}C isotope effect, suggests a change in the partitioning of the oxaloacetate intermediate favors decarboxylation, i.e., a decrease in c_r; a lower value of c_r is calculated, Table 2.4. A decrease in the forward commitment factor was also estimated, Table 2.4. All of the mutant enzymes have similar intrinsic deuterium and ^{13}C isotope effect values compared to wild type, suggesting similar transition states

for the hydride transfer and decarboxylation. All of the S433 and N434 mutant enzymes exhibited a smaller value of ^{13}C isotope effect with deuterated malate, consistent with a stepwise mechanism.

Data for the S433C mutant enzyme exhibit a $^{D}(V/K)$ value similar to that of wt, while there is a decrease in the ^{13}C isotope effect. Data suggest a change in the partitioning of the oxaloacetate intermediate to favor decarboxylation. In agreement, the estimated value of c_r has decreased considerably, compared to wt.

In addition to its interaction with the nicotinamide ribose, N434 also interacts with the β-carboxylate of malate. If the interaction is eliminated, the positioning of malate may change, resulting in changes in the rates of hydride transfer and decarboxylation. ^{D}V and $^{D}(V/K)$ values for the N434A mutant enzyme are equal, within error, to the wild type values, while $^{13}(V/K)_{H}$ is greater than that of the wt enzyme. Data suggest a more rate-limiting decarboxylation. The commitment factors and the intrinsic isotope effects were almost identical to the wt values. However, 3,500-fold decrease in $V/\mathbf{E_t}$ suggests that only a small fraction of the dinucleotide is productively bound, as for N479S. The rates of the steps within the catalytic pathway slow down with the same ratio relative to one another.

In the case of the N434M mutant enzyme, the longer methionine side chain sticks into the active site, in close proximity to C4 of malate, likely causing a change in the orientation of malate and slowing down decarboxylation. The ^{13}C isotope effects were not determined for this mutant enzyme since $V/\mathbf{E_t}$ decreased 10,000-fold. However, it would be expected that ^{D}V and $^{D}(V/K_{malate})$, unity within error, most likely reflect the

decarboxylation step becoming totally rate-limiting. Isotope effects were not determined for the N434Q mutant enzyme since the rate was too low (14,000-fold decrease in $V/\mathbf{E}_t$).

2.4.5. Conclusion.

Results obtained for the N479 mutant enzymes, indicate that the hydrogen bond donated by N479 to the carboxamide side chain of the nicotinamide ring is crucial for proper orientation in the hydride transfer step of the *Ascaris* NAD-malic enzyme reaction. This is very reasonable if one considers the structure of the enzyme.

S433 and N434 residues are very important in positioning the dinucleotide. Data obtained for all mutant enzymes suggest the following: 1. The orientation of the nicotinamide is very strictly controlled, because any mutation, whether it is conservative or not, caused considerable decrease in the rate of the reaction. 2. S433 provides significant binding affinity for NAD, and its replacement with A generates significant nonproductive binding of the cofactor. 3. The effect of N434 mutant enzymes is more pronounced in terms of the positioning of NAD and malate. 4. Differences in the dissociation constants for NAD and NADH indicate the enzyme sees the oxidized and reduced forms of the cofactor differently.

CHAPTER 3:

3.1. Introduction

Malic enzymes are a distinct class of oxidative decarboxylases, that catalyze the divalent metal ion dependent (Mg^{2+} or Mn^{2+}) conversion of L-malate to pyruvate and CO_2, with the reduction of NAD(P) to NAD(P)H [1,6,42]. The malic enzyme has been found in many organisms, and in 1956, was isolated from the parasitic roundworm, *Ascaris suum*. [21] The metabolism of the nematode strictly depends on the mitochondrial malic enzyme reaction, which is the main source of NADH for ATP production [62,63].

Crystal structures of *Ascaris* mitochondrial malic enzyme in complex with NAD and NADH have shown that the enzyme is a homotetramer with a molecular weight of around 68 kDa [33,34]. It is composed of four domains. Domains A and B are associated with dimer and tetramer interactions. The active site residues are contributed mainly by domains B and C, while domain D contains the amino- and carboxyl-termini. The cofactor binds to a modified Rossmann fold in the C domain of the enzyme. The third β strand of the Rossmann fold is replaced by a β-turn, an antiparallel β strand (361-366) and a segment (367-389) that contains a short helix (375-380). This difference in the Rossmann dinucleotide binding domain in the *Ascaris* malic enzyme was also observed in the human enzyme [32,38]. Aspartate-361 begins the antiparallel β strand of the Rossmann fold, and is located in close proximity to the 2'-OH group of the NAD adenosine. As a result, D361 could provide binding specificity for NAD and exclude the 2'-phosphate group of NADP. However, in the crystal structure of the *Ascaris* enzyme

with NAD bound, the D361 side chain is directed away from the cofactor, leaving enough space for NADP binding [33]. Furthermore, D361 is conserved in NADP-specific malic enzymes (Figure 3.1), which suggests that it has no role in determining cofactor specificity [71]. The possible importance of D361 may be associated with a salt bridge it makes with R370; this ionic interaction is also highly conserved in malic enzymes, and can likely be attributed to the stabilization of one of the dinucleotide adenosine binding loops (361-362).

It has been shown that both human and *Ascaris* malic enzymes prefer NAD under physiological conditions, but they can also use NADP [53,72]. The pigeon liver cytosolic malic enzyme utilizes only NADP as the cofactor [73]. Interaction of the cofactor with a lysine residue in the pigeon cytosolic enzyme was proposed to be one of the main determinants for cofactor specificity [71]. Sequence alignment of NADP-specific malic enzymes indicates that the lysine residue is completely conserved (Figure 3.1). In the human mitochondrial NAD(P)-dependent malic enzyme, this lysine residue is replaced by a glutamine (Q362), while it is a histidine (H377) in the *Ascaris* malic enzyme. Hsieh *et al.*[74], reported that the specificity of the human mitochondrial NAD(P)- dependent malic enzyme could be changed to favor NADP with the mutation of Q362 to lysine.

Previously, the possible functional roles of residues interacting with the nicotinamide and its ribose ring were investigated, and it was concluded that the positioning of the nicotinamide ring is very important for the *Ascaris* malic enzyme reaction [75]. In this study, several residues that form the adenosine binding site of NAD were examined to determine their functional roles in binding of NAD and/or catalysis, by mutating them to different amino acids. In addition, the importance of H377 was

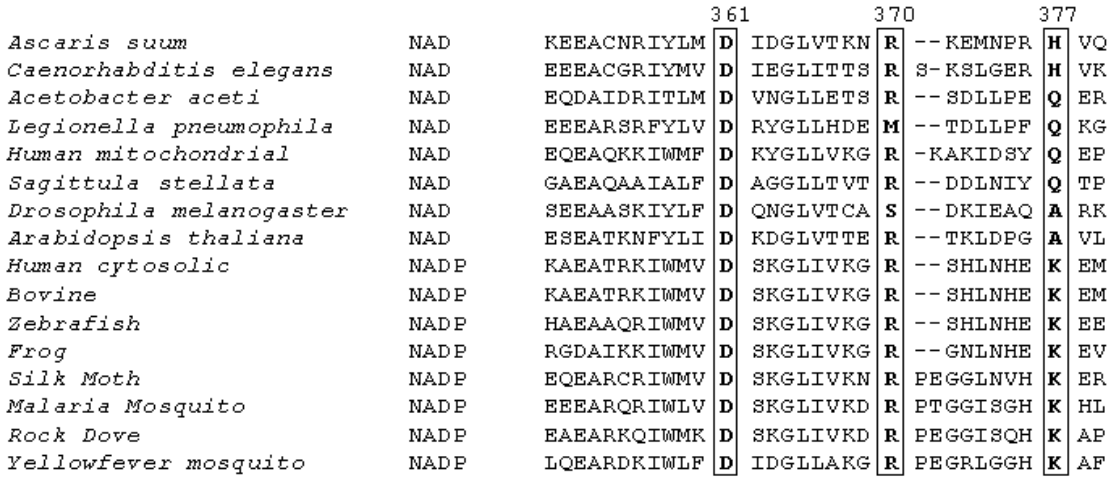

Figure 3.1 Multiple sequence alignment of malic enymes around the adenosine binding site of NAD(P). The conserved residues (D361, R370 and H377) that are investigated in this study are shown in a box.

investigated. Mutant enzymes were characterized by initial rate and kinetic isotope effect studies, and results are described in terms of the mechanism of the malic enzyme.

3.2. Materials and methods.

3.2.1. Chemicals and enzymes.

Malate, NAD and NADH were obtained from USB. Magnesium sulfate and manganese sulfate were purchased from Fisher Scientific. Sodium borodeuteride (98 atom %) was from Aldrich and IPTG was from GoldBio Tech. Hepes and Ches buffers were from Research Organics, while Pipes buffer and fumarate were purchased from Sigma. The QuikChange site-directed mutagenesis kit was from Stratagene. The recombinant *A. suum* malic enzyme used in these studies has a 6-histidine N-terminal tag, and both the wild type and mutant enzymes were prepared and purified as described previously [28]. Protein concentrations were obtained using the method of Bradford [65]. L-Malate-2-d was synthesized by the reduction of oxaloacetate with sodium borodeuteride, and the D-malate eliminated using the tartrate dehydrogenase reaction, as described previously [75]. All other chemicals and reagents used were obtained commercially and were of the highest purity available.

3.2.2. Enzyme assays.

Enzyme assays were carried out at 25°C in 1 cm cuvettes using a Beckman DU640 UV-visible spectrophotometer. In the direction of oxidative decarboxylation of malate, malic enzyme activity was measured at varying concentrations of L-malate, divalent metal ion, and NAD, keeping the non-varied substrate at least 10 times its K_m value. Reaction mixtures were maintained at pH 7 with 100 mM Hepes buffer. The

reaction was followed at 340 nm to monitor the production of NADH (ε_{340}, 6220 $M^{-1}cm^{-1}$). Malic enzyme binds the uncomplexed forms of metal ion and substrates and corrections for chelate complexes were made using the following dissociation constants: Mg-malate, 25.1 mM; Mn-malate 5.4 mM; Mg-NAD 19.6 mM; Mn-NAD and Mn-NADH 12.6 mM [75]. All substrate concentrations reported in the text refer to the uncomplexed concentrations of substrates, and divalent metal ion.

The primary kinetic deuterium isotope effects were determined by direct comparison of initial velocities using 100 mM Hepes, pH 7, at saturating concentrations of metal ion and the cofactor, and varied concentrations of L-malate-2-h(d).

3.2.3. Fluorescence titration.

Fluorescence spectra were collected using an SLM 8100 spectrophotometer. Quartz cuvettes with an inner volume of 3 mL were used. All spectra were collected at pH 7, 100 mM Hepes and 25˚C, with 150 µg/mL malic enzyme. The excitation wavelength was 280 nm, and emission spectra were measured between 320 and 600 nm at 2-nm intervals. A bandwidth of 5 nm was used for excitation and emission monochromators. Blank spectra, containing all components except enzyme, were collected and subtracted from sample spectra. The titration was carried out by sequentially adding 5µL from a concentrated stock malate solution. All spectra were corrected for dilution resulting from the addition of malate.

3.2.4. ^{13}C Kinetic isotope effects.

The ^{13}C isotope effects on the malic enzyme reaction were determined using the natural abundance of ^{13}C in the substrate as the label [66]. The low conversion reactions

(15%) contained 25 mM Hepes, pH 7, 10 mM NAD, 20 mM $MnSO_4$, and 12 mM L-malate-2-h(d), in a total volume of 33 mL. The high-conversion sample (100%) contained the same components, with the exception that the concentration of L-malate-2-h(d) was 2 mM. The reaction mixtures were adjusted to pH ~6 and sparged with CO_2 free nitrogen for at least 3 hours. The pH was then adjusted to 8.2 with KOH and the mixture was sparged for an additional 2 hours. The high-conversion reaction was initiated by the addition of wild type malic enzyme (0.6 mg) and the reaction was incubated overnight. The completeness of the reaction was determined by taking an aliquot of the sample mixture and determining the absorbance at 340 nm. The low-conversion reaction was initiated by the addition of one of the mutant enzymes. The progress of the reaction was checked by measuring the absorbance of the aliquots at 340 nm. All the reactions were quenched by the addition of 100 µL of concentrated sulfuric acid prior to CO_2 isolation. The $^{12}C/^{13}C$ ratio of the isolated CO_2 was determined using an isotope ratio mass spectrometer (Finnigan Delta E). All ratios were corrected for ^{17}O according to Craig [67].

3.2.5. Data analysis.

Initial velocity data were fitted with BASIC versions of the FORTRAN programs developed by Cleland [68]**.** Saturation curves for malate, NAD and the metal ion were fitted using equation 1. Data conforming to a sequential kinetic mechanism were fitted using equations 2.

$$v = \frac{V\mathbf{A}}{K_a + \mathbf{A}} \qquad (1)$$

$$v = \frac{V\mathbf{AB}}{K_{ia}K_b + K_a\mathbf{B} + K_b\mathbf{A} + \mathbf{AB}} \quad (2)$$

In equations 1and 2, v represents the initial velocity, V is the maximum velocity, **A** and **B** are reactant concentrations, K_a and K_b are the Michaelis constants for **A** and **B**, K_{ia} is the inhibition constant for **A**.

Data for primary kinetic deuterium isotope effects were fitted using equation 3, where F_i is the fraction of deuterium in the labeled compound, and $E_{V/K}$ and E_V are the isotope effects minus 1 on *V/K* and *V*, respectively.

$$v = \frac{V\mathbf{A}}{K_a(1 + F_i E_{V/K}) + \mathbf{A}(1 + F_i E_V)} \quad (3)$$

^{13}C isotope effects were calculated using equation 4. f is the fraction of completion of reaction, and R_f and R_o are the ^{12}C/^{13}C isotopic ratios of CO_2 at low and complete (representing the ratio in the substrate) conversion, respectively. Isotope ratios are measured as δ^{13}C, equation 5, where R_{smp} and R_{std} are ^{12}C/^{13}C isotopic ratios for sample and standard, respectively. The standard for CO_2 was Pee Dee Belemnite with a ^{12}C/^{13}C of 0.0112372 [67].

$$^{13}\left(\frac{V}{K}\right) = \frac{\log(1-f)}{\log\left(1 - f\left[\frac{R_f}{R_0}\right]\right)} \quad (4)$$

$$\delta^{13}C = (R_{smp} / R_{std} - 1) \times 1000 \quad (5)$$

3.3. Results.

The mutant enzymes were characterized by initial rate and kinetic isotope effect studies. The initial rate was measured as a function of NAD at varied concentrations of malate, maintaining metal ion concentration at saturation ($10K_m$). The results are shown in Table 3.1 and Table 3.2.

3.3.1. Aspartate-361 mutant enzymes.

Aspartate-361 was mutated to asparagine, glutamate and alanine. The D361A and D361E mutant enzymes showed no activity even at high concentrations of enzyme (>1 mg/ml) and substrates (~50 mM). Titrations with malate were carried out monitoring changes in intrinsic tryptophan fluorescence to determine if the active sites of these mutant enzymes were intact. The K_d for the E-malate complex in the wild type malic enzyme was 40 ± 11 mM, while it was 32 ± 10 mM and 38 ± 12 mM for the D361E and D361A mutant enzymes, respectively. The very similar values of K_d indicated that the site for malate binding was intact. There is no good probe of NAD binding. However, there is synergism in the binding of malate and NAD, and it's believed that data are suggestive of a native conformation of the mutant enzymes. The complete loss of activity is thus likely due to the local changes in the NAD site.

The D361N mutant enzyme showed no significant change in K_{malate}, and a 3-fold increase in K_{NAD}. However, $V/\mathbf{E_t}$ decreased by 1400-fold, giving a 4400-fold decrease in V/K_{NAD};.Table 3.1

Table 3.1 Kinetic parameters for the D361 and R370 mutant enzymes.

Parameter	Wild Type	D361N	R370K	R370A
K_{malate} (mM)	0.8 ± 0.1	0.81 ± 0.04	1.0 ± 0.1	0.83 ± 0.02
F old increase		-	1.3	-
K_{NAD} (mM)	0.032 ± 0.004	0.10 ± 0.01	0.038 ± 0.003	0.030 ± 0.001
Fold increase		3	1.2	-
$V/\mathbf{E_t}$ (s^{-1})	31 ± 1	(23 ± 3) x 10^{-3}	12 ± 2	(1.7 ± 0.3)
Fold decrease		1400	2.6	18
$V/(K_{malate}.\mathbf{E_t})$ ($M^{-1}s^{-1}$)	(3.8 ± 0.5) x10^4	32 ± 3	(1.2 ± 0.2) x10^3	(2.0 ± 0.1) x10^3
Fold decrease		1200	32	20
$V/(K_{NAD}.\mathbf{E_t})$ ($M^{-1}s^{-1}$)	(1.0 ± 0.2) x 10^6	230 ± 20	(3.2 ± 0.2) x10^5	(5.7 ± 0.8) x10^4
Fold decrease		4400	3	17

3.3.2. Arginine-370 mutant enzymes.

Arginine-370 which forms a salt bridge with D361 (Figure 3.2), was mutated to alanine and lysine. No significant change in K_m values for the substrates were observed for either of the mutant enzymes, Table 1. However, $V/\mathbf{E_t}$ was decreased by 2.5- and 20-fold for the R370K and R370A mutant enzymes, respectively. The more significant decrease in $V/\mathbf{E_t}$ for R370A mutant enzyme, compared to that of R370K mutant enzyme, suggested that the charge at position 370 is somewhat important.

3.3.3. Histidine-377 mutant enzymes.

On the basis of studies of the human mitochondrial malic enzyme [74], histidine-377 was thought to be a critical residue for cofactor specificity and was mutated to lysine and alanine. Initial rates were determined with NAD and NADP, as cofactors. Both mutant enzymes exhibited only modest changes in K_{malate}, K_{NAD} and $V/\mathbf{E_t}$, Table 3.2. Contrary to results expected for a specificity determinat, the mutant enzymes showed an increase in K_{NADP}; 8- and 1.5-fold for H377K and H377A mutant enzymes, respectively.

3.3.4. Isotope effects.

Deuterium isotope effects were measured with L-malate-2-d as the labeled substrate and the results are summarized in Table 3.3. Values of ^{D}V and $^{D}(V/K_{malate})$ are the mean average of at least six separate determinations. No significant change was observed in the isotope effect data for the mutant enzymes. ^{13}C kinetic isotope effects were also determined for H377K (1.0333 ± 0 .001) and H377A (1.0315 ± 0.004) mutant enzymes and found to be very similar to that of wild type (1.0342 ± 0.0002).

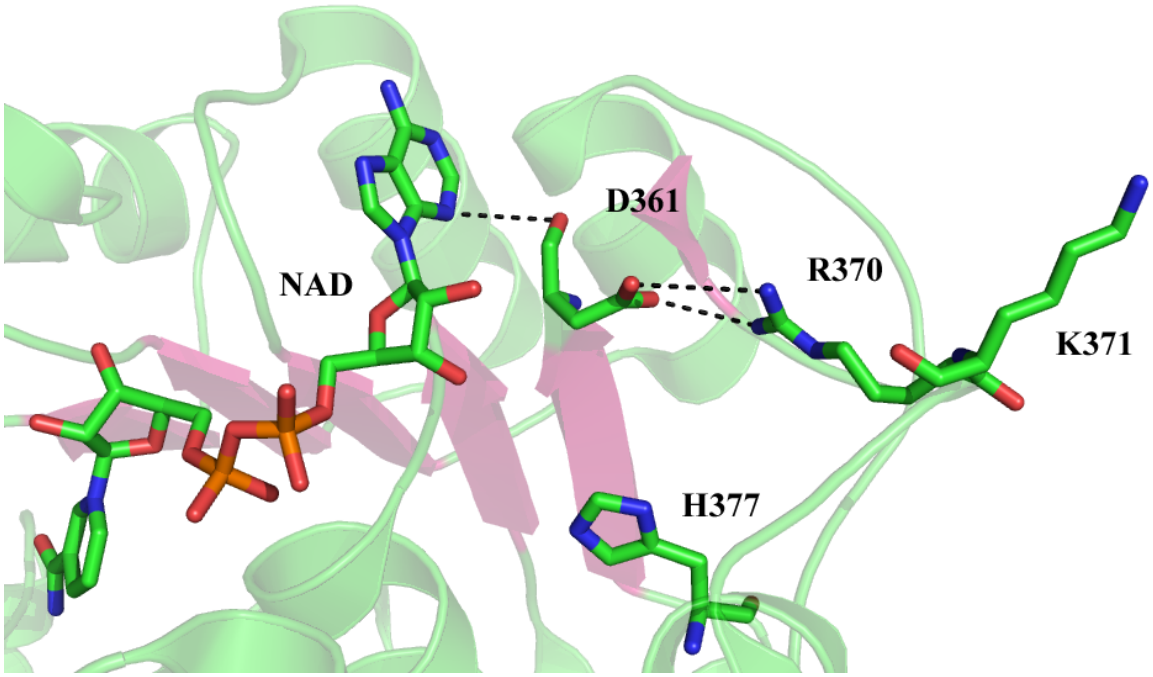

Figure 3.2 The NAD binding site of the *Ascaris suum* mitochondrial malic enzyme (PDB code 1llq). The residues that directly or indirectly interact with the cofactor are shown. The interactions between the residues are shown with dash lines. The hydrogen-bonding distance between adenine-N3A and D361 backbone carbonyl is 3.4 Å, whereas the ionic interaction distance between D361 and R370 is around 3.6 Å. This figure was generated using the PyMOL molecular visualization program (website: http://pymol.sourceforge.net/).

Table 3.2 Kinetic Parameters for the H377 Mutant Enzymes with both NAD and NADP.

Mn^{2+} as metal ion	Wild Type		H377K		H377A	
	With **NAD**	With **NADP**	With **NAD**	With **NADP**	With **NAD**	With **NADP**
K_{malate} (mM)	0.24 ± 0.08	0.36 ± 0.08	0.52 ± 0.09	1.1 ± 0.3	0.28 ± 0.08	0.76 ± 0.16
Fold increase			2.1	3	1.2	2.1
$K_{NAD(P)}$ (mM)	0.07 ± 0.01	0.05 ± 0.01	0.30 ± 0.02	0.4 ± 0.1	0.07 ± 0.01	0.07 ± 0.01
Fold increase			4.3	8	-	1.4
$V/\mathbf{E_t}$ (s^{-1})	45 ± 4	33 ± 2	14 ± 1	7.7 ± 0.7	19 ± 1	14.0 ± 1.5
Fold decrease			3.2	4.3	2.4	2.4
$V/(K_{malate}.\mathbf{E_t})$ ($M^{-1}s^{-1}$)	(19 ± 7) x10^4	(9.2 ± 2.1) x10^4	(2.7 ± 0.5) x10^4	(7.0 ± 0.4) x10^3	(7 ± 2) x10^4	(1.8 ± 0.1) x10^4
Fold decrease			7	13	2.7	5.1
$V/(K_{NAD(P)}.\mathbf{E_t})$ ($M^{-1}s^{-1}$)	(6.4 ± 1.1) x 10^5	(6.6 ± 1.4) x 10^5	(4.7± 0.7) x 10^4	(1.9 ± 0.2) x 10^4	(2.7 ± 0.4) x 10^5	(2.0 ± 0.1) x 10^5
Fold decrease			14	35	2.4	3.3

Table 3.3 Primary Deuterium Kinetic Isotope Effects for The Wild Type and Mutant Malic Enzymes.

	Wild Type	D361N	R370K	R370A	H377K	H377A
^{D}V	2.0 ± 0.1	2.3 ± 0.2	2.1 ± 0.2	2.4 ± 0.3	2.1 ± 0.2	2.4 ± 0.3
$^{D}(V/K)$	1.6 ± 0.3	1.8 ± 0.1	1.6 ± 0.2	1.7 ± 0.2	1.6 ± 0.2	1.7 ± 0.2

3.4. Discussion.

In this study, site-directed mutagenesis, initial rate and kinetic isotope effect studies were carried out to obtain a better understanding of the cofactor binding site of the *Ascaris* mitochondrial NAD-malic enzyme. Residues that interact directly or indirectly with the adenosine moiety of the cofactor were mutated to different amino acids to determine their possible functional roles in binding and/or catalysis.

3.4.1. The D361-R370 salt bridge.

Aspartate-361 is located in the dinucleotide binding Rossmann fold and is a part of a cap surrounding the adenosine moiety of NAD. D361 is in close proximity to the 2'-OH group of the NAD-adenosine and was thought to be important in cofactor specificity, by excluding the 2'-phosphate group of NADP. However, in the crystal structure of *Ascaris* m-NAD-ME, the 361 side chain is directed away from the ribose of the cofactor, and forms a salt bridge with R370, leaving sufficient space for the 2'-phosphate of NADP [33]. Furthermore, D361 is also completely conserved in NADP-specific malic enzymes (Figure 3.1), suggesting that it likely does not play a role in cofactor specificity [71]. When D361 is mutated to alanine or glutamate, the enzyme loses all of its activity. Fluorescence titrations suggest the loss of activity of the enzymes is likely localized to the NAD-binding site. Since the ionic interaction is still possible, it is likely that the loss of activity of D361E enzyme results from the increase in molecular volume, with E being a methylene longer than D. Visualization of the D to E mutation using PyMOL software indicates the longer side chain of glutamate clashes with the adenosine ribose of NAD and also with the loop (326-329) that contains the GAGAA signature motif for cofactor

binding. The mutation would thus be expected to change the positioning of NAD leading to either nonproductive or no binding of the cofactor.

D361N exhibited no or modest changes in the K_m values of the substrates. As expected, D361N did not show a significant change in K_{NADP} (data not shown). However, $V/\mathbf{E_t}$ decreased by 1400-fold, which is most likely caused by the loss of the salt bridge between D361 and R370. Unlike D361A and E mutant enzymes, D361N mutant enzyme exhibited activity; the asparagine side chain is essentially isosteric with aspartate and still retains H-bonding capability to R370. Data suggest that the salt bridge between D361 and R370 is important for the productive binding of the cofactor and indirectly for catalysis. The electrostatic interaction stabilizes one of the loops, containing D361 and I362, that aids in binding the cofactor. A shift in the position of the loop, in addition to causing ineffective cofactor binding, relocates I362, one of the 3 residues forming the hydrophobic pocket for adenosine binding. Movement of D361 would also affect the hydrogen-bonding interaction of the backbone carbonyl of D361 with N3A of the adenine ring (3.4 Å), Figure 3.2.

The importance of the salt bridge between D361 and R370 is also confirmed by mutation of R370. R370K showed modest changes in the kinetic parameters, consistent with the maintenance of the ionic interaction between D361 and K370. However, the R370A mutant enzyme showed no change in K_m values for the substrates, and a decrease in $V/\mathbf{E_t}$ of only 20-fold, compared to the wild type enzyme. Conversion of D361 to N, on the other hand gave a 1400-fold decrease in $V/\mathbf{E_t}$, and D361A was inactive. There are two possible explanations for this behavior. First of all, H377 could possibly maintain an electrostatic interaction with D361. In the crystal structures, H377 is around 6 Å away

from D361. However, there is no crystal structure for the closed form of the *Ascaris* malic enzyme yet. When the active site closes upon binding of malate, the conformational changes may cause H377 to get closer to D361, making it possible to have an interaction between these residues, allowing the R370A mutant enzyme to retain partial activity. A second possible reason for retaining activity may be a result of K371 (Figure 3.2), which is in close proximity to R370. When R370 is mutated to alanine, the loop on which K371 is located may move, placing K371 in a reasonable interaction distance with D361.

There are a number of cases in the literature for which mutation gives no or little change in kinetic parameters, but a significant change in isotope effects. That is not the case with the D361 and R370 mutant enzymes characterized in these studies. ^{D}V and $^{D}(V/K)$ values of the mutant enzymes were very similar to those of wild type malic enzyme, suggesting similarity in the relative rates of steps that contribute to rate limitation. The portion of the mechanism of the wild type enzyme that contributes to rate limitation of the overall reaction, includes a conformational change, followed by hyride transfer and decarboxylation. At saturating concentrations of reactants an isomerization of E-NAD also contributes to rate limitation [50]. Although the K_m for the substrates and isotope effect values of the mutant enzymes are very similar to those of wild type, there is still change in $V/\mathbf{E_t}$ values. Data suggest it's likely that the cofactor binds nonproductively, with a small fraction of the enzyme being active (0.07%, 6% and 40% for D361N, R370A and R370K, respectively, calculated as the ratio of k_{cat} values).

3.4.2. H377 is not a cofactor specificity determinant of the Ascaris malic enzyme.

In NADP-specific malic enzymes, like pigeon cytosolic malic enzyme, the residue corresponding to 377 in the *Ascaris* malic enzyme is a lysine that is strictly conserved among species, while in the NAD malic enzymes this residue varies, Figure 3.1. The human mitochondrial malic enzyme can use either NAD or NADP as a substrate and has a Q at position 377 [72], while the residue is H in the *Ascaris* enzyme.

In 2000, Kuo *et al*. [76], performed alanine-scanning site-directed mutagenesis to change the conserved lysine residues in NADP-dependent pigeon malic enzyme. When K340 (which corresponds to H377 in *Ascaris* and Q362 in human malic enzymes, respectively) is mutated to alanine, the K_m for NADP was increased by 65-fold, whereas the K_m for malate and metal ion, and k_{cat} were not affected. Therefore, they proposed that K340 plays an important role in determining the specificity for NADP. A structure of the E-NADP-Mn-oxalate quaternary complex of the pigeon liver cytosolic malic enzyme showed that the 2'-phosphate group of NADP interacts with S346 (which corresponds to I362 in the *Ascaris* malic enzyme) and the side chain ammonium group of K340, which was proposed to be one of the important determinants of cofactor specificity in the pigeon malic enzyme (The authors numbered the residues in pigeon liver cytosolic malic enzyme according to their equivalents in human mitochondrial malic enzyme for a more convenient comparison. Therefore, K340 in pigeon malic enzyme is numbered as K362) [71]. The difference between NAD(P) binding site of the pigeon liver cytosolic malic enzyme and the NAD binding site of the human mitochondrial malic enzyme is shown in Figure 3.3.

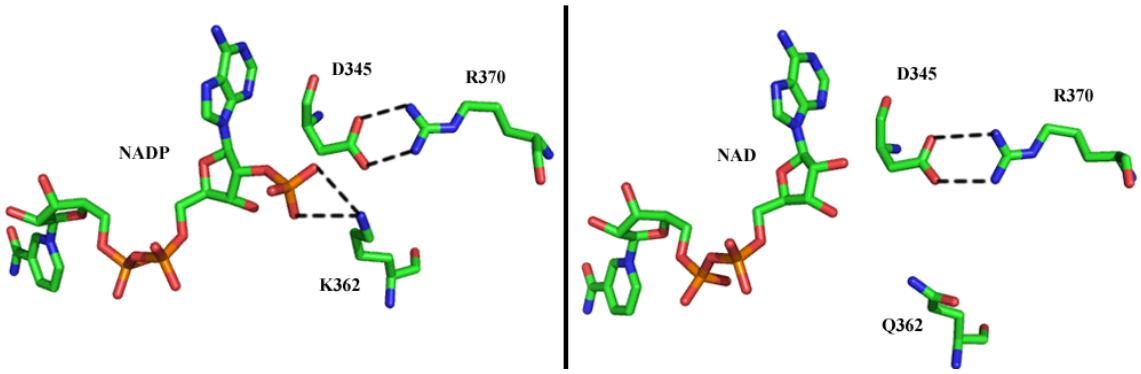

Figure 3.3 The NADP binding site of the pigeon cytosolic malic enzyme (PDB code 1GQ2) and the NAD binding site of the human mitochondrial malic enzyme (PDB code 1QR6). The residues in the pigeon liver malic enzyme are numbered according to their structural equivalents in the human malic enzyme. The residues that directly or indirectly interact with the cofactor are shown. The ionic interactions are shown with dash lines. The average distance between K362 and 2'-phosphate group of the NADP is 3.5 Å. This figure was generated using the PyMOL molecular visualization program (website: http://pymol.sourceforge.net/).

Recently, the importance of Q362 in cofactor specificity of the human mitochondrial malic enzyme was studied [74]. The Q362K mutant enzyme shifted preference from NADP to NAD. k_{cat} /K_m for NADP increased by 35-fold, whereas it decreased by 7-fold for NAD.

Site-directed mutagenesis has been used in other studies to shift the specificity of the enzymes for their cofactors. Scrutton *et al*. [77], mutated specific residues that interact with the cofactor in glutathione reductase and they observed that although the specificity of glutathione reductase for NADP did not change, the preference of the enzyme for NAD increased. Hurley *et al*. [78], mutated 7 residues in *E. coli* isocitrate dehydrogenase and converted the cofactor specificity of the enzyme from a 7000-fold preference for NADP to a 200-fold preference for NAD.

Mutation of H377 in *Ascaris* malic enzyme to lysine gave no shift in cofactor preference. In the *Ascaris* enzyme, H377 is almost 8 Å away from the 2'-OH group of the adenosine ring of NAD. Therefore, the interaction between these two is not likely. When NADP is modeled in the active site of the *Ascaris* malic enzyme using PyMOL software, H377/H377K and 2'-phosphate groups of NADP are still not close enough to be able to maintain an interaction. Although H377 doesn't have a cofactor specificity determining role, it could be an important second layer residue that affects the residues it is packed against, and directly interacts with the cofactor. In the H377K mutant enzyme structure created using PyMOL program, the side chain of lysine clashes with one of the loops that binds the cofactor. It specifically clashes with A328 and G329, which form a part of the cofactor binding signature motif. This may cause nonproductive binding of

the cofactor. This was confirmed by almost no change in kinetic parameters for H377A mutant enzyme, compared to those of wild type.

^{13}C kinetic isotope effects were also determined for H377K and H377A mutant enzymes and found to be very similar to that of the wild type, indicating a similar contribution to rate limitation of the decarboxylation step.

3.4.3. Conclusion.

Data obtained for the D361 and R370 mutant enzymes indicate that the ionic interaction between the two residues is important for the binding of the adenosine portion of the cofactor in *Ascaris* malic enzyme. This interaction stabilizes a part of the Rossmann fold that NAD binds. A mutation to D361 can lead to nonproductive binding of the cofactor to the active site. When R370 is mutated, the interaction between D361 and R370 may be maintained, at least partially, by interaction with other residues. The mutation of H377 to lysine, which is conserved in NADP-specific malic enzymes and proposed to be a cofactor specificity determinant, did not cause a shift in cofactor specificity of the *Ascaris* malic enzyme from NAD to NADP. In the available crystal structures of the NADP malic enzymes this lysine residue is in close proximity to 2'-phosphate group of NADP to maintain an ionic interaction, whereas in NAD(P) specific enzymes the residue(s) corresponding to this lysine is (are) distant. However, H377 may be an important second layer residue that affects the packing of the first layer residues that directly interact with the cofactor.

CHAPTER 4:

4.1. Introduction

β-Hydroxyacid oxidative decarboxylation is catalyzed by a class of enzymes that utilize a pyridine dinucleotide, NAD(P). The enzyme class includes the well-studied malic enzyme (ME), isocitrate dehydrogenase (IcDH) and 6-phosphogluconate dehydrogenase (6PGDH), as well as homoisocitrate dehydrogenase (HIcDH), isopropylmalate dehydrogenase (IPMDH) and tartrate dehydrogenase (TDH). The β-hydroxyacid oxidative decarboxylases can be classified on the basis of their metal ion dependence. The ME [6,21,79,80], ICDH [81-83] and IPMDH [84,85] require a divalent metal ion, Mg^{2+} or Mn^{2+}, for activity. In addition to the divalent metal ion, a monovalent ion, usually K^{+}, is required for optimal activity of the HICDH [86,87] and TDH [88,89] reactions . Finally, 6PGDH is divalent and monovalent metal ion independent [90,91]. This review will focus on the metal ion-dependent enzymes. In terms of overall structure, the metal ion dependent enzymes can be divided into two distinct groups. The first includes ICDH, IPMDH, HICDH and TDH, while ME is in a class of its own.

The reactions catalyzed by the enzymes are listed in Figure 1.1. Note that the substrates of these enzymes, isocitrate, isopropylmalate, homoisocitrate and tartrate, have a common malate backbone, and differ only in the substituent on the carbon beta to the 1-carboxylate. The enzymes thus differ in their substrate specificity, and are strict in their selection of the substrate for the oxidative decarboxylation reaction. (TDH catalyzes reactions other than oxidative decarboxylation [92]).

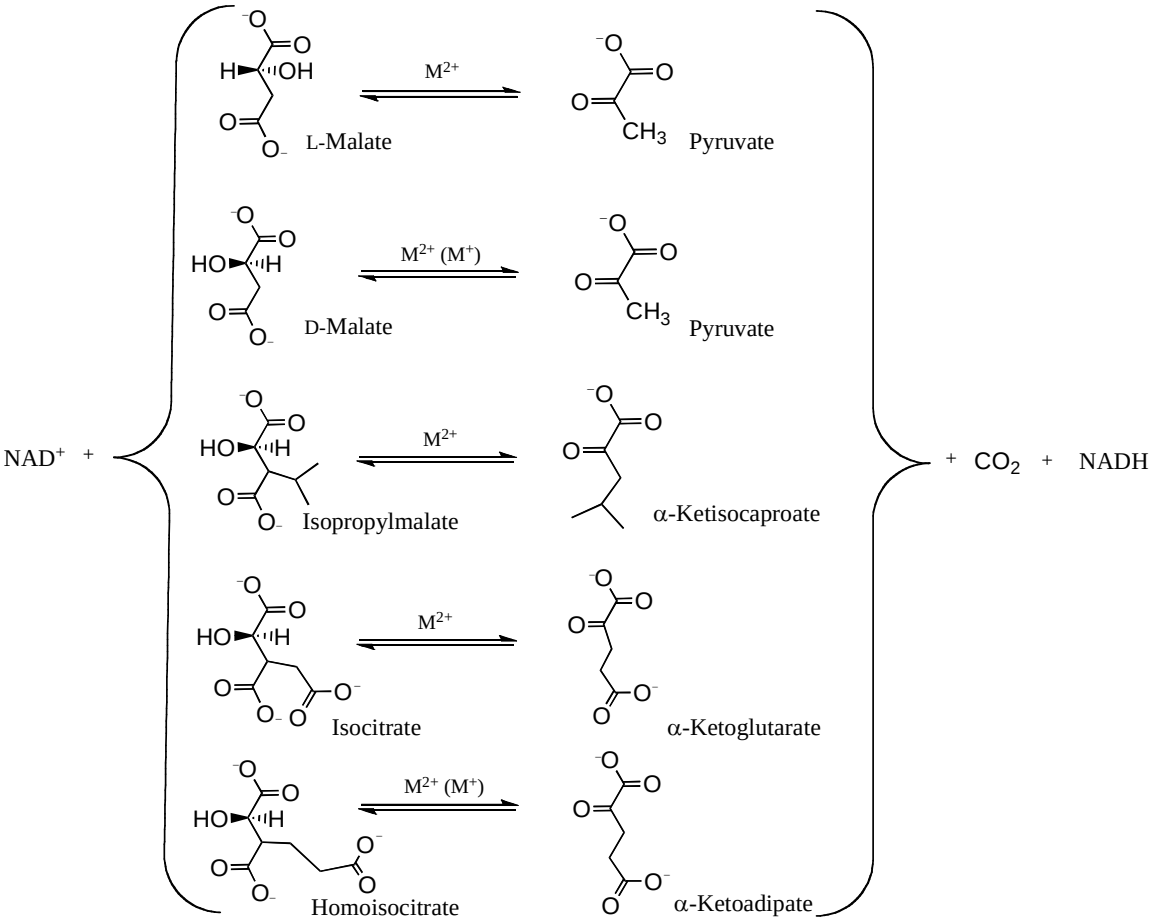

Figure 4.1 Reactions catalyzed by the metal ion-dependent pyridine dinucleotide–linked β-hydroxyacid oxidative decarboxylases. The dinucleotide substrate and product, and CO_2 are common to all reactions. The β-hydroxyacid and ketone product for each of the reactions are shown in parantheses. The metal ion dependencies of each of the enzymes are provided above the arrow. Reactions from top to bottom are catalyzed by ME, TDH, IPMDH, IcDH, and HIcDH, respectively.

In spite of the differences in metal ion requirement and structure, all of the pyridine dinucleotide-linked β-hydroxyacid oxidative decarboxylases catalyze the same general reaction. The overall reaction proceeds via three steps, oxidation of the β-hydroxyacid to a β-ketoacid, decarboxylation to generate an enol, and tautomerization to give a ketone product. As an example, the mechanism for oxidative decarboxylation of malate is given in Scheme 4.1.

All the enzymes in the class of metal ion dependent β-hydroxyacid oxidative decarboxylases exhibit a steady-state random kinetic mechanism [45,48,92-96]. The acid-base chemical mechanisms of some of the enzymes have been proposed and there are significant differences in the proposed mechanisms [55,56,97-101]. In this manuscript we propose a unified acid-base mechanism for the metal ion dependent enzymes on the basis of the similarity in the active sites and data presently in the literature. There are a number of reviews that cover aspects other than those considered in this manuscript, and the reader is referred to these for additional information [1,102-104].

4.2. Overall Structure

As suggested in the introduction, the metal ion dependent β-hydroxyacid oxidative decarboxylases apparently fall into two general classes. An overlay of a dimer of IcDH [100], IPMDH [105], and HIcDH [106] is shown in Figure 4.2A. (No structure is available for TDH). There is remarkably good agreement of the backbone structures of all three of the enzymes; they are clearly in the same fold family, which for convenience we will call the IcDH subfamily. The malic enzyme, on the other hand, neither aligns well, nor has a structure similar to those of the other enzymes. A superposition of a dimer

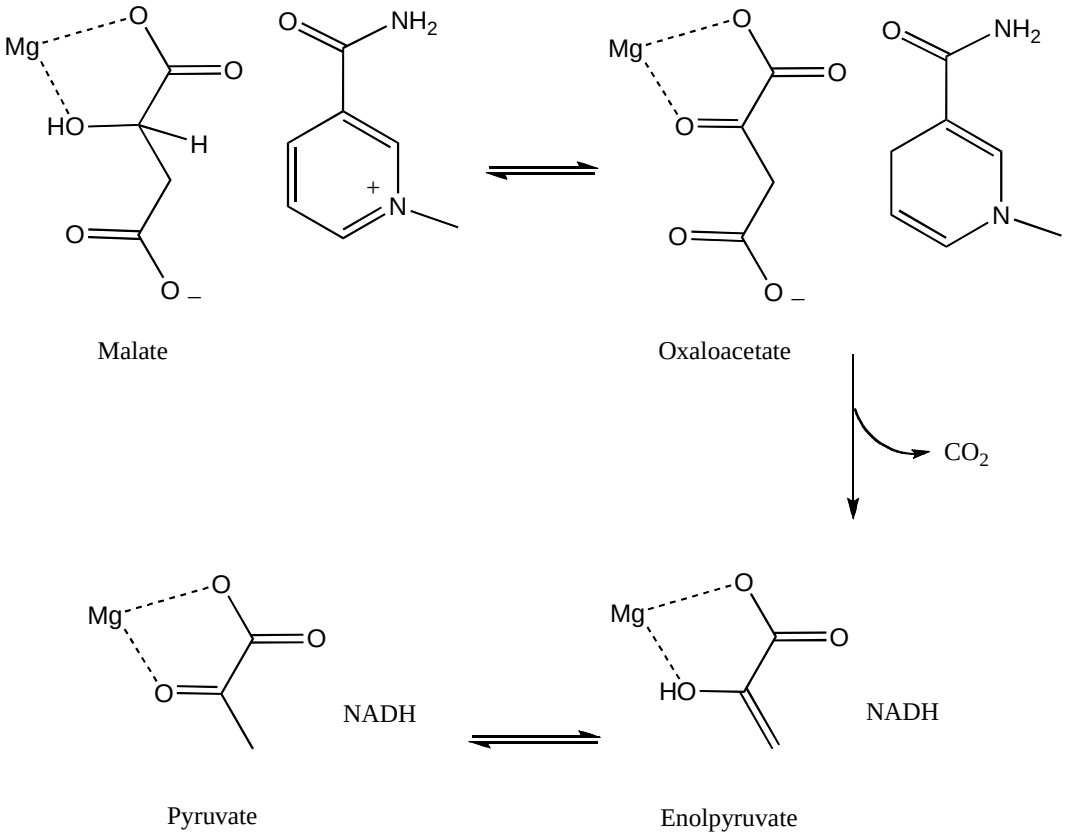

Scheme 4.1 Proposed three-step mechanism of oxidative decarboxylation of malate.

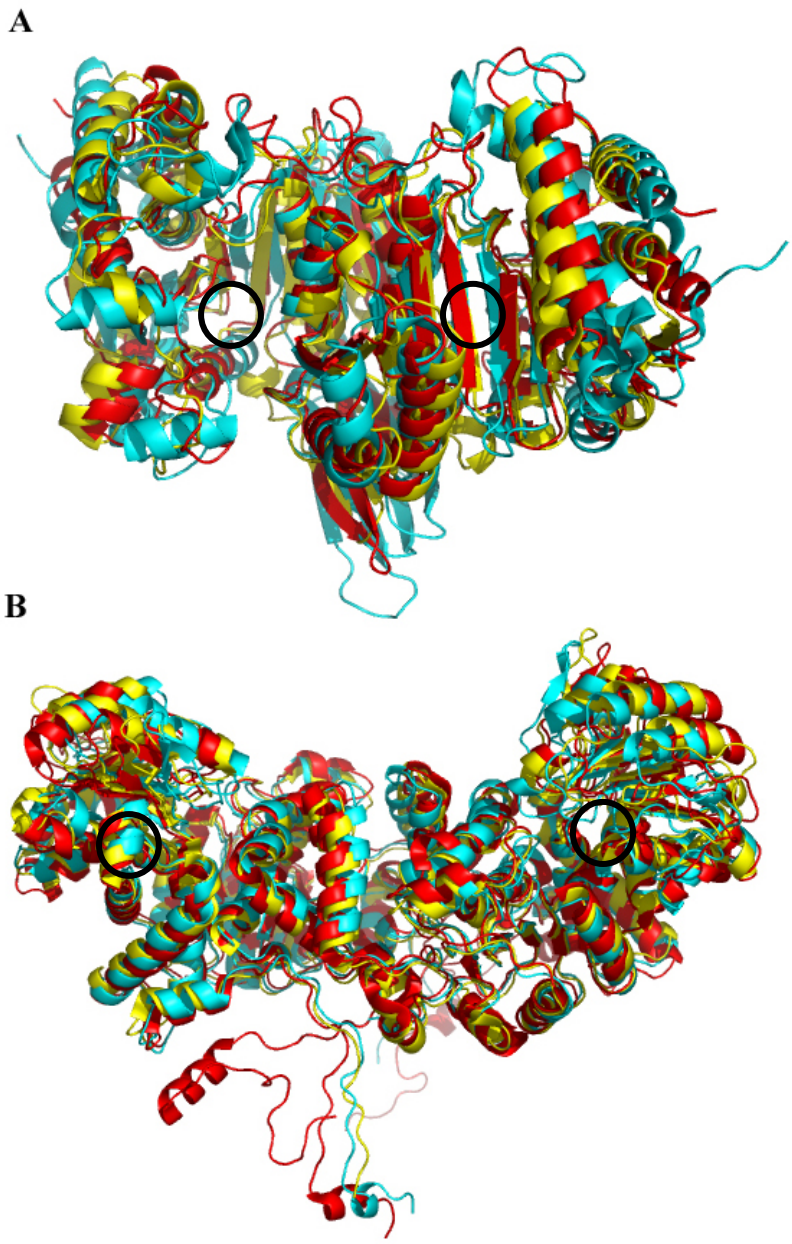

Figure 4.2 Structural overlay. A) The structures of a dimer of three members of the IcDH subfamily are superimposed. The enzymes are ICDH (cyan, PDB), IPMDH (red, PDB 1A05) and HICDH (yellow, PDB 1X0L). B) *Ascaris* ME (red, PDB 1LLQ), pigeon liver ME (cyan, PDB 1GQ2) and human ME (yellow, PDB 1PJ2) are superimposed. The location of the active sites are shown with a circle. The figures were generated using the PyMOL molecular visualization program (website: http://pymol.sourceforge.net/).

of the malic enzymes from *Ascaris suum* [33] and human mitochondria [107], and pigeon liver cytosol [71] is shown in Figure 4.2B; the enzyme is tetrameric overall. All are αβ proteins with a modified Rossmann fold for cofactor binding. The active site is located in the cleft between two subunits for IPMDH and ICDH, while for ME the active site is in a cleft with contributions from three domains [33,100,105]. All enzymes adopt a closed conformation of the active site upon substrate binding, via rigid body movement of one domain relative to the other.

A multiple sequence alignment of the members of the IcDH subfamily is shown in Figure 4.3. As can be seen, active site residues important for reactant and metal ion binding and catalysis are completely conserved in all of the family members. On the other hand, the malic enzymes do not align with the IcDH subfamily members, but align with high homology to one another, Figure 4.4. Of interest, alignment of the mitochondrial NAD- and cytosolic NADP-dependent MEs also exhibit high (~50%) homology, while the NAD- and NADP-dependent isocitrate dehydrogenases exhibit low (~10%) homology.

4.2.1. Active site

As expected on the basis of the similarity of the overall structures, the location of the active site within a monomer is the same for all of the enzymes in the IcDH subfamily. In the case of the IcDH subfamily, active site residues are contributed by two subunits, with the catalytic lysine and an aspartate metal-ligand contributed by one subunit and the remaining residues contributed by the other. The active sites of the MEs are completely contained in each of the four subunits of the tetramer. A close-up view of

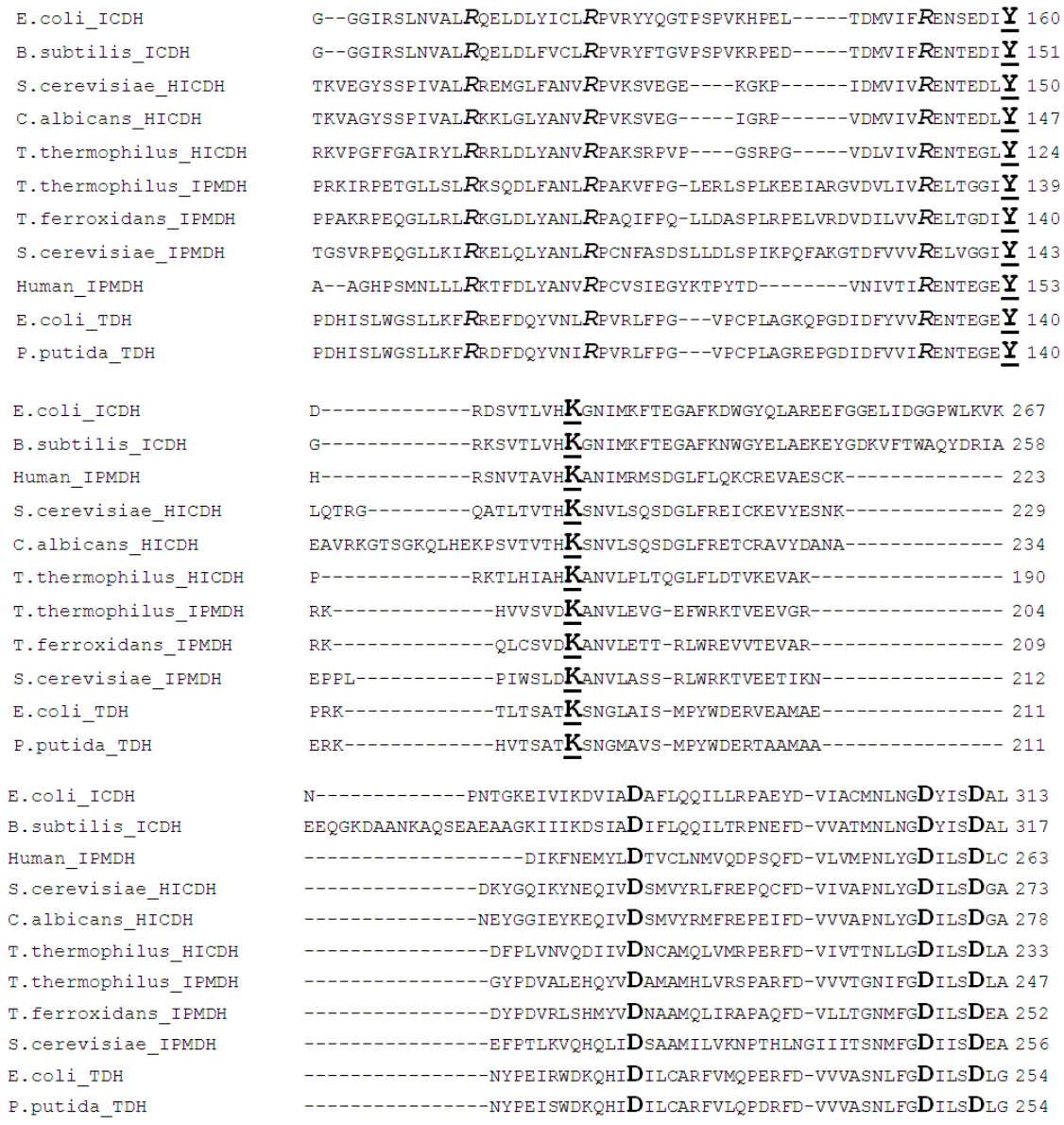

Figure 4.3 Multiple sequence alignment for ICDH, IPMDH, HICDH and TDH, showing important conserved residues. The residues coordinating the metal ion are shown in bold, while the residues coordinating the substrate are bold and italicized. The catalytic residues are shown as bold and underlined. The multiple sequence alignment was carried out using the ClustalW program.

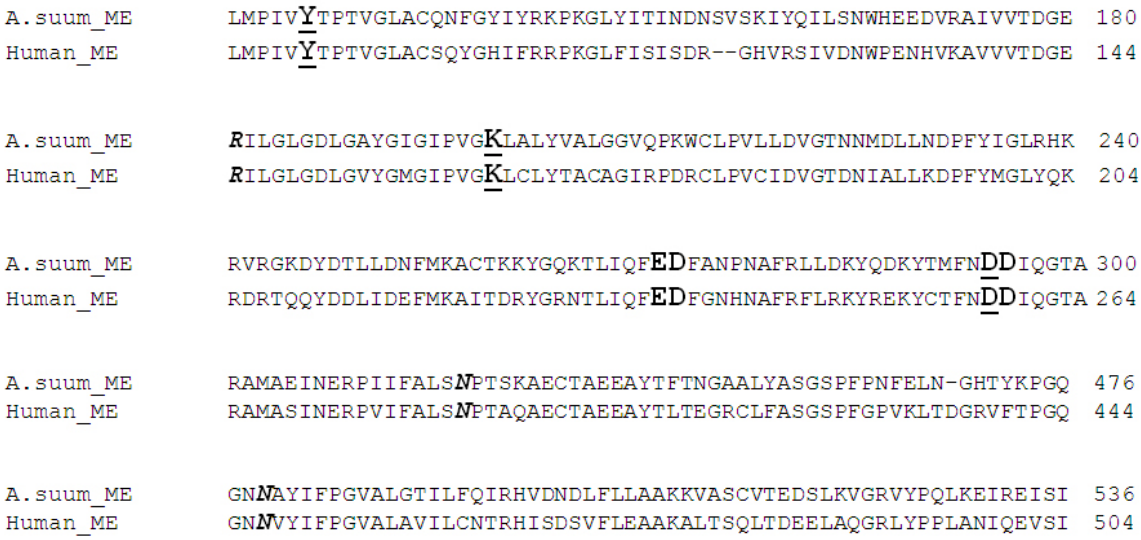

Figure 4.4 Multiple sequence alignment for *Ascaris* and human MEs, showing important conserved residues. Residues coordinating the metal ion are shown in bold, while the residues coordinating the substrate are bold and italicized. The catalytic residues are shown in bold and are underlined. The multiple sequence alignment was carried out using the ClustalW program.

the NAD-malic enzyme showing the catalytic residues and those involved in metal ion binding is shown in Figure 4.5A

A general acid/general base mechanism and the identities of the catalytic residues have been proposed and will be discussed in "**Acid-base Chemical Mechanism**" below. A catalytic triad has been suggested for *Ascaris* ME, consisting of a lysine, a tyrosine, and an aspartic acid [56]. In the substrate bound form, the metal ion exhibits octahedral coordination, and all of the ligands are oxygens, and include three side chain carboxylates, a water molecule and two substrate functional groups, the α-carboxylate and α-hydroxyl. In addition, the α-carboxylate of malate is further oriented by hydrogen bonding interactions with the side chains of an arginine and two asparagine residues (not shown). The active site of the NADP-malic enzymes is virtually identical to that of the NAD-malic enzymes.

Active site close-ups of IPMDH, IcDH, and HIcDH are shown in Figure 4.5B-D. The similarity in the active site residues and overall geometry of the active sites of IcDH and IPMDH is remarkable, as is the similarity to the active site of ME. The tyrosine and lysine, as putative catalytic residues, are conserved, as is the arginine that hydrogen bonds the α-carboxylate of the substrate, and three of the ligands to the metal ion, two aspartate carboxylates and a water molecule. In the IcDH subfamily, one of the aspartates that coordinates the metal ion in ME is replaced by a second water molecule and the two asparagine residues that hydrogen bond the α-carboxylate of the substrate in ME are replaced by arginine residues. The active site of HIcDH has identical residues, but the tyrosine is away from the lysine. However, the structure is an open form, and it is known that a conformational change is required to close the site upon substrate binding and that

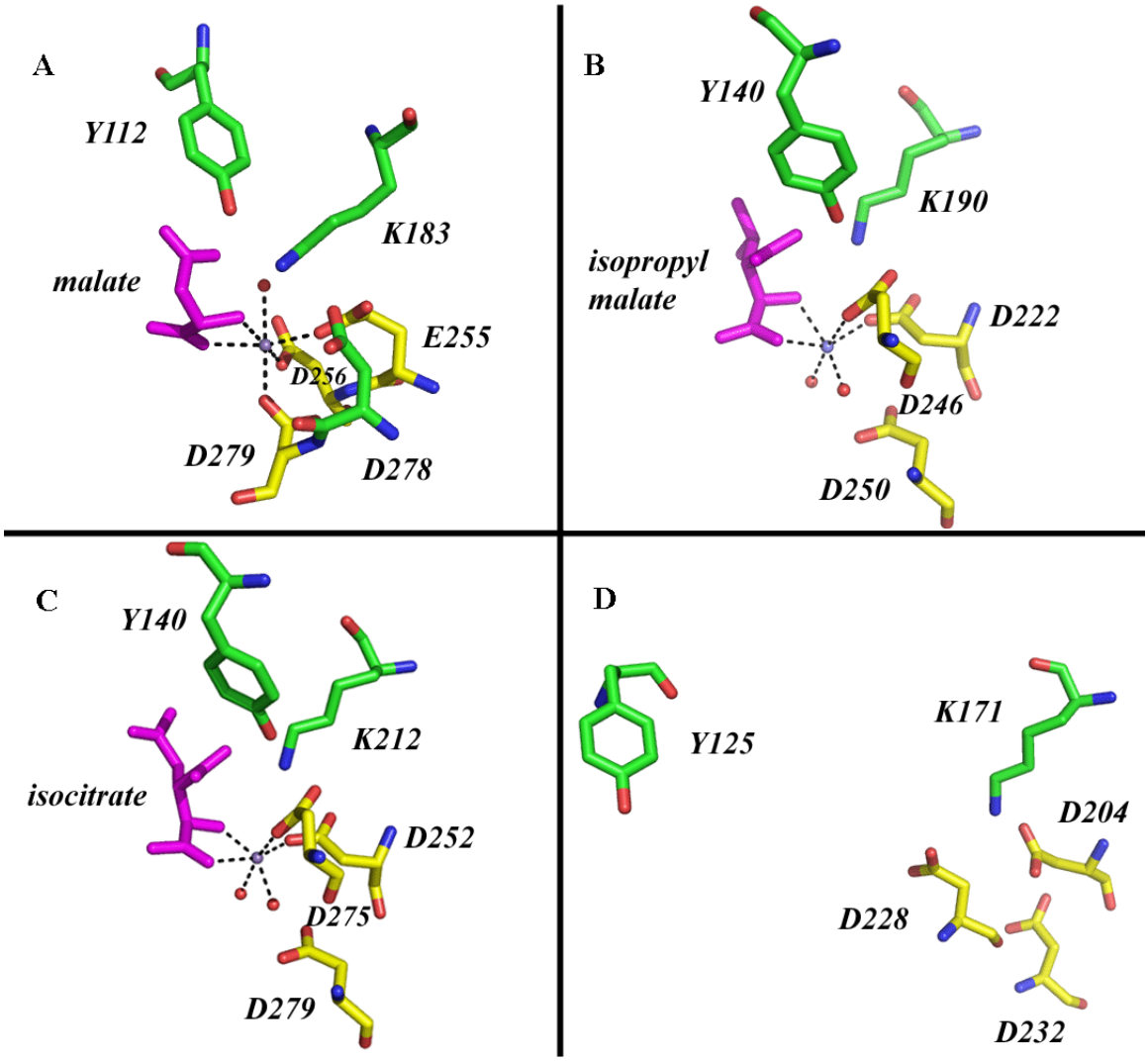

Figure 4.5 Close-up view of active sites. Enzymes with active sites pictured are A) ME, B) IPMDH, C) ICDH, and D) HICDH. Residues that coordinate the metal ion are shown; the metal ion is purple and coordinating residues are yellow. Substrates are colored magenta. The structures for ME and HICDH are the open conformation. The PDB codes for figures A, B, C and D are 1PJ2, 1A05, 1LWD and 1X0L, respectively. The figures are generated using the PyMOL molecular visualization program (website: http://pymol.sourceforge.net).

the tyrosine is then in close proximity to homoisocitrate [106,108]. As shown in Figure 4.2 and 4.3, the overall structure and all of the active site residues are conserved in TDH.

The three dimensional arrangement of active site residues is identical in IPMDH and IcDH, and in fact the two can be superposed, Figure 4.6A. The HIcDH active site will likely also be identical with Mg-homoisocitrate bound. This is not surprising given the similarity of overall fold and complete conservation of all active site residues. The three dimensional arrangement of active site residues in the MEs is very similar to that of IcDH, but the active sites are mirror images, Figure 4.6B. This is consistent with the opposite stereochemistry at the Cα alcohol of L-malate and the D-isocitrate (and isopropylmalate). One of the water molecules in the metal ion coordination sphere in the IcDH subfamily takes the place of D279 in ME. The distance between the active site lysine ε-amine and tyrosine phenolic hydroxyl in the binary complex of ME is 3.3Å [32], but decreases to 2.9 Å in the closed quaternary E-NAD-Mg-malate complex form [107]. In the quaternary E-NAD-Mg-malate complex the distance from the lysine ε-amine and the malate α-hydroxyl is 2.8 Å, and it is thus set to act as a base in the overall reaction. The tyrosine phenolic hydroxyl is also in position to donate a proton to C3 of enolpyruvate. In the IcDH and IPMDH ternary E-M^{2+}-substrate complexes, the distance between the active site lysine ε-amine and tyrosine phenolic hydroxyl is ~3.7 Å, similar to that found in the open form of the MEs, while the distance between the lysine ε-amine and the substrate α-hydroxyl is ~3.5 Å, and is expected to be within hydrogen bonding distance in the closed form of the enzyme [100,105]. In addition to the difference in the active site stereochemistry between the MEs and IcDH subfamily, there are two other differences. First, the MEs have a catalytic aspartate (D278 in the human enzyme; see

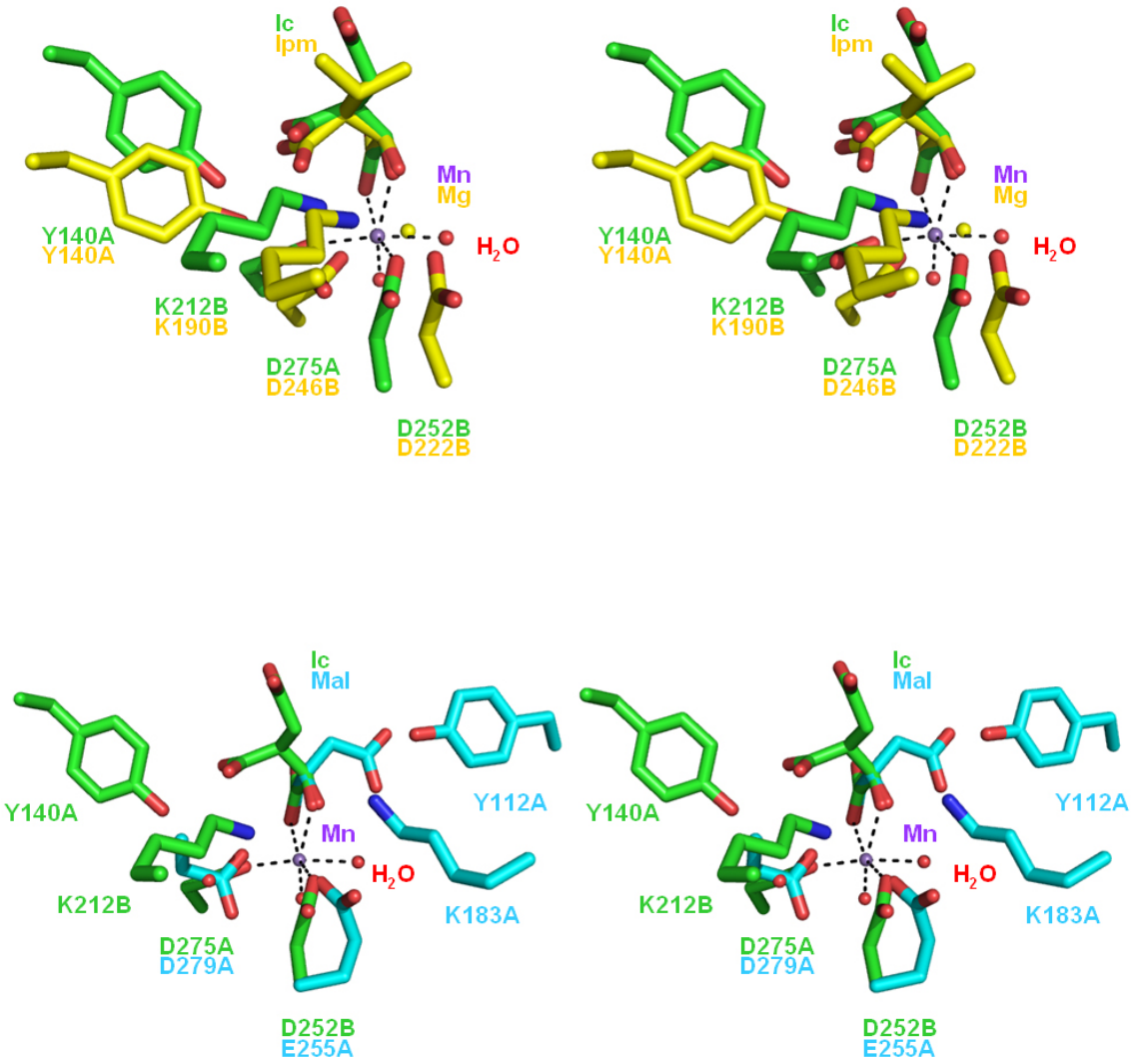

Figure 4.6 Stereoview of active site superpositions. A) The active sites of IcDH (PDB 1LWD) and IPMDH (PDB 1A05) are shown in green and yellow, respectively. The metal ion is shown as a purple ball (yellow for Mg) and water molecules are shown as red balls. B) The active sites of IcDH and ME (PDB 1PJ2) are shown in green and cyan, respectively. Coordination bonds to the metal ion are shown for one of the enzymes in both A and B. (This picture was created by Dr. Babak Andi).

Acid-base Chemical Mechanism below) that is absent in the IcDH subfamily. Second, two asparagine residues and an arginine are hydrogen-bonded to the substrate α-carboxylate in the MEs, while there are three arginine residues in the case of the IcDH subfamily. These changes almost certainly contribute to the catalytic mechanism in these two subfamilies.

Details of mechanism are discussed below. We begin with a discussion of the mechanism of the MEs and then discuss similarities and differences between the two subfamilies. Although the exact mechanism of the other oxidative decarboxylases (TDH and IPMDH) has not yet been determined, the arrangement of their active site residues and their spatial positions in those enzymes are very similar to those that have been well studied. Their chemical mechanisms are thus likely to be very similar to those discussed in detail below.

4.3. Acid-base chemical mechanism

4.3.1. Malic enzyme

The MEs are perhaps the best studied of any member of the class of pyridine dinucleotide-linked, metal ion-dependent β-hydroxyacid oxidative decarboxylases. The proposed acid-base mechanism is based on extensive kinetic studies including pH-rate profiles [43,46,109] and isotope effects [25,53,54,110-113], structural studies [32-35,38,107], and site-directed mutagenesis [3,28,55,56]. The current general acid/general base chemical mechanism was proposed on the basis of the E-NADH-Mn-malate structure [107] and site-directed mutagenesis studies of Karsten *et al.* [56]. The mechanism proceeds via the use of a catalytic triad.

In the open form of the enzyme, the active site lysine is within hydrogen-bonding distance to an active site aspartate, but not to the active site tyrosine. The structure of the closed form of the human and *Ascaris* NAD-malic enzymes [34,107], with cofactor, metal ion and substrate (or substrate analog) bound show the active site lysine within hydrogen-bonding distance to the substrate hydroxyl, and the active site tyrosine, which is properly positioned to deliver a proton to C3 of the enolpyruvate intermediate that results from oxidative decarboxylation. In addition, an aspartate that does not participate in coordination of the metal ion is in strong hydrogen-bonding distance to a glutamate that participates in coordinating the metal ion, Figure 5A. There is a net negative charge in the active site of the quaternary E-NAD-M^{2+}-malate complex. Four side chain carboxylates and the substrate carboxylates are partially balanced by the charge on the metal ion, the arginine that ion pairs the substrate α-carboxylate, the charge on the pyridine ring of the cofactor, and the charge of the catalytic lysine. Lysine requires assistance to act as a base and this is supplied by the aspartate that is in close proximity to the glutamate, which serves as a ligand to the metal ion, Figure 4.7.

The proposed mechanism of the *Ascaris* NAD-malic enzyme reaction, as an example, is shown in Figure 8 [56]. A catalytic triad, comprised of K199, Y126, and D294, was proposed to function for the MEs. The pH dependence of $V/K_{mal}\mathbf{E_t}$ decreases at low pH, giving a global pK_a of 5.6 reflecting the general base. Given the net negative active site, the initial hydrogen bonding of K199 and D294 in the open form, and close approach of D294 and E271 in the closed form suggests a strong hydrogen bond between D294 and E271, and a neutral K199 that can serve as a base, as suggested in Figure 4.8 (II). The lysine then serves to accept a proton from the hydroxyl of malate in the

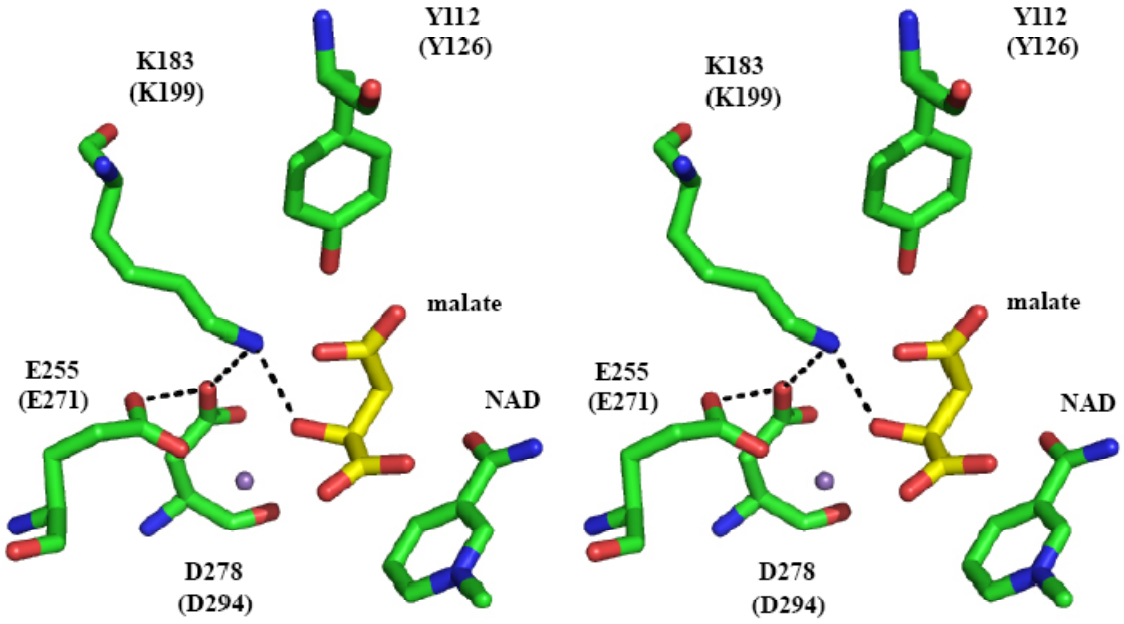

Figure 4.7 Stereoview of the active site structure and catalytic triad in the human ME (PDB 1PJ2). The corresponding residues for the *Ascaris* ME are shown in parenthesis. Distances between K183-D278 (2.8 Å), the malate 2'-OH and K183 (2.78 Å), and E255-D278 (2.6 Å) in the closed structure are shown; Mn^{2+} is shown as a purple ball. The figures are generated using the PyMOL molecular visualization program (website: http://pymol.sourceforge.net/).

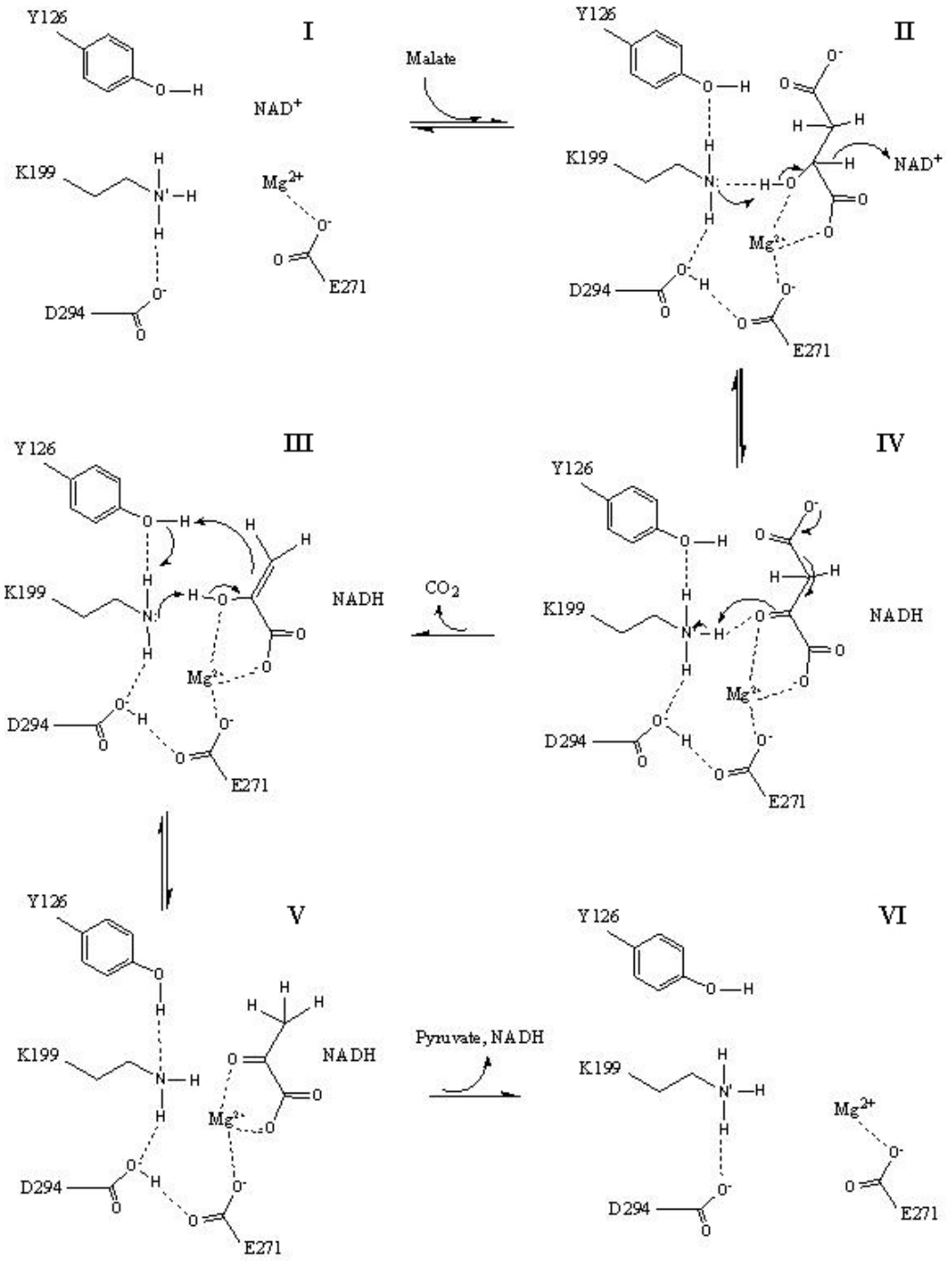

Figure 4.8 Proposed general acid/general base mechanism for *Ascaris* ME [56].

oxidation step to generate the oxaloacetate intermediate (III). The β-ketoacid is then activated for decarboxylation, and the majority of catalysis of this step is provided by the metal ion, acting as a Lewis acid to produce enolpyruvate, and with K199 donating a proton to the enol oxygen (IV). In agreement, kinetic ^{13}C isotope effects measured for divalent metal ion-catalyzed decarboxylation of oxaloacetate are very similar to the intrinsic ^{13}C kinetic isotope effects for decarboxylation of the oxaloacetate intermediate in the malic enzyme reaction, suggesting the enzyme simply provides the site for binding metal ion and reactant, and plays only a small catalytic role in this step of the reaction [52]. Finally, tautomerization of enolpyruvate to pyruvate proceeds via general base/general acid catalysis, with K199 accepting a proton from the enol and Y126 donating a proton to C3 to give pyruvate (V). Release of products, and proton rearrangement gives the catalytic triad in the same protonation state as at the beginning of the reaction (VI).

In support of the proposed mechanism are the structural studies cited above and studies of site-directed mutations of the three participants in the catalytic triad [56]. Mutation of K199 to R gave a 10-fold decrease in k_{cat}, but no change in the pK_a of the putative general base. However, mutation of D294, which is very close to E271, to A gave a 13,000-fold decrease in the rate, and a shift in the pK_a on the acid side to about 9.7 from 5.6. Thus, removal of the auxiliary catalyst that is required to deprotonate K199 so that it can serve as a base results in a pH dependence that is expected if K199 were acting alone.

Tautomerization is generally very fast compared to other steps along the ME reaction pathway, and as a result, the pK_a for the Y126 is not observed in the pH-rate

profiles. Mutation of Y126 to F gives a 60,000-fold reduction in the rate, consistent with its important role in catalysis. However, the pK_a of the general base in the Y126F mutant enzyme is 5.6, identical to that of the wild type enzyme.

Given the similarity in the active sites of the IcDH subfamily to that of ME, it is highly likely the same general mechanism applies in all cases. Of the enzymes in the IcDH subfamily, IcDH has been well studied, while data for HIcDH and TDH are not as extensive and only structural data are available for IPMDH. Each of these enzymes will be discussed below in terms of the mechanism proposed for the MEs.

4.3.2. Isocitrate dehydrogenase

The porcine ICDH has been extensively studied. The overall mechanism of the enzyme follows that shown in Scheme 1. We propose that, as is true for the MEs, the acid-base chemistry of the IcDH overall reaction is catalyzed by an active site lysine-tyrosine. On the basis of available structures [98,100,114,115], kinetic studies and site-directed mutagenesis [98-101,114,116-118], a mechanism has been proposed for IcDH. The wild type enzyme exhibits a pK_a of about 5.2 for a group that must be unprotonated for optimal activity [101]. The pK_a was assigned to the ionization of the metal-bound hydroxyl of isocitrate. Tyrosine 140, which corresponds to Y126 in the *Ascaris* ME was proposed to be the general acid that protonates the enol to give α-ketoglutarate [116]. Below, the proposed mechanism will first be considered, and then data obtained for IcDH will be considered in terms of a catalytically active Lys-Tyr pair.

Data support the proposed role of Y140 as the general acid that must protonate the enol of α-ketoglutarate to generate the ketone product [116]. Changing the tyrosine to a side chain that cannot function over the pH range 5-9, i.e., phenylalanine which is

missing the phenolic hydroxyl, and threonine, which has a pK_a >14, results in a very low pH independent basal activity that is 400-fold lower than that of wild type. A change to glutamate and lysine gives enzymes that exhibit pH dependence with observed pK_a values of 6.4 and 6.75, respectively, for a group that must be protonated for optimal activity. Finally, the detritiation of α-ketoglutarate requires the presence of Y140.

Data are not as clear in the assignment of the group with a pK_a of 5.2 observed in the k_{cat} profile of the wild type enzyme. Changing K212 to Q, which does not allow it to function as a base, does not eliminate the pH dependence of k_{cat}, but does give a 540-fold decrease in the rate and a shift in the pK_a to 7.5; a pH independent basal level of activity about 1000-fold lower than that of wild type is observed at pH values <6.5. On the other hand, a change to R, gives only a 10-fold change, and no change in the observed pK_a, similar to the behavior of ME [56]. Clearly, the observed pK_a does not reflect K212, but its value is influenced by the positively-charged side chain in agreement with the authors' suggestion [116]. The lysine side chain must have a function in the reaction in addition to an electrostatic effect on the pK_a of another group, however, since the activity is decreased >500-fold. Two other lines of evidence are used to assign the pK_a of 5.2 to the hydroxyl of isocitrate, *viz*., site-directed mutagenesis to change conserved active site aspartate side chains and replacement of the metal ion that chelates isocitrate [101]. On the basis of structural data, two of the aspartate residues serve as ligands to the metal ion in the active site, D252 and D275, while the third, D279, is in the vicinity of the metal-isocitrate complex and hydrogen-bonded to two water molecules [34]. Replacement of D252 or D275 by cysteine gives similar pK_a values for k_{cat} but a decrease in rate by 3.6-fold and 2.7-fold, respectively, consistent with a change in the electronic properties of the

metal ion, which must serve as a Lewis acid in the decarboxylation reaction. Of interest, the observed pK_a is unchanged, which is not consistent with the ionization of the metal bound hydroxyl of isocitrate. Replacement of D279 by C, however, gives a lower pK_a of 4.7, and a 240-fold lower rate, consistent with the weaker hydrogen-bonding ability of the cysteine thiol(ate). Metal ion replacement, e.g., Mn^{2+} to Co^{2+} gave observed pK_a values in k_{cat} of 5.24 to 5.07, which the authors suggest are significantly different in support of ionization of the metal coordinated isocitrate hydroxyl [101]. The pK_a values 5.24 and 5.07 are likely actually within error equal (standard errors obtained are too low given the data reported by the authors. On the basis of hundreds of pH-rate profiles obtained by PFC, the standard errors on the pK_a values are likely about 0.2. It is likely that at least a portion of the difference results from log to ln conversions, in the error analysis). In agreement, a similar metal replacement study by Auld and Valee [119] gave a shift in the pK_a of carboxypeptidase from 6.36 to 5.33 as expected given the pK_a values of 10.6 and 9.7 for hydrolysis $(Mn\text{-}OH_2)^{2+}$ and $(Co\text{-}OH_2)^{2+}$, respectively [120]. Also of interest, changing R110 and R133 (within hydrogen-bonding distance to the substrate α-carboxylate of isocitrate) to Q results in increasing the pK_a in the k_{cat} pH-rate profile to 6.4 and 7.4, respectively [34]. Thus, positive charge in the active site is clearly important.

If the pK_a observed in the k_{cat} pH-rate profile is not that of the metal-isocitrate hydroxyl, how can the data be reconciled? It is likely given the close similarity in the active sites of the MEs and the IcDH subfamily that the lysine-tyrosine pair functions in an acid-base role in IcDH as for ME. However, it is clear that the residue responsible for the pK_a in the k_{cat} pH-rate profile is not lysine, but is influenced greatly by its

environment. Specifically, a decrease in positive charge results in an increase in the pK_a, suggesting either a positively-charged group in the vicinity of K212, which would have a lower pK_a as a result of electrostatic repulsion of the two groups when protonated, or a neutral acid, which would be preferentially ionized in a positive site. The only positively charged groups in the active site, beside K212 and the metal ion are the three arginine residues in the vicinity of the substrate α-carboxylate and the nicotinamide of NAD^+. However, D279 or one of the other aspartate side chains, either directly or via hydrogen-bonded water, could certainly function to deprontonate K212 in a manner similar to that proposed for ME. In this regard, one must remember that the structure available is that of the E-Mn-isocitrate complex. It is possible, for example, that one of the two aspartates that serves as metal ion ligands serves as a catalyst to deprotonate K212 and that D279 acts as a ligand to the metal ion in the quaternary E-NADP-Mn-isocitrate complex. We suggest a triad similar to that observed for ME functions to catalyze the Ic oxidative decarboxylation with another active site group, e.g., an aspartate, required to deprotonate K212, which functions as the general base to deprotonate the Ic hydroxyl, while Y140 functions as the general acid to protonate the enol. Elimination of positive charge in the site will cause an increase in the pK_a of the aspartate, while elimination of the aspartate will give the pK_a of the lysine unless the new side chain can function as a base, as in H or C. The proposed mechanism also explains the relatively high activity observed for the K212R mutant enzyme. The pK_a of the δ-guanidinium of arginine is 2 pH units higher than that of the ε-amine of lysine, and thus one might expect a 100-fold decrease in the rate with R212 as the base catalyst in place of K212, and not the 10-fold change observed. However, the chemical steps do not contribute to rate limitation in the case of

the wild type enzyme and must be at least 10-times faster than structural changes required to set up the site for catalysis. In agreement, on the basis of the pH dependence of isotope effects, Grissom and Cleland estimate that catalysis is 16 times faster than substrate dissociation [52].

A pH independent basal level of activity was observed for several mutant enzymes. The K212Q mutant enzyme exhibits a 1000-fold lower rate than k_{cat} of the wild type enzyme at pH values <6.5. The Y140F and Y140T mutant enzymes exhibit a 400-fold lower rate than that of the wild type enzyme over the pH range 5-9. The basal activity is still much greater than that of the uncatalyzed reaction, and must be due to a combination of catalysis by the remaining catalytic group, water and the metal ion. A series of double mutations could be used to sort this out using a mutant cycle analysis.

4.3.3. Homoisocitrate dehydrogenase

Although not as much data are available for HIcDH, data are consistent with the action of a lysine-tyrosine pair, consistent with the active site structure of the enzyme. The pH-rate profiles obtained with HIc as the substrate exhibit significant pK_a perturbation as a result of substrate stickiness [27]. However, Ic is a slow substrate for HIcDH, and was very useful in interpreting the pH-rate profiles in general. A single base was observed in the k_{cat} and k_{cat}/K_{Ic} profiles with a pK_a of about 7. Site-directed mutagenesis of K206 and Y150 resulted in dramatic changes in the pH-rate profiles. The k_{cat} for the K206M mutant enzyme is pH independent below pH 8, and increases at higher pH values to a constant value above pH 9.5, giving a pK_a of about 9.3 (unpublished data of Y. Lin in this lab). The Y150F mutant enzyme is pH independent above pH 7, and increases as the pH is decreased to a constant value below 5.5, giving a pK_a of about 6

(unpublished data of Y. Lin in this lab). Data are consistent with Y150 acting as a base in the reaction catalyzed by the Y150F mutant enzyme, and K206 acting as an acid in the K206M mutant enzyme. The pK_a of the Y150 in the absence of K206 is 9.3, while that of K206 in the absence on Y150 is about 6. The most reasonable explanation is the presence of a Lys-Tyr ion pair in the wild type enzyme with a pK_a of about 7. The low pK_a for K206 in the mutant enzyme likely results from the highly positive nature of the active site, with 3 arginine residues, the positive charge on NAD, and the metal ion. The pH independent basal activity exhibited by K206M below pH 8 and Y150F above pH 7 is likely explained as for the IcDH mutant enzymes (see above).

4.3.4. Isopropylmalate and tartrate dehydrogenases

There is only very limited data in available for possible catalytic residues of IPMDH and TDH. Miyazaki *et al*. [121] mutated Y139, which corresponds to the general acid in other enzymes, to F in *Thermus thermophilus* IPMDH, and observed the k_{cat} was reduced to 7% of the wild type, confirming the importance of the hydroxyl group of the tyrosine in catalysis.

For TDH, there is no study that points out the importance of any of the conserved residues, however, as for IPMDH, the similarity of the arrangement of the lysine-tyrosine pair to the one in the MEs, IcDH, HIcDH, and IPMDH, suggests a chemical mechanism very similar to that of the other enzymes.

4.4. Overall

All of the metal ion-dependent, pyridine nucleotide-dependent β-hydroxyacid oxidative decarboxylases utilize a lysine-tyrosine pair to carry out the acid-base catalysis

in the oxidation, decarboxylation, and tautomerization steps of the overall reaction. The lysine ε-amine functions as the base in the reaction, and the phenolic hydroxyl of tyrosine functions as the proton donor in the tautomerization reaction. However, the way the enzymes utilize the catalytic pair differs. In the case of the MEs and IcDH, there is apparently a group, an aspartate carboxylate in the case of ME, that assists in generating the neutral amine, while for HIcDH, this auxiliary catalyst is not utilized and the lysine-tyrosine pair functions directly. Some of the differences are almost certainly due to the amount of positive charge in the active sites of the respective enzymes. The MEs have less positive charge because two of the three arginines that interact with the substrate α-carboxylate in the IcDH subfamily are asparagines in the MEs.

A number of enzymes have a lysine and tyrosine in their active site. This pair of residues provides advantages for enzymes that catalyze acid-base chemistry. Given their equal solution pK_a values of 10.5, the two residues, if in close proximity, can ion pair as NH_3^+--O^- or hydrogen bond as NH_2--HO, such that reactant binding can select one or the other form. In addition, since one is a neutral acid, and the other a cationic acid the environment of the active site, once it closes in preparation for catalysis can generate differences in the pK_a values of the two residues, resulting in a broader pH independent reaction range.

CHAPTER 5:

5.1. Overall Discussion and Conclusion

Malic enzyme has been studied for more than 60 years. Its overall kinetic and chemical mechanisms are well determined, and its structure was obtained from various organisms. Although vast amount of information exists on this enzyme, there are still gaps to be filled in on the cofactor binding site and the role of residues surrounding the site. This work has focused on the detailed mechanism of NAD binding and specificity and it has contributed to the overall knowledge of the reaction catalyzed by malic enzyme, specifically, and the class of pyridine nucleotide β-hyroxyacid oxidative decarboxylases in general.

The first part of the project was to investigate the contribution of binding energy and catalysis of the groups that interact with the nicotinamide and ribose rings of NAD. The results suggested that the correct orientation of the NAD is crucial for the reaction. If it is not in the proper position, significant decrease in the rate of the reaction, nonproductive binding of the cofactor and even a change in the kinetic mechanism of the enzyme can be observed. The second part of the project focused on the roles of residues surrounding the adenosine binding site of NAD. It was shown that eliminating a single ionic interaction between residues in the NAD adenosine binding site was enough to decrease or eliminate all catalytic activity of the enzyme. In addition, cofactor specificity could not be changed to favor NADP. Thus, binding of cofactor 2'-phosphate requires a collective interaction of many residues.

Single mutations to specific residues interacting with the nicotinamide ring, where hydride transfer occurs, was enough to change how the enzyme worked and indicated the delicate balance in the overall enzymatic reaction. As an example, one of the mutant enzymes (N479Q) exhibited a concerted oxidative decarboxylation of malate, instead of the stepwise mechanism observed for the wild type. The most likely explanation for this behavior was that the malate should be able to bind in the proper conformation for the decarboxylation to happen simultaneously with hydride transfer. In the wild type enzyme, hydride transfer precedes decarboxylation because when malate is bound with its C4 in the C2-C3 plane it is not able to undergo decarboxylation. However, in a concerted mechanism, malate is already bound with its β-carboxyl group out of C2-C3 plane and trans to the hydride to be transferred to C4 of the nicotinamide ring of NAD. This might give an impression that this is a more efficient way to catalyze the reaction, whereas the wild type enzyme has to do it by a stepwise mechanism. However, in this case the overall rate of the reaction decreased more than three orders of magnitude, indicating there was something not feasible with this mechanism. The switch from stepwise to concerted mechanism was also observed with alternative nucleotides. These data suggest that NAD binding has an important role in orienting malate for catalysis. Therefore, N479Q mutation caused the cofactor to bind a in a different conformation which in turn affected the bound configuration of malate, changing its binding orientation for catalysis. For the fully active enzyme, both NAD and malate must bind in proper conformation and orientation. This is only one of the examples indicating how the nature of the active site of this enzyme has been perfected through evolution.

Although the nicotinamide portion of the cofactor has a role in the hydride transfer, the binding of the adenosine portion of NAD, which is relatively distant from the active site, is also important. A single point mutation, changing an aspartate residue (D361) that helps to orient the adenine ring of the cofactor results in an inactive enzyme. When the closed structure of the enzyme with NAD-Mn-malate bound is overlayed against the structure with ATP-Mn-malate bound, the spatial positions and orientations of the catalytic residues and substrates are the same, Figure 5.1 . Data indicate that binding of the adenosine portion of the cofactor, rather than the nicotinamide portion, is important for the catalytic conformation of the enzyme.

Information on a particular enzyme can be helpful when it comes to interpret data for another one, especially if the enzymes are in the same class. It will also be helpful generalizing the working principles of the class by projecting the knowledge obtained from one enzyme to others in the same class that have little mechanistic information available. The last part of this dissertation on oxidative decarboxylases provides an example of this. The extensive knowledge we have obtained on malic enzymes was used as a probe to interpret the data obtained for other oxidative decarboxylases, such as isocitrate dehydrogenase.

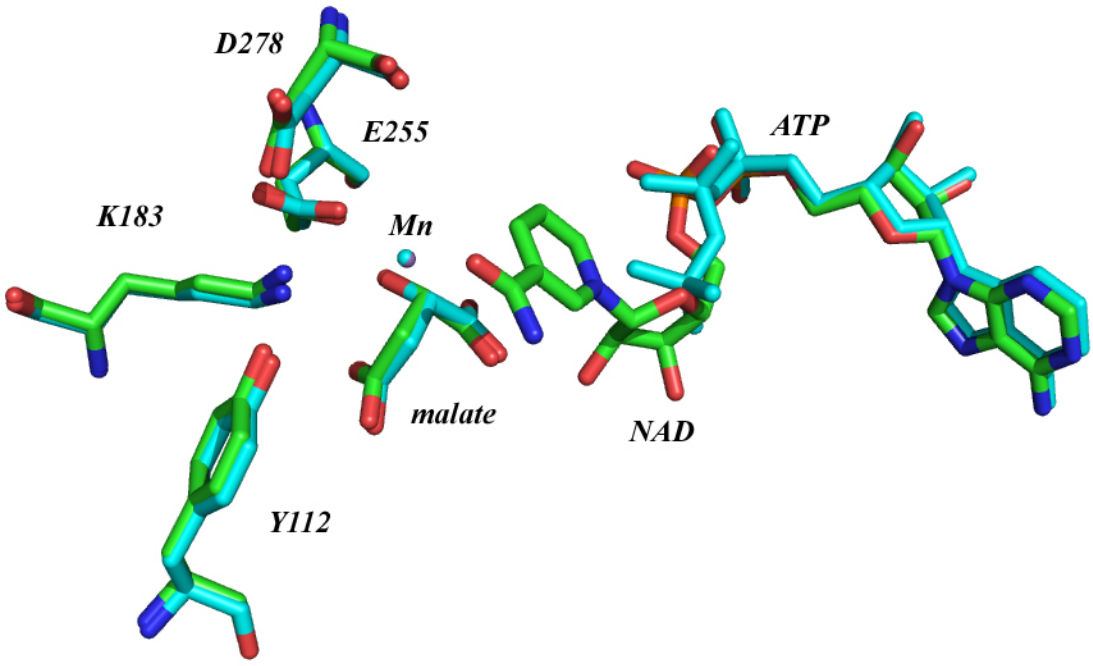

Figure 5.1 Overlay of human ME with NAD-Mn-malate bound (PDB:1PJ2) against ATP-Mn-malate bound (PDB:1PJ4) structure. NAD bound structure is shown in green, whereas ATP bound structure is shown in cyan. The figures are generated by PyMOL molecular visualization program (website: http://pymol.sourceforge.net/).

REFERENCES

1. Karsten, W. E. and Cook, P. F. (2000) Pyridine nucleotide-dependent beta-hydroxyacid oxidative decarboxylases: An overview, *Protein and Peptide Lett. 7*, 281-286.

2. Zhang, L. and Cook, P. F. (2000) Chemical mechanism of 6-phosphogluconate dehydrogenase via kinetic studies and site-directed mutagenesis, *Protein and Peptide Lett. 7*, 313-322.

3. Dali Liu (2001) Elucidating the catalytic mechanism of malic enzyme via site-directed mutagenesis studies, PhD Dissertation, The University of Oklahoma, Norman, Oklahoma, USA.

4. Evans, E. A. and Slotin, L. (1940) The utilization of carbon dioxide in the synthesis of alpha-ketoglutaric acid, *J. Biol. Chem. 136*, 301-302.

5. Moulder, J. W., Vennesland, B., and Evans, E. A. (1945) A study of enzymic reactions catalyzed by pigeon liver extracts, *J. Biol. Chem. 160*, 305-325.

6. Ochoa, S., Mehler, A. H., and Kornberg, A. (1947) Reversible oxidative decarboxylation of malic acid, *Fed. Proc. 6*, 282.

7. Ochoa, S., Mehler, A., Blanchard, M. L., Jukes, T. H., Hoffmann, C. E., and Regan, M. (1947) Biotin and carbon dioxide fixation in liver, *J. Biol. Chem. 170*, 413-414.

8. Maurino, V. G., Drincovich, M. F., Casati, P., Andreo, C. S., Edwards, G. E., Ku, M. S. B., Gupta, S. K., and Franceschi, V. R. (1997) NADP-malic enzyme: Immunolocalization in different tissues of the C-4 plant maize and the C-3 plant wheat, *J. Exp. Bot. 48*, 799-811.

9. Maurino, V. G., Drincovich, M. F., and Andreo, C. S. (1996) NADP-malic enzyme isoforms in maize leaves, *Biochem. Mol. Biol. Int. 38*, 239-250.

10. Pinto, M. E., Casati, P., Hsu, T. P., Ku, M. S. B., and Edwards, G. E. (1999) Effects of UV-B radiation on growth, photosynthesis, UV-B-absorbing compounds and NADP-malic enzyme in bean (Phaseolus vulgaris L.) grown under different nitrogen conditions, *J. Photoch. Photobio. B 48*, 200-209.

11. Casati, P., Drincovich, M. F., Edwards, G. E., and Andreo, C. S. (1999) Malate metabolism by NADP-malic enzyme in plant defense, *Photosynth. Res. 61*, 99-105.

12. Rognstad, R. and Katz, J. (1966) Balance of pyridine nucleotides and ATP in adipose tissue, *P. Natl. Acad. Sci. USA 55*, 1148-1150.

13. Rognstad, R. and Katz, J. (1979) Effects of 2,4-dihydroxybutyrate on lipogenesis in rat hepatocytes, *J. Biol. Chem. 254*, 1969-1972.

14. Kuriharcuch, W. and Green, H. (1977) Increasing activity of enzymes on pathway of triacylglycerol synthesis during adipose conversion of 3T3 cells, *J. Biol. Chem. 252*, 2158-2160.

15. Ayala, A., Flobato, M., and Machado, A. (1986) Malic enzyme levels are increased by the activation of NADPH-consuming pathways - Detoxification processes, *FEBS Lett. 202*, 102-106.

16. Sauer, L. A. and Dauchy, R. T. (1978) Activity and properties of NAD(P)-dependent malic enzyme in mouse ascites tumor mitochondria, *Fed. Proc. 37*, 1717.

17. Sauer, L. A., Dauchy, R. T., Nagel, W. O., and Morris, H. P. (1980) Mitochondrial malic enzymes - Mitochondrial $NAD(P)^+$-dependent malic enzyme activity and malate-dependent pyruvate formation are progression linked in morris hepatomas, *J. Biol. Chem. 255*, 3844-3848.

18. Loeber, G., Dworkin, M. B., Infante, A., and Ahorn, H. (1994) Characterization of cytosolic malic enzyme in human tumor cells, *FEBS Lett. 344*, 181-186.

19. Reitzer, L. J., Wice, B. M., and Kennell, D. (1979) Evidence that glutamine, not sugar, is the major energy source for cultured hela cells, *J. Biol. Chem. 254*, 2669-2676.

20. Mckeehan, W. L. (1982) Glycolysis, glutaminolysis and cell proliferation, *Cell Biol. Int. Rep. 6*, 635-650.

21. Saz, H. J. and Hubbard, J. A. (1957) The oxidative decarboxylation of malate by *Ascaris lumbricoides*, *J. Biol. Chem. 225*, 921-933.

22. Saz, H. J. (1981) Energy metabolisms of parasitic helminths - Adaptations to parasitism, *Annu. Rev. of Physiol. 43*, 323-341.

23. Allen, B. L. and Harris, B. G. (1981) Purification of malic enzyme from *Ascaris suum* using NAD^+-agarose, *Mol. Biochem. Parasit. 2*, 367-372.

24. Lai, C. J., Harris, B. G., and Cook, P. F. (1992) Mechanism of activation of the NAD-malic enzyme from *Ascaris suum* by fumarate, *Arch. Biochem. Biophys. 299*, 214-219.

25. Karsten, W. E. and Cook, P. F. (1994) Stepwise versus concerted oxidative decarboxylation catalyzed by malic enzyme - A reinvestigation, *Biochemistry 33*, 2096-2103.

26. Kulkarni, G., Cook, P. F., and Harris, B. G. (1993) Cloning and nucleotide-sequence of a full-length cDNA-encoding *Ascaris suum* malic enzyme, *Arch. Biochem. Biophys. 300*, 231-237.

27. Chooback, L., Karsten, W. E., Kulkarni, G., Nalabolu, S. R., Harris, B. G., and Cook, P. F. (1997) Expression, purification, and characterization of the recombinant NAD-malic enzyme from *Ascaris suum*, *Protein Expres. Purif. 10*, 51-54.

28. Karsten, W. E., Chooback, L., Liu, D., Hwang, C. C., Lynch, C., and Cook, P. F. (1999) Mapping the active site topography of the NAD-malic enzyme via alanine-scanning site-directed mutagenesis, *Biochemistry 38*, 10527-10532.

29. Baker, P. J., Thomas, D. H., Barton, C. H., Rice, D. W., and Bailey, E. (1987) Crystallization of an $NADP^+$-dependent malic enzyme from rat liver, *J. Mol. Biol. 193*, 233-235.

30. Clancy, L. L., Rao, G. S. J., Finzel, B. C., Muchmore, S. W., Holland, D. R., Watenpaugh, K. D., Krishnamurthy, H. M., Sweet, R. M., Cook, P. F., Harris, B. G., and Einspahr, H. M. (1992) Crystallization of the NAD-dependent malic enzyme from the parasitic nematode *Ascaris suum*, *J. Mol. Biol. 226*, 565-569.

31. Tsai, L. C., Kuo, C. C., Chou, W. Y., Chang, G. G., and Yuan, H. S. (1999) Crystallization and preliminary X-ray diffraction analysis of malic enzyme from pigeon liver, *Acta Crystallogr .D. 55*, 1930-1932.

32. Xu, Y. W., Bhargava, G., Wu, H., Loeber, G., and Tong, L. (1999) Crystal structure of human mitochondrial $NAD(P)(^+)$-dependent malic enzyme: A new class of oxidative decarboxylases, *Struct. Fold. Des. 7*, 877-889.

33. Coleman, D. E., Rao, G. S. J., Goldsmith, E. J., Cook, P. F., and Harris, B. G. (2002) Crystal structure of the malic enzyme from *Ascaris suum* complexed with nicotinamide adenine dinucleotide at 2.3 angstrom resolution, *Biochemistry 41*, 6928-6938.

34. Rao, G. S. J., Coleman, D. E., Karsten, W. E., Cook, P. F., and Harris, B. G. (2003) Crystallographic studies on *Ascaris suum* NAD-malic enzyme bound to reduced cofactor and identification of an effector site, *J. Biol. Chem. 278*, 38051-38058.

35. Chang, G. G. and Tong, L. (2003) Structure and function of malic enzymes, a new class of oxidative decarboxylases, *Biochemistry 42*, 12721-12733.

36. Hung, H. C., Chang, G. G., Yang, Z. R., and Tong, L. (2000) Slow binding of metal ions to pigeon liver malic enzyme: A general case, *Biochemistry 39*, 14095-14102.

37. Landsperger, W. J. and Harris, B. G. (1976) NAD^+-malic enzyme - Regulatory properties of enzyme from *Ascaris suum*, *J. Biol. Chem. 251*, 3599-3602.

38. Yang, Z. R., Floyd, D. L., Loeber, G., and Tong, L. (2000) Structure of a closed form of human malic enzyme and implications for catalytic mechanism, *Nat. Struct. Biol. 7*, 251-257.

39. Karsten, W. E. and Cook, P. F. (2007) The multiple roles of arginine-181 in binding and catalysis in the NAD-malic enzyme from *Ascaris suum*, *Biochemistry 46*, 14578-14588.

40. Cervellati, C., Dallocchio, F., Bergamini, C. M., and Cook, P. F. (2005) Role of methionine-13 in the catalytic mechanism of 6-phosphogluconate dehydrogenase from sheep liver, *Biochemistry 44*, 2432-2440.

41. Li, L., Zhang, L., and Cook, P. F. (2006) Role of the S128, H186, and N187 triad in substrate binding and decarboxylation in the sheep liver 6-phosphogluconate dehydrogenase reaction, *Biochemistry 45*, 12680-12686.

42. Hsu, R. Y. and Lardy, H. A. (1967) Pigeon liver malic enzyme. 2. Isolation crystallization and some properties, *J. Biol. Chem. 242*, 520-526.

43. Park, S. H., Harris, B. G., and Cook, P. F. (1986) pH-dependence of kinetic parameters for oxalacetate decarboxylation and pyruvate reduction reactions catalyzed by malic enzyme, *Biochemistry 25*, 3752-3759.

44. Landsperger, W. J., Fodge, D. W., and Harris, B. G. (1978) Kinetic and isotope partitioning studies on NAD^+-malic enzyme from *Ascaris suum*, *J. Biol. Chem. 253*, 1868-1873.

45. Park, S. H., Kiick, D. M., Harris, B. G., and Cook, P. F. (1984) Kinetic mechanism in the direction of oxidative decarboxylation for NAD-malic enzyme from *Ascaris suum*, *Biochemistry 23*, 446-5453.

46. Kiick, D. M., Harris, B. G., and Cook, P. F. (1986) Protonation mechanism and location of rate-determining steps for the *Ascaris suum* nicotinamide adenine-dinucleotide malic enzyme reaction from isotope effects and pH studies, *Biochemistry 25*, 227-236.

47. Chen, C. Y., Harris, B. G., and Cook, P. F. (1988) Isotope partitioning for NAD malic enzyme from *Ascaris suum* confirms a steady-state random kinetic mechanism, *Biochemistry 27*, 212-219.

48. Mallick, S., Harris, B. G., and Cook, P. F. (1991) Kinetic mechanism of NAD-malic enzyme from *Ascaris suum* in the direction of reductive carboxylation, *J. Biol. Chem. 266*, 2732-2738.

49. Cook, P. F. and Cleland, W. W. (1981) pH variation of isotope effects in enzyme-catalyzed reactions. 1. Isotope-dependent and pH-dependent steps the same, *Biochemistry 20*, 1797-1805.

50. Rajapaksa, R., Abusoud, H., Raushel, F. M., Harris, B. G., and Cook, P. F. (1993) Pre-steady-state kinetics reveal a slow isomerization of the enzyme-NAD complex in the NAD-malic enzyme reaction, *Biochemistry 32*, 1928-1934.

51. Hermes, J. D., Roeske, C. A., Oleary, M. H., and Cleland, W. W. (1982) Use of multiple isotope effects to determine enzyme mechanisms and intrinsic isotope effects - Malic enzyme and glucose-6-phosphate-dehydrogenase, *Biochemistry 21*, 5106-5114.

52. Grissom, C. B. and Cleland, W. W. (1988) Isotope effect studies of chicken liver NADP malic enzyme - Role of the metal-ion and viscosity dependence, *Biochemistry 27*, 2927-2934.

53. Weiss, P. M., Gavva, S. R., Harris, B. G., Urbauer, J. L., Cleland, W. W., and Cook, P. F. (1991) Multiple isotope effects with alternative dinucleotide substrates as a probe of the malic enzyme reaction, *Biochemistry 30*, 5755-5763.

54. Edens, W. A., Urbauer, J. L., and Cleland, W. W. (1997) Determination of the chemical mechanism of malic enzyme by isotope effects, *Biochemistry 36*, 1141-1147.

55. Liu, D., Karsten, W. E., and Cook, P. F. (2000) Lysine 199 is the general acid in the NAD-malic enzyme reaction, *Biochemistry 39*, 11955-11960.

56. Karsten, W. E., Liu, D. L., Rao, G. S. J., Harris, B. G., and Cook, P. F. (2005) A catalytic triad is responsible for acid-base chemistry in the *Ascaris suum* NAD-malic enzyme, *Biochemistry 44*, 3626-3635.

57. Karsten, W. E., Pais, J. E., Rao, G. S. J., Harris, B. G., and Cook, P. F. (2003) *Ascaris suum* NAD-malic enzyme is activated by L-malate and fumarate binding to separate allosteric sites, *Biochemistry 42*, 9712-9721.

58. Sauer, L. A. (1973) NAD-dependent malic enzyme and NADP-dependent malic enzyme with regulatory properties in rat liver and adrenal cortex mitochondrial fractions, *Biochem. Bioph. Res. Co. 50*, 524-531.

59. Dozin, B., Magnuson, M. A., and Nikodem, V. M. (1985) Tissue-specific regulation of 2 functional malic enzyme messenger-RNAs by triiodothyronine, *Biochemistry 24*, 5581-5586.

60. Tepperman, H. M., Tepperman, J., Pownall, J. D., and Branch, A. (1964) Patterns of dietary hormonal induction of certain NADP-linked liver enzymes, *Am. J. Physiol. 206*, 357-361.

61. Goldman, M. J., Back, D. W., and Goodridge, A. G. (1985) Nutritional regulation of the synthesis and degradation of malic enzyme messenger-RNA in duck liver, *J. Biol. Chem. 260*, 4404-4408.

62. Saz, H. J. (1971) Anaerobic phosphorylation in *Ascaris* mitochondria and effects of anthelmintics, *Comp. Biochem. Phys. 39*, 627-637.

63. Seidman, I. and Entner, N. (1961) Oxidative enzymes and their role in phosphorylation in sarcosomes of adult *Ascaris lumbricoides*, *J. Biol. Chem. 236*, 915-919.

64. Chen, C. Y., Harris, B. G., and Cook, P. F. (1988) Isotope partitioning for NAD malic enzyme from *Ascaris suum* confirms a steady-state random kinetic mechanism, *Biochemistry 27*, 212-219.

65. Bradford, M. M. and Williams, W. L. (1976) New, rapid, sensitive method for protein determination, *Fed. Proc. 35*, 274.

66. O'Leary, M. H. (1980) Determination of heavy-atom isotope effects on enzyme-catalyzed reactions., *Methods Enzymol. 64 (Enzyme Kinet. Mech., Part B)*, 83-104.

67. Craig, N. (1957) Isotopic standards for carbon and oxygen and correction factors for mass-spectrometric analysis of CO_2, *Geochim. Cosmochim. Acta. 12*, 133-140.

68. Cleland, W. W. (1979) Statistical analysis of enzyme kinetic data, *Methods Enzymol. 63*, 103-138.

69. Cook, P. F., Blanchard, J. S., and Cleland, W. W. (1980) Primary and secondary deuterium isotope effects on equilibrium constants for enzyme catalyzed reactions, *Biochemistry 19*, 4853-4858.

70. Klinman, J. P. and Matthews, R. G. (1985) Calculation of substrate dissociation constants from steady-state isotope effects in enzyme catalyzed reactions, *J. Am. Chem. Soc. 107*, 1058-1060.

71. Yang, Z. R., Zhang, H. L., Hung, H. C., Kuo, C. C., Tsai, L. C., Yuan, H. S., Chou, W. Y., Chang, G. G., and Tong, L. (2002) Structural studies of the pigeon cytosolic NADP($^+$)-dependent malic enzyme, *Protein Sci. 11*, 332-341.

72. Loeber, G., Infante, A. A., Maurerfogy, I., Krystek, E., and Dworkin, M. B. (1991) Human NAD^+-dependent mitochondrial malic enzyme, *FASEB J. 5*, A839.

73. Hsu, R. Y. and Lardy, H. A. (1967) Pigeon liver malic enzyme. 3. Fluorescence studies of coenzyme binding, *J. Biol. Chem. 242*, 527-532.

74. Hsieh, J. Y., Liu, G. Y., Chang, G. G., and Hung, H. C. (2006) Determinants of the dual cofactor specificity and substrate cooperativity of the human

mitochondrial NAD(P)($^+$)-dependent malic enzyme - Functional roles of glutamine 362, *J. Biol. Chem. 281*, 23237-23245.

75. Aktas, D. F. and Cook, P. F. (2008) Proper positioning of the nicotinamide ring is crucial for the *Ascaris suum* malic enzyme reaction, *Biochemistry 47*, 2539-2546.

76. Kuo, C. C., Tsai, L. C., Chin, T. Y., Chang, G. G., and Chou, W. Y. (2000) Lysine residues 162 and 340 are involved in the catalysis and coenzyme binding of NADP($^+$)-dependent malic enzyme from pigeon, *Biochem. Biophys. Res. Co. 270*, 821-825.

77. Scrutton, N. S., Berry, A., and Perham, R. N. (1990) Redesign of the coenzyme specificity of a dehydrogenase by protein engineering, *Nature 343*, 38-43.

78. Hurley, J. H., Chen, R. D., and Dean, A. M. (1996) Determinants of cofactor specificity in isocitrate dehydrogenase: Structure of an engineered NADP($^+$)-NAD($^+$) specificity reversal mutant, *Biochemistry 35*, 5670-5678.

79. Ochoa, S., Mehler, A. H., and Kornberg, A. (1948) Biosynthesis of dicarboxylic acids by carbon dioxide fixation. 1. Isolation and properties of an enzyme from pigeon liver catalyzing the reversible oxidative decarboxylation of L-malic acid, *J. Biol. Chem. 174*, 979-1000.

80. Kaufman, S., Korkes, S., and Delcampillo, A. (1951) Biosynthesis of dicarboxylic acids by carbon dioxide fixation. 5. Further study of the malic enzyme of *Lactobacillus arabinosus*, *J. Biol. Chem. 192*, 301-312.

81. Kornberg, A. and Pricer, W. E. (1951) Diphosphopyridine and triphosphopyridine nucleotide isocitric dehydrogenases in yeast, *J. Biol. Chem. 189*, 123-136.

82. Agosin, M. and Weinbach, E. C. (1956) Partial purification and characterization of the isocitric dehydrogenase from *Trypanosoma cruzi*, *Biochim. Biophys. Acta 21*, 117-126.

83. Moyle, J. (1956) Some properties of purified isocitric enzyme, *Biochem. J. 63*, 552-558.

84. Burns, R. O., Umbarger, H. E., and Gross, S. R. (1963) Biosynthesis of leucine. 3. Conversion of alpha-hydroxy-beta-carboxyisocaproate to alpha-ketoisocaproate, *Biochemistry 2*, 1053-1058.

85. Hsu, Y. P. and Kohlhaw, G. B. (1980) Leucine biosynthesis in *Saccharomyces cerevisiae* - Purification and characterization of beta-isopropylmalate dehydrogenase, *J. Biol. Chem. 255*, 7255-7260.

86. Strassman, M. and Ceci, L. N. (1965) Enzymatic formation of alpha-ketoadipic acid from homoisocitric acid, *J. Biol. Chem. 240*, 4357-4361.

87. Rowley, B. and Tucci, A. F. (1970) Homoisocitric dehydrogenase from yeast, *Fed. Proc. 29*, A922-933.

88. Kohn, L. D., Packman, P. M., Allen, R. H., and Jakoby, W. B. (1968) Tartaric acid metabolism. V. Crystalline tartrate dehydrogenase, *J. Biol. Chem. 243*, 2479-2485.

89. Giffhorn, F. and Kuhn, A. (1983) Purification and characterization of a bifunctional l-(+)-tartrate dehydrogenase-d-(+)-malate dehydrogenase (decarboxylating) from *Rhodopseudomonas sphaeroides-y*, *J. Bacteriol. 155*, 281-290.

90. Dickens, F. and Glock, G. E. (1951) Direct oxidation of glucose-6-phosphate, 6-phosphogluconate and pentose-5-phosphates by enzymes of animal origin, *Biochem. J. 50*, 81-95.

91. Dyson, J. E. D., Dorazio, R. E., and Hanson, W. H. (1973) Sheep liver 6-phosphogluconate dehydrogenase - Isolation procedure and effect of pH, ionic-strength, and metal-ions on kinetic parameters, *Arch. Biochem. Biophys. 154*, 623-635.

92. Tipton, P. A. (1993) Intermediate partitioning in the tartrate dehydrogenase-catalyzed oxidative decarboxylation of D-malate, *Biochemistry 32*, 2822-2827.

93. Uhr, M. L., Thompson, V. W., and Cleland, W. W. (1974) Kinetics of pig heart triphosphopyridine nucleotide-isocitrate dehydrogenase. 1. Initial velocity, substrate and product inhibition, and isotope-exchange studies, *Journal of Biological Chemistry 249*, 2920-2927.

94. Northrop, D. B. and Cleland, W. W. (1974) Kinetics of pig heart triphosphopyridine nucleotide-isocitrate dehydrogenase. 2. Dead-end and multiple inhibition studies, *J. Biol. Chem. 249*, 2928-2931.

95. Dean, A. M. and Dvorak, L. (1995) The role of glutamate-87 in the kinetic mechanism of *Thermus thermophilus* isopropylmalate dehydrogenase, *Protein Sci. 4*, 2156-2167.

96. Lin, Y., Alguindigue, S. S., Volkman, J., Nicholas, K. M., West, A. H., and Cook, P. F. (2007) Complete kinetic mechanism of homoisocitrate dehydrogenase from *Saccharomyces cerevisiae*, *Biochemistry 46*, 890-898.

97. Hurley, J. H., Dean, A. M., Koshland, D. E., and Stroud, R. M. (1991) Catalytic Mechanism of $NADP^+$-dependent isocitrate dehydrogenase - Implications from the structures of magnesium isocitrate and $NADP^+$ complexes, *Biochemistry 30*, 8671-8678.

98. Bolduc, J. M. (1995) Mutagenesis and Laue Structures of enzyme intermediates - Isocitrate dehydrogenase, *Science 270*, 365.

99. Grodsky, N. B., Soundar, S., and Colman, R. F. (2000) Evaluation by site-directed mutagenesis of aspartic acid residues in the metal site of pig heart NADP-dependent isocitrate dehydrogenase, *Biochemistry 39*, 2193-2200.

100. Ceccarelli, C., Grodsky, N. B., Ariyaratne, N., Colman, R. F., and Bahnson, B. J. (2002) Crystal structure of porcine mitochondrial NADP(+)-dependent isocitrate dehydrogenase complexed with Mn^{2+} and isocitrate - Insights into the enzyme mechanism, *J. Biol. Chem. 277*, 43454-43462.

101. Huang, Y. C., Grodsky, N. B., Kim, T. K., and Colman, R. F. (2004) Ligands of the Mn^{2+} bound to porcine mitochondrial NADP-dependent isocitrate dehydrogenase, as assessed by mutagenesis, *Biochemistry 43*, 2821-2828.

102. Dalziel, K. (1980) Isocitrate dehydrogenase and related oxidative decarboxylases, *FEBS Lett. 117*, K45-K55.

103. Dalziel, K. (1984) Kinetics of oxidative decarboxylases, *NATO ASI Series, Series A: Life Sciences 81 (Dyn. Biochem. Systs.)*, 65-81.

104. Cleland, W. W. (1999) Mechanisms of enzymatic oxidative decarboxylation, *Accounts Chem. Res. 32*, 862-868.

105. Imada, K., Inagaki, K., Matsunami, H., Kawaguchi, H., Tanaka, H., Tanaka, N., and Namba, K. (1998) Structure of 3-isopropylmalate dehydrogenase in complex with 3-isopropylmalate at 2.0 angstrom resolution: the role of Glu88 in the unique substrate-recognition mechanism, *Struct. Fold. Des. 6*, 971-982.

106. Miyazaki, J., Asada, K., Fushinobu, S., Kuzuyama, T., and Nishiyama, M. (2005) Crystal structure of tetrameric homoisocitrate dehydrogenase from an extreme thermophile, *Thermus thermophilus*: Involvement of hydrophobic dimer-dimer interaction in extremely high thermotolerance, *J. Bacteriol. 187*, 6779-6788.

107. Tao, X., Yang, Z. R., and Tong, L. (2003) Crystal structures of substrate complexes of malic enzyme and insights into the catalytic mechanism, *Structure 11*, 1141-1150.

108. Lin, Y., Volkman, J., Nicholas, K. M., Yamamoto, T., Eguchi, T., Nimmo, S. L., West, A. H., and Cook, P. F. (2008) Chemical mechanism of homoisocitrate dehydrogenase from *Saccharomyces cerevisiae*, *Biochemistry 47*, 4169-4180.

109. Schimerlik, M. I. and Cleland, W. W. (1977) pH variation of kinetic parameters and catalytic mechanism of malic enzyme, *Biochemistry 16*, 576-583.

110. Gavva, S. R., Harris, B. G., Weiss, P. M., and Cook, P. F. (1991) Modification of a thiol at the active site of the *Ascaris suum* NAD-malic enzyme results in changes in the rate-determining steps for oxidative decarboxylation of L-malate, *Biochemistry 30*, 5764-5769.

111. Karsten, W. E., Lai, C. J., and Cook, P. F. (1995) Inverse solvent isotope effects in the NAD-malic enzyme reaction are the result of the viscosity difference between D_2O and H_2O - Implications for solvent isotope effect studies, *J. Am. Chem. Soc. 117*, 5914-5918.

112. Karsten, W. E., Hwang, C. C., and Cook, P. F. (1999) Alpha-secondary tritium kinetic isotope effects indicate hydrogen tunneling and coupled motion occur in the oxidation of L-malate by NAD-malic enzyme, *Biochemistry 38*, 4398-4402.

113. Schimerlik, M. I. and Cleland, W. W. (1975) Deuterium-isotope effects and substrate specificity of malic enzyme, *Fed. Proc. 34*, 495.

114. Huang, Y. C. and Colman, R. F. (2005) Location of the coenzyme binding site in the porcine mitochondrial NADP-dependent isocitrate dehydrogenase, *J. Biol. Chem. 280*, 30349-30353.

115. Imada, K., Tamura, T., Takenaka, R., Kobayashi, I., Namba, K., and Inagaki, K. (2008) Structure and quantum chemical analysis of NAD($^+$)-dependent isocitrate dehydrogenase: Hydride transfer and co-factor specificity, *Proteins 70*, 63-71.

116. Kim, T. K., Lee, P., and Colman, R. F. (2003) Critical role of Lys(212) and Tyr(140) in porcine NADP-dependent isocitrate dehydrogenase, *J. Biol. Chem. 278*, 49323-49331.

117. Lee, P. and Colman, R. F. (2006) Thr(373), Asp(375), and Lys(260) are in the coenzyme site of porcine NADP-dependent isocitrate dehydrogenase, *Arch. Biochem. Biophys. 450*, 183-190.

118. Bzymek, K. P. and Colman, R. F. (2007) Role of alpha-Asp(181), beta-Asp(192), and gamma-Asp(190) in the distinctive subunits of human NAD-specific isocitrate dehydrogenase, *Biochemistry 46*, 5391-5397.

119. Auld, D. S. and Vallee, B. L. (1970) Kinetics of carboxypeptidase-A - pH dependence of tripeptide hydrolysis catalyzed by zinc, cobalt, and manganese enzymes, *Biochemistry 9*, 4352-&.

120. Smith, R. M. and Martell, A. E. (1976) *Critical Stability Constants, Vol 4: Inorganic complexes* Plenum Press, New York and London.

121. Miyazaki, K. and Oshima, T. (1993) Tyr-139 in *Thermus thermophilus* 3-isopropylmalate dehydrogenase is involved in catalytic function, *FEBS Lett. 332*, 37-38.

APPENDIX

LIST OF ABBREVIATIONS

APAD, 3-acetylpyridine adenine dinucleotide

ADP, adenosine diphosphate

ATP, adenosine triphosphate

BSA, bovine serum albumin

Ches, 2-(*N*-cyclohexylamino)ethanesulfonic acid

Hepes, *N*-(2-hydroxyethyl)piperazine-*N'*-2-ethanesulfonic acid

HICDH, homoisocitrate dehydrogenase

Ic, isocitrate

IcDH, isocitrate dehydrogenase

Ipm, isopropylmalate

IPMDH, isopropylmalate dehydrogenase

IPTG, isopropyl β-D-1-thiogalactopyranoside

LDH, lactate dehydrogenase

ME, malic enzyme

NAD, nicotinamide adenine dinucleotide

NADH, reduced nicotinamide adenine dinucleotide

NADP, nicotinamide adenine dinucleotide 2'-phosphate

NADPH, reduced nicotinamide adenine dinucleotide 2'-phosphate

Ni-NTA, Ni^{2+}-nitrilo-tri-acetic acid

OAA, oxaloacetate

PAAD, 3-pyridinealdehyde adenine dinucleotide

PCR, polymerase chain reaction

6PGDH, 6-phosphogluconate dehydrogenase

Pipes, piperazine-*N*,*N'*-bis-(2-ethanesulfonic acid)

SDS, sodium dodecyl sulfate

TDH, tartrate dehydrogenase

WT, wild type